

Dissertation zur Erlangung des Doktorgrades
der Fakultät für Chemie und Pharmazie
der Ludwig-Maximilians-Universität München

Structural and Biochemical Characterization of
IFT-B proteins

Sagar Bhogaraju

aus

Nizamabad, Indien.

2013

Erklärung

Diese Dissertation wurde im Sinne von § 7 der Promotionsordnung vom 28. November 2011 von Frau Prof. Dr. Elena Conti betreut.

Eidesstattliche Versicherung

Diese Dissertation wurde eigenständig und ohne unerlaubte Hilfe erarbeitet.

München, 19.04.2013

.....
Sagar Bhogaraju

Dissertation eingereicht am	19.04.2013
1. Gutachterin	Prof. Dr. Elena Conti
2. Gutachter	Prof. Dr. Karl-Peter Hopfner
Mündliche Prüfung am	18.07.2013

Dedicated to my father, B. Venugopala Rao. Despite all the odds, he made this possible.

Table of Contents

1. Preface	3
2. Contributions	4
3. Summary	5
4. Introduction.....	8
4.1 Architecture of the cilium	8
4.2 Functions of cilia	13
4.2.1 Cilia in development.....	13
4.2.2 Cilia in photoreception and olfaction	14
4.2.3 Cilia in mechanosensing.....	16
4.2.4 Miscellaneous functions of cilia	17
4.3 Intraflagellar transport.....	17
4.3.1 Domain architecture and function of individual IFT proteins.....	21
4.3.1.1 IFT-B proteins.....	21
4.3.1.1.1 IFT27, 25 and 22	21
4.3.1.1.2 IFT20, 54, 57, 74 and 81	23
4.3.1.1.3 IFT46, 52, 70 and 88.....	25
4.3.1.1.4 IFT172 and 80.....	27
4.3.1.2 IFT-A proteins.....	29
4.4 Ciliary length control	31
5. Aim of research.....	34
6. Results	35
Chapter I.....	35
Crystal structure of the intraflagellar transport complex IFT25/27.....	35

Extended discussion.....	55
Finding a RabGAP specific for IFT25/27	55
IFT25 as a Ca ²⁺ sensor in the Shh pathway.....	56
Chapter II	59
Intraflagellar transport proteins IFT74 and IFT81 form a tubulin-binding module required for ciliogenesis.....	59
Extended discussion.....	111
The IFT74/81 tubulin binding module in mitosis	111
The life cycle of ciliary tubulin	111
7. Abbreviations.....	114
8. References.....	115
9. Acknowledgements.....	125
10. Curriculum Vitae.....	127

1. Preface

This thesis describes the work that I did in the lab of Dr. Esben Lorentzen for the last three and a half years. I have worked on two distinct but related projects and the results section in the thesis is thus divided into two main chapters. The results described in the first chapter were published as a research article in EMBO J with the title: “Crystal structure of the intraflagellar transport complex 25/27”. The second chapter is named “The IFT74/81 complex contains a tubulin binding module required for ciliogenesis” and is also presented in the form of a manuscript. As both manuscripts are comprehensive with regard to results and analyses, these are inserted “as is” into the thesis. A detailed introduction to the field of research precedes these two chapters. An extended discussion section follows each chapter that presents the implications of the results that are not part of the manuscript and the scope for further research.

2. Contributions

As the projects described in this thesis are a collaborative effort, a number of people have contributed scientific and technical expertise at various stages. Except for the experiments mentioned below, Sagar Bhogaraju designed and carried out all the experiments in this thesis under the supervision of Dr. Esben Lorentzen.

Purification of IFT complexes from insect cells: Dr. Michael Taschner

The following experiments were carried out by collaborators:

- 1) Functional experiments in human RPE-1 cells: Dr. Lukas Cajanek (Prof. Dr. Erich Nigg's lab, University of Basel)
- 2) Electron Microscopy of MT with binding partners: Dr. Naoko Mizuno

The following people provided technical help to Sagar Bhogaraju:

- 1) Isothermal titration calorimetry: Dr. Claire Basquin
- 2) Microscale thermophoresis: Christophe Jung and Kristina Weber
- 3) Molecular cloning: Michaela Morawetz and Marc Stiegler

3. Summary

Cilia/flagella are microtubule (MT) based membrane protrusions present on the surface of many eukaryotic cells. Once regarded as vestigial organelles without much functionality, cilia are now acknowledged to play critical roles in many aspects of human development, health and disease phenotypes through functions in cellular motility, signaling and sensory pathways. Cilia exist in many forms and serve a wide variety of tissue-specific functions. Given that cilia do not contain ribosomes and ciliary components are constantly turning over at the tip, proteins destined for cilia are synthesized in the cytoplasm and have to be actively transported into the cilium. Almost all cilia rely on a dedicated transport process called intraflagellar transport (IFT) for assembly and maintenance. IFT involves a multi-protein mega-dalton complex, known as the IFT complex that binds ciliary cargoes and transports them into and out of the cilium. IFT proteins are highly conserved in ciliated organisms ranging from the unicellular biflagellate green alga *Chlamydomonas reinhardtii* (*Chlamydomonas* or *Cr*) to higher eukaryotes including humans. Mutations in IFT genes lead to severe defects in cilia formation and are the primary cause of many ciliopathies (diseases caused by ciliary dysfunction). *Chlamydomonas* is an important model organism to study ciliary assembly and major discoveries such as the process of IFT, purification of IFT particles and tubulin turnover were made using simple but elegant experiments in this biflagellate. Although IFT is implicated in the transport of major axonemal components such as tubulin and outer dynein arms, a direct link between an IFT protein and a ciliary cargo was still missing prior to this study, largely due to the inadequate characterization of individual IFT proteins. This thesis describes the structural and biochemical characterization of 4 IFT proteins - namely IFT27, IFT25, IFT74 and IFT81 - from human and/or *Chlamydomonas*.

The first half of my thesis deals with the characterization of the heterodimeric IFT25/27 complex. *Chlamydomonas* IFT25 and IFT27 were recombinantly co-expressed in *E.coli* and purified to homogeneity as a stoichiometric heterodimeric complex. The purified IFT25/27 complex yielded crystals that diffracted to 2.6Å and allowed for structure determination using molecular replacement. The crystal structure of IFT25/27 revealed that IFT25 adopts a jellyroll fold and binds Ca²⁺. IFT27 adopts a small GTPase fold that is most similar to the family of Rab GTPases, and has a longer C-terminal helix that forms extensive hydrophobic and polar contacts with the Ca²⁺ binding loop of IFT25. The binding interface between IFT25 and IFT27 seen in the crystal structure was further verified using structure-guided point mutations that disrupted complex formation. Isothermal titration calorimetry (ITC) revealed that IFT27 binds to both GTP (K_d=19µM) and GDP (K_d=37µM) but does not bind ATP. Sequence comparison of IFT27 to other small Rab GTPases revealed that it lacks a critical catalytic residue involved in the hydrolysis of GTP. Consistent with this observation, GTP hydrolysis measurements on IFT27 revealed a very slow catalytic rate (2.1×10⁻³ min⁻¹), indicating that it might need a GTPase activating protein (GAP) to stimulate its activity *in vivo*. Indeed, binding of such a GAP fits with the surface conservation analysis of IFT25/27 complex, and BLAST searches revealed that several candidate GAPs exist in the *Chlamydomonas* genome that may function in the regulation of IFT by acting upon IFT27.

As a second project, I have characterized the N-terminal domains of IFT81 (IFT81N) and IFT74 (IFT74N). To this end, the crystal structure of the *Chlamydomonas* IFT81N was determined at 2.3Å resolution using anomalous dispersion methods. Interestingly, the structure showed that IFT81N adopts a calponin-homology (CH) domain fold and showed highest 3D structural similarity to CH domain of NDC80, a

kinetochore protein that was shown to interact with MTs. *In vitro* binding experiments showed that IFT81N interacts with both MT and $\alpha\beta$ -tubulin heterodimers. Affinity in terms of the dissociation constant (K_d) of the IFT81N-tubulin interaction was measured using Microscale thermophoresis (MST) experiments as $\sim 15\mu\text{M}$. Point mutations of several conserved positively charged residues in IFT81N severely affected its binding to tubulin. Careful sequence inspection revealed that IFT74, a direct interacting partner of IFT81 contains a highly basic N-terminal end (IFT74N). Knowledge of a similar basic region in NDC80 that plays an important role in the binding of NDC80 to MTs, prompted me to test the role of IFT74N in the context of IFT81N-tubulin/MT interaction. For this purpose, the IFT81/74_CC complex containing both the N-termini and proximal coiled-coil parts of IFT74 and IFT81 was produced. This complex bound MTs with increased affinity and the K_d for tubulin was measured using MST to be $0.9\mu\text{M}$. Further binding experiments with subtilisin-treated tubulin and MTs revealed that the IFT81N binds to the globular domain of tubulin whereas IFT74N binds to the acidic C-terminal tails. These results suggest that the N-termini of IFT74 and IFT81 form a tubulin-binding module that may be involved in the transport of tubulin to the tip of the cilium.

In collaboration with the group of Prof. Erich Nigg at University of Basel, we characterized the role of this tubulin-binding module in ciliogenesis of human RPE-1 cells. siRNA knockdown of IFT81 expression led to severe ciliogenesis defects. Although expressing RNAi resistant wild-type IFT81 rescued this phenotype completely, expression of IFT81 with tubulin-binding point mutations failed to do so. These functional analyses are consistent with the structural and biochemical data and suggest a conserved tubulin transport mechanism mediated through the N-termini of IFT74 and IFT81.

4. Introduction

Cilia are tail-like organelles that project from the surface of most eukaryotic cells with the exception of fungi and higher plants. Cilia are typically 2-15 μ M in length. Mammalian cilia were first observed by a Swiss anatomist, K.W. Zimmermann, on kidney cells in 1898 and later were also discovered on cells in the brain, liver, testis, eyes and many other tissue types (Figure 4.1). For the majority of the last century, this organelle was considered an evolutionary remnant acquired from a unicellular common ancestor having a motility-specific cilium. Recently, however, several human diseases were linked to defects in cilia (Badano et al., 2006). These diseases are collectively known as ciliopathies, as they all have been associated with defects in ciliary assembly and function. Some notable ciliopathies include polycystic kidney disease (PKD), primary ciliary dyskinesia, Bardet-Biedl syndrome (BBS), Joubert syndrome and Meckel-Gruber syndrome.

4.1 Architecture of the cilium

Cilium and flagellum are interchangeable terms used to describe the hair-like organelle on cells of mammals and other eukaryotic organisms, but are not to be confused with the structurally and functionally different bacterial flagellum. One of the earliest glimpses into the structure of the cilium came from electron microscopy studies on sea urchin sperm flagella (Afzelius, 1959). Technological advances in electron microscopy and cryo-electron tomography have greatly increased our knowledge of ciliary ultra structure and has enabled the detailed visualization of axonemal components (Nicastro, 2006; Nicastro et al., 2005; Sui and Downing, 2006).

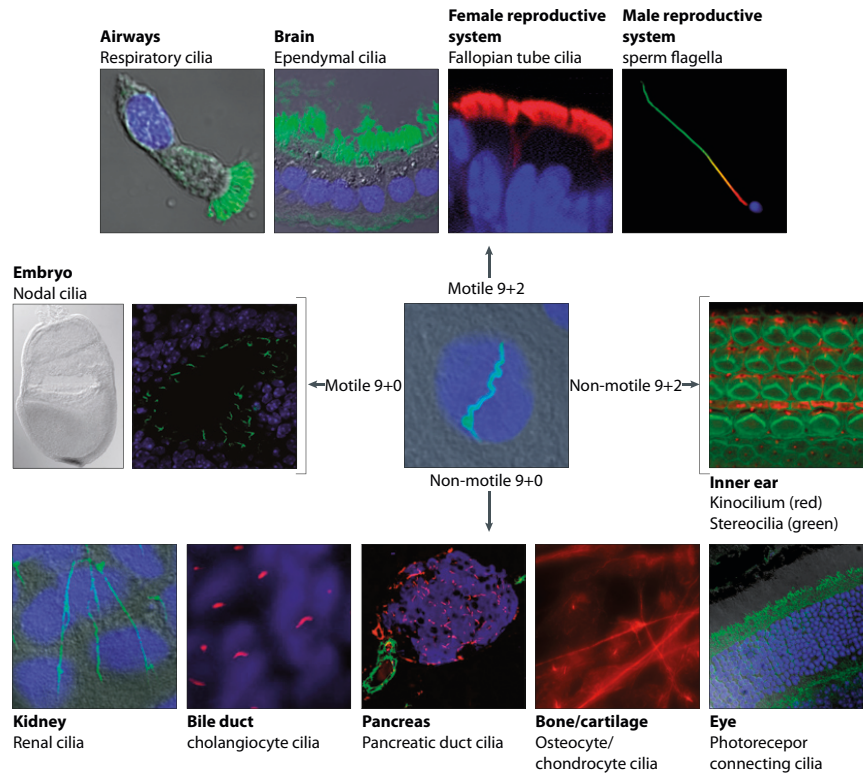


Figure 4.1. Four main classes of mammalian cilia constitute “motile 9+0”, “motile 9+2”, “non-motile 9+0” and “non-motile 9+2”. Each class of cilia is associated with cells of specific tissues and performs unique functions (see section 4.2, adapted from (Fliegeauf et al., 2007)).

The basic backbone of the cilium is a microtubule (MT)-based structure called the axoneme. The axoneme is typically composed of 9 outer doublet MTs, with or without a central pair of MTs; this arrangement of MTs in an axoneme is referred to as “9+2 arrangement” or “9+0 arrangement”, respectively (Figure 4.2, Axoneme). The two MTs in a doublet are referred as the A- and B-tubule. The A-tubule of the doublet is “complete” with 13 protofilaments whereas the B-tubule is only composed of 10 protofilaments. Similar to their cytoplasmic counterparts, axonemal MTs are formed by polymerization of $\alpha\beta$ -tubulin heterodimers and grow from their ‘+’ end which is at the ciliary tip (Figure 4.2). The 9+2 arrangement of MTs is often associated with motile cilia such as respiratory cilia and the sperm flagellum, whereas

the 9+0 arrangement is typically associated with the non-motile cilium also called the primary cilium. In addition to the central pair of MTs, motile ciliary axonemes also contain various appendage structures attached to the doublet MTs that facilitate ciliary beating. These include nexins that connect adjacent MT-doublets (Figure 4.2, Axoneme). The inner sheath is another appendage structure that is composed of fibrous protein complexes surrounding the central pair. Dynein arms are key components of the motile cilium as they are directly responsible for generating the force required for ciliary movement. Dynein arms emanate from the A-tubule of the doublet towards the B-tubule of the adjacent doublet in the direction of the flagellar membrane (outer dynein arms) and into the lumen of the axoneme (inner dynein arms) (Mitchell, 2001; Warner and Satir, 1974). They contain motor proteins (ATPases) that undergo large conformational changes and reversibly bind to the adjacent B-tubule (Nicastro, 2006) to create a sliding motion of a doublet with respect to its adjacent doublet. Since doublets are connected to each other via nexins and are connected to the basal body at one end, this sliding motion translates into bending of the cilium (Lindemann and Lesich, 2010). Radial spokes are also motility specific structures and connect the A-tubules of each outer doublet to the central pair. Together with the central pair, radial spokes regulate the beating pattern of the cilium (Barber et al., 2012; Mitchell, 2001; Warner and Satir, 1974). The ciliary membrane is continuous with the cellular plasma membrane and surrounds the axoneme. There are many variations in the ultra-structure and appearance of cilia from various organisms or different tissue types of the same organism (for examples, see Figure 4.4). Non-motile cilia that lack the central pair of MTs (primary cilia) also lack the accessory proteins such as dynein arms, nexins and radial spokes necessary for motility. Embryonic nodal cilia have a 9+0 arrangement but are still motile (Nonaka

et al., 1998). These cilia lack the central pair of MTs but have retained the motor machinery required for motility (Figure 4.1) (Fliegauf et al., 2007). On the contrary, kinocilia present in the inner ear possess a central pair but still are immotile as they specifically lack outer dynein arms and nexins (Kikuchi et al., 1989; Sobkowicz et al., 1995) (Figure 4.1).

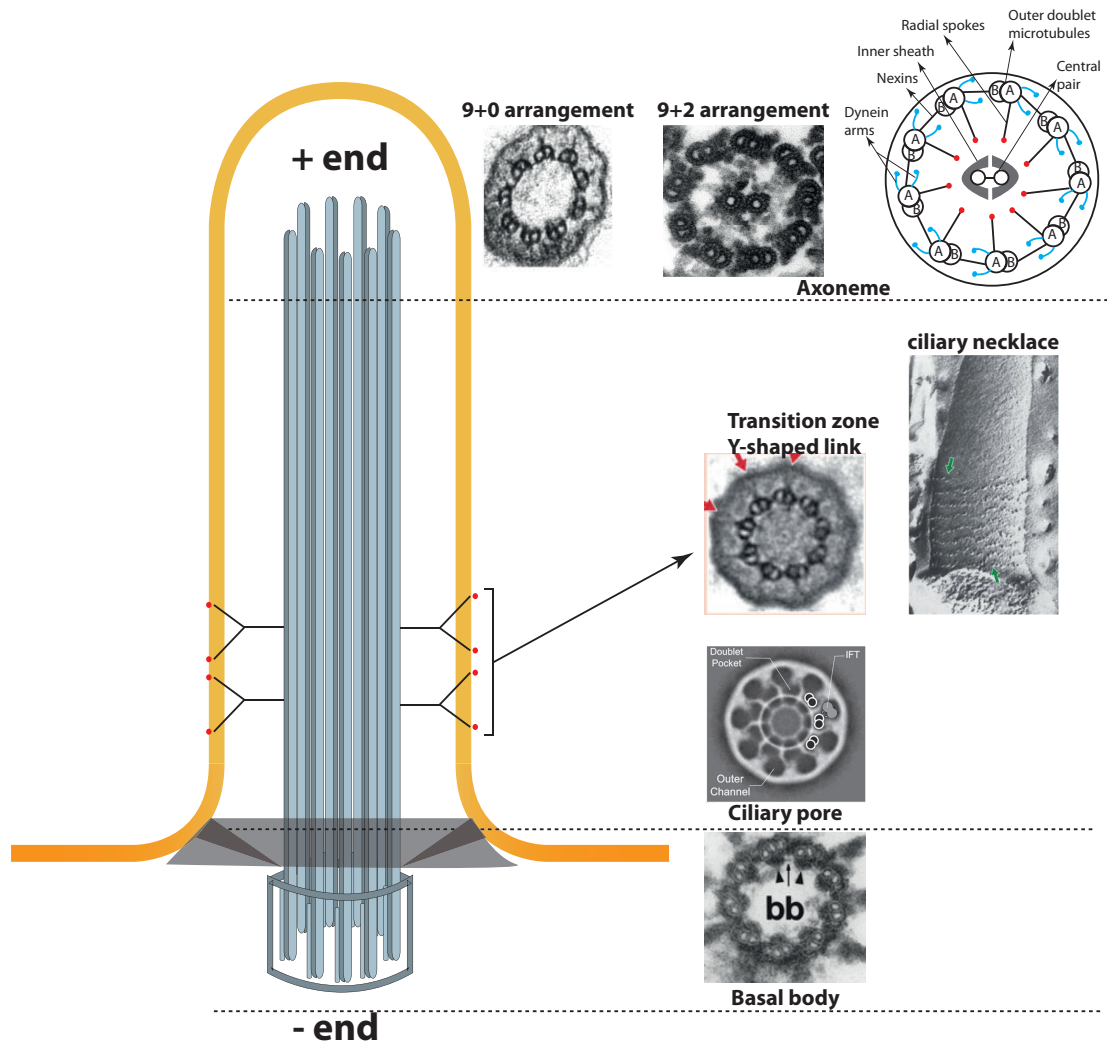


Figure 4.2: Ultra structure of the cilium. A cartoon representation of a cilium is shown on the left and on the right, cross sections at various positions along the cilium are shown. The axoneme forms the backbone of the cilium extending from the basal body triplets. The ciliary pocket and transition zone together form a barrier preventing free diffusion of proteins. The ciliary necklace works as a membrane barrier and prevents free diffusion of membrane proteins into and out of the ciliary membrane.

The axoneme is connected to a cytoplasmic structure known as the basal body, which is a modified form of the mother centriole (Bornens, 2012; Gönczy, 2012; Nigg and Raff, 2009). It has 9 triplet MTs arranged in a cartwheel-like fashion. As two MTs (A-tubule & B-tubule) in each triplet extend to form the ciliary axoneme, the cartwheel symmetry of these triplets is translated into the symmetry of the axonemal outer doublet MTs (Figure 4.2, Basal body) (Mizuno et al., 2012; Ringo, 1967). As is true for any organelle in the cell, maintenance of homeostasis by preventing the entry of meandering non-native cytosolic proteins and complexes is of great importance for the cilium. For this purpose, the cilium has specialized structures that connect the axoneme to the ciliary membrane and act as diffusion barriers. Although a lot is known about the overall protein composition of these barriers (Garcia-Gonzalo et al., 2011; Sang et al., 2011), the exact mechanism of “sieving” for ciliary proteins is still not known. A barrier-like structure exists just proximal to the basal body preventing free diffusion of cytosolic proteins into the cilium. This structure is called the ciliary pore. Recent electron tomography analysis of the ciliary pore revealed that it has 9 holes arranged symmetrically through which 9 outer doublet MTs of the ciliary axoneme protrude (Ounjai et al., 2013). It also contains a 53nm wide hole adjacent to the B-tubule of each outer doublet that could allow the passage of the ciliary protein trafficking machinery such as Intraflagellar transport (IFT) particles (Figure 4.2, Ciliary pore). Upstream to the ciliary pore, another barrier like region called ‘transition zone’ exists. It contains several Y-shaped structures that connect the axoneme and the ciliary membrane. These structures are also thought to be involved in sorting the ciliary proteins. The membrane component of the transition zone is called ciliary necklace and is proposed to act as a barrier for membrane proteins entering cilia (Fisch and Dupuis-Williams, 2012; Gilula, 1972). In summary, cilia

possess all the characteristic features of a distinct compartment and thus can be considered as a *bona fide* cellular organelle.

4.2 Functions of cilia

4.2.1 Cilia in development

A single copy of a motile cilium is present on each of the embryonic nodal cells. Nodal cilia undergo leftward rotation with a regular frequency to create extracellular fluid flow that is responsible for establishing the left-right asymmetry in the embryo (Figure 4.3). It is proposed that the vigorous circular motion of the nodal cilia concentrates the morphogens packaged into nodal vesicular parcels (NVPs) to the left side of the node where they interact with signaling proteins thus initiating the establishment of asymmetry (Nonaka et al., 1998). Consistent with this hypothesis, artificial fluid flow simulating the ciliary nodal flow induces asymmetry in cultured mouse embryonic cells (Nonaka et al., 2002). PKD2, a ciliary transmembrane protein and a Ca^{2+} ion channel expressed in the cells at the edge of the embryonic node, senses the nodal flow and is found to play a pivotal role in the formation of left-right asymmetry (Yoshihara et al., 2012). Defects in nodal cilia are common causes of *situs-inversus* in humans where left-right asymmetry during development is dysfunctional leading to an inverted position of vital internal organs such as lungs, heart, spleen and stomach.

Another role of cilia in mammalian development is the regulation of the Hedgehog (Hh) signaling pathway. Binding of the signaling ligand Hh to the ciliary membrane receptor Patched-1 (Ptch1) stimulates the Hh pathway. Upon Hh ligand binding, activated Ptch1 is displaced from the ciliary membrane and in turn triggers the

accumulation of another transmembrane protein Smoothed (Smo) in the ciliary membrane (Rohatgi et al., 2007).

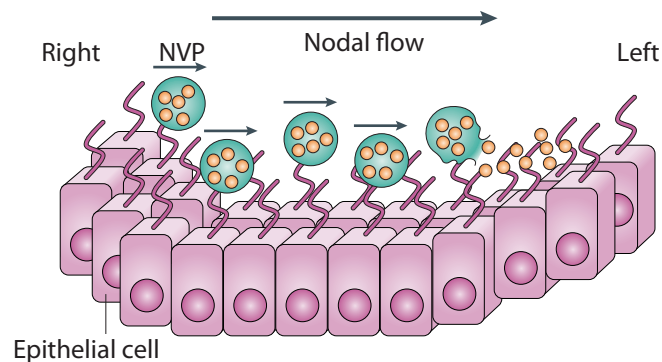


Figure 4.3: Schematic representation of embryonic nodal cilia. Ciliary beating creates a leftward fluid flow establishing a gradient of nodal vesicular parcels (NVPs) that triggers the left-right asymmetry (adapted form (Fliegeauf et al., 2007)).

The ciliary Smo activates Gli transcription factors that further localize to the nucleus and trigger the Hh signaling response by activating Hh pathway target genes (Haycraft et al., 2005; Kim et al., 2009; Tukachinsky et al., 2010). Major players in this pathway Ptc, Smo and Gli transcription factors have been shown to localize to the cilium. Mutations in the genes responsible for cilium formation compromise the Hedgehog signaling pathway, leading to developmental abnormalities such as polydactyly and neural tube closure/patterning defects (Badano et al., 2006; Han et al., 2008; Mukhopadhyay et al., 2013).

4.2.2 Cilia in photoreception and olfaction

Rod and cone photoreceptor cells have specialized sensory cilia with an expanded tip referred to as the outer segment (Figure 4.4, Photoreceptor cell). The outer segment hosts the opsin G-protein coupled receptors (GPCRs) that respond to light and transduce the signal to the inner segment by activating the hydrolysis of cGMP and thereby closing the cGMP gated channels (Elias et al., 2004; Osawa et al., 2011; Strissel, 2005). The heterotrimeric G-protein transducin and rhodopsin kinase (GRK1)

that are part of this signal transduction pathway undergo active transport via the connecting cilium (Figure 4.4, Photoreceptor cell) to their site of function in the outer segment. Mutations that compromise outer segment formation (ciliogenesis) leads to diseases such as Retinitis pigmentosa (RP) which is associated with progressive degeneration of rod photoreceptors leading to blindness (Badano et al., 2006; Khanna, 2005).

Cilia also play a significant role in olfaction. Each olfactory receptor cell (ORC) contains several cilia attached to the dendritic knob (Figure 4.4, Olfactory receptor cell). The apical part of the ORCs containing the cilia is exposed to the environment while the rest of the cell surface is immersed in the epithelium. In this way, the ciliary membrane is perfectly placed to sense environmental odors. Olfactory specific membrane receptors belong to the GPCR superfamily and are localized to cilia where they interact with extracellular odorants and transduce the signal via an olfactory specific heterotrimeric G protein called G_{olf} . This leads to increased levels of cAMP inside the cilium, an important second messenger in the olfaction pathway for a wide variety of odorants (McEwen et al., 2008). ORCs with defective cilia cannot respond to odorants (Benton et al., 2006; Kulaga et al., 2004).

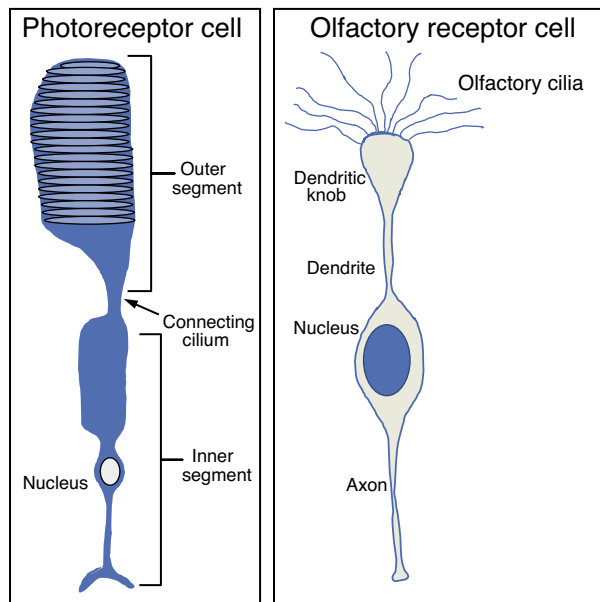


Figure 4.4: Schematic representation of photoreceptor and olfactory receptor cells showing various component parts (adapted from (Berbari et al., 2009)).

4.2.3 Cilia in mechanosensing

The first hint that cilia play a role in mechanosensing came from the finding that mono cilia in cultured renal epithelial cells respond to fluid flow by increasing the intracellular Ca^{2+} levels (Nauli et al., 2003). It was later discovered that ciliary transmembrane proteins polycystin-1 (PC1) and polycystin-2 (PC2), mutated in polycystic kidney disease (PKD), play an important role in this pathway (Stayner and Zhou, 2001). Patients with PKD have unusually large kidneys with multiple cysts, compromising kidney function and thereby making them extensively dependent on dialysis. Mono cilia on the apical surface of epithelial cells lining the renal collecting duct bend in response to the urine flow, which leads to activation of PC1. This in turn activates PC2, a physical PC1 interacting partner and a Ca^{2+} ion channel (Nauli et al., 2003; Qian et al., 1997). PC2 upon activation pumps Ca^{2+} into the cell leading to increased intracellular calcium levels. Absence of cilia or mutated PC1 or PC2 results in cells that cannot sense the urine flow and this leads to decreased intracellular

calcium levels. As a result of this, intracellular cAMP levels increase, leading to activation of MAP kinase signaling and to uncontrolled cell proliferation and cyst formation (Nagao et al., 2007). Similar to the renal cysts, dysfunctional cilia are also proposed to cause pancreatic cysts that arise from the uncontrolled proliferation of epithelial cells lining the pancreatic duct (Cano et al., 2006).

4.2.4 Miscellaneous functions of cilia

Apart from the functions mentioned above, motile cilia are also known to play a role in the smooth flow of the cerebrospinal fluid in the brain ventricles (Banizs, 2005; Ibanez-Tallon, 2004). Furthermore, motile cilia on respiratory epithelial cells are responsible for mucociliary clearance (Duchateau et al., 1985). Normal beating of cilia lining the fallopian tube epithelium is essential for pregnancy as these cilia drive the movement of the zygote from the ovary to the uterus (Lyons, 2006). A failure to do so is an important cause of ectopic pregnancy. Mutations in ciliary assembly machinery proteins (IFT), leading to defects in the assembly of the sperm flagellum, are known to cause male sterility (Fliegauf et al., 2007).

4.3 Intraflagellar transport

Cilia do not contain ribosomes for the synthesis of their protein components. Given that axonemal components are assembled and turned over at the distal end (ciliary tip) (Johnson and Rosenbaum, 1992; Marshall and Rosenbaum, 2001b), cilia depend on a bi-directional active transport of ciliary precursors for their formation and maintenance. This transport process is called Intraflagellar transport (IFT). IFT was first discovered in *Chlamydomonas* flagella by digital interference contrast (DIC) microscopy as a motility that is different from the flagellar beating (Kozminski et al., 1993). The speed of IFT was measured at 2 $\mu\text{m}/\text{sec}$ in the anterograde direction (from

the base to the ciliary tip) and 3.5 $\mu\text{m}/\text{sec}$ in the retrograde direction (from ciliary tip to the base). Transmission electron microscopy of *Chlamydomonas* flagella revealed linear arrays of electron dense matter dispersed over the length of the flagellum and connected to both the ciliary membrane and the B-tubule of the outer doublet MTs (Figure 4.5 A and B). These linear arrays are referred to as “IFT trains” and the repetitive components of the trains are known as “IFT particles”. It was later discovered that a hetero-trimeric kinesin (also known as kinesin-2) motor is responsible for the anterograde IFT while the cytoplasmic dynein 2 (previously called cytoplasmic dynein 1b) motor drives the retrograde IFT (Figure 4.5 B) (Cole et al., 1998; Kozminski et al., 1995; Pazour et al., 1999).

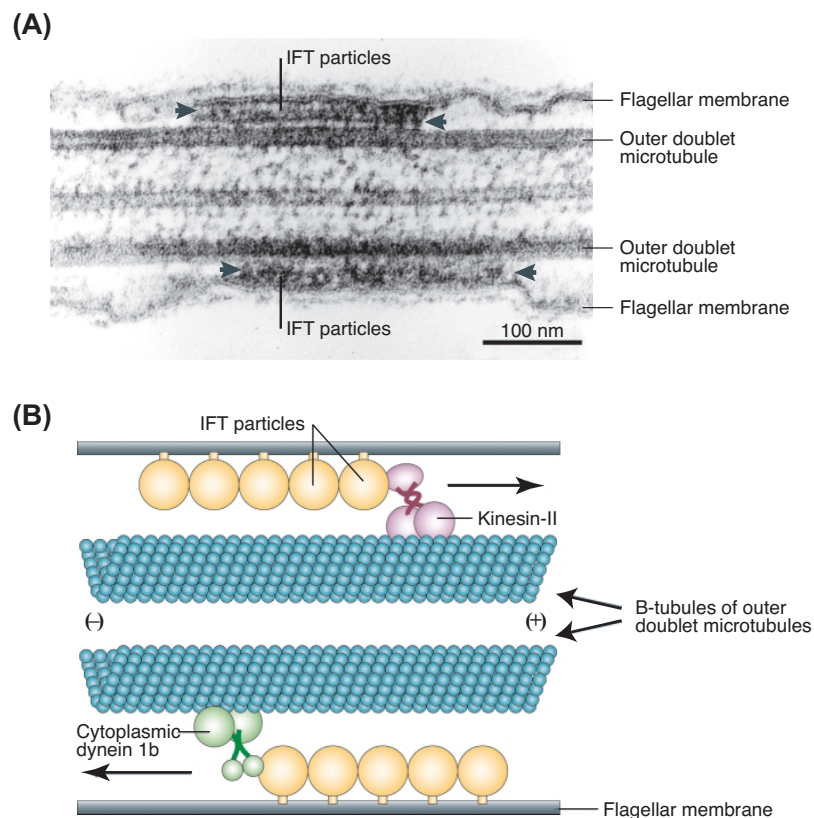


Figure 4.5: A) Electron micrograph of the *Chlamydomonas* flagellum showing the IFT trains lying in between the flagellar membrane and the axoneme. B) Schematic representation of anterograde and retrograde IFT powered by kinesin-2 and dynein 1b, respectively (adapted from (Rosenbaum and Witman, 2002)).

The first breakthrough linking the polypeptides in the IFT particle to cilia assembly came from the finding that the purified *Chlamydomonas* IFT particle proteins are homologous to the proteins required for the assembly of *C.elegans* sensory cilia (Cole et al., 1998). The proteins of the IFT particles were first purified by sucrose density gradient centrifugation from isolated *Chlamydomonas* flagella and were later also characterized in *C.elegans* and mouse (Cole et al., 1998; Follit et al., 2009; Piperno and Mead, 1997). These proteins form a 17S complex (IFT complex) composed of 20 different polypeptides (see Table 4.1). Each polypeptide is named according to its apparent molecular weight on an SDS gel. During the initial sucrose density gradient centrifugation of isolated *Chlamydomonas* IFT complexes, it was observed that by increasing the ionic strength, the IFT complex is separated into two sub-complexes called IFT-A and IFT-B (Cole et al., 1998). Further increase of ionic strength during purification of the IFT complex led to the dissociation of IFT-B peripheral proteins from the salt stable IFT-B “core” (see Table 4.1 for the list of proteins) (Lucker et al., 2005). Mutational inhibition of IFT-A components in *C.elegans* and *Chlamydomonas* led to the formation of short and stumpy cilia with large amounts of IFT material accumulated inside the cilium (Piperno et al., 1998; Qin et al., 2001). However, mutations in the IFT-B proteins in multiple organisms invariably led to the complete loss of ciliary assembly (Gorivodsky et al., 2009; Pazour et al., 2000; Yoshida et al., 2012). These observations led to the notion that the IFT-A complex plays a role in the retrograde transport, whereas the IFT-B complex is involved in the anterograde IFT. Mutational studies of IFT motors and polypeptides in *Chlamydomonas* revealed the essential role of IFT in the formation and maintenance of cilia. Mutations in IFT proteins are also found to affect ciliary assembly in numerous mammalian cilia systems such as renal mono cilia, embryonic nodal cilia and photoreceptor cells

(Pazour, 2004; Sedmak and Wolfrum, 2012; Yoshiba et al., 2012) suggesting that IFT proteins play an important role in the assembly of a wide variety of cilia. Consistent with their role in ciliary assembly, IFT proteins are highly conserved in all ciliated eukaryotes but are absent from the non-ciliated plants and fungi.

IFT polypeptide	<i>Chlamydomonas reinhardtii</i>	<i>C.elegans</i>	<i>Homo sapiens</i>
<i>IFT-A complex</i>			
IFT144	IFT144/FAP66 (A9XPA7)	DYF-2 (G5ECZ4)	WDR19 (Q8NEZ3)
IFT140	IFT140 (A8J4D9)	CHE-11 (P90757)	IFT140/WDTC2 (Q96RY7)
IFT139	IFT139 (A9XPA6)	ZK328.7/TTC21 (Q20255)	TTC21B (Q7Z4L5)
IFT122	IFT122 (H9CTG6)	DAF-10 (G5EFW7)	IFT122/WDR10 (Q9HBG6)
IFT121	FAP118 (A8JFR3)	IFTA-1 (Q18859)	IFT121/WDR35 (Q9P2L0)
IFT43	IFT43/MOT1 (A8HYP5)	Absent	IFT43/ C14orf179 (Q96FT9)
<i>IFT-B complex</i>			
<i>IFT-B "Core"</i>			
IFT88	IFT88 (Q9FPW0)	OSM-5 (G5ED37)	IFT88/Tg737 (Q13099)
IFT81	IFT81 (Q68RJ5)	IFT81 (A8DYR7)	IFT81/CDV1 (Q8WYA0)
IFT74	IFT74/72 (Q6RCE1)	IFT74 (Q18106)	IFT74/CMG1 (Q96LB3)
IFT70	FAP259 (A8ITN7)	DYF-1 (Q817G4)	TTC30B (Q8N4P2)
IFT52	IFT52 (Q946G4)	OSM-6 (G5EDF6)	IFT52 (Q9Y366)
IFT46	IFT46/FAP32 (A2T2X4)	DYF-6 (Q0G838)	IFT46 (Q9NQC8)
IFT27	IFT27/FAP156 (A8HN58)	Absent	IFT27/RABL4 (Q9BW83)
IFT25	IFT25 (B8LIX8)	Absent	Hspb11 (Q9Y547)
IFT22*	IFT22/FAP9 (A8HME3)	IFTA-2 (Q9XUC2)	RABL5 (Q9H7X7)
<i>IFT-B "Peripheral"</i>			
IFT172	IFT172/FLA11 (Q5DM57)	OSM-1 (Q22830)	IFT172 (Q9UG01)
IFT80	IFT80 (A5Z0S9)	CHE-2 (G5EGF0)	IFT80/WDR56 (Q9P2H3)
IFT57	IFT57 (Q2XQY7)	CHE-13 (Q93833)	IFT57/HIPPI (Q9NWB7)
IFT54	FAP116 (A8JBY2)	DYF-11 (Q17595)	IFT54/TRAF3IP1/MIPT3 (Q8TDR0)
IFT20	IFT20 (Q8LLV9)	IFT20 (Q8TA52)	IFT20 (Q8IY31)

*Unpublished data (Dr. Michael Taschner)

Table 4.1: List of IFT proteins. IFT proteins in *Chlamydomonas reinhardtii*, *Homo sapiens* and *Caenorhabditis elegans* are listed along with their respective Uniprot identifiers in the brackets. Proteins not present are listed as "Absent".

4.3.1 Domain architecture and function of individual IFT proteins

Given that IFT proteins play a role in binding and transport of ciliary cargo and exist in the form of a ~1.5MDa complex, it is not surprising that many of the IFT proteins are predicted to be composed of domains consisting of TPR repeats, β -propellers and coiled-coils which are known to mediate protein-protein interactions (Figure 3.6). The IFT complex contains 20 proteins in total, with 14 proteins in IFT-B and 6 in IFT-A. Notably, except for the crystal structure of IFT25, no other structural information was available for any of the IFT proteins prior to the work described in this thesis. In the following sections proteins belonging to IFT-A and IFT-B are discussed separately. The fourteen IFT-B proteins are further divided into a few biochemical and structural sub-groups based on the analysis of the literature available. Proteins belonging to each sub-group will be introduced and their possible molecular role in IFT and ciliogenesis will be discussed.

4.3.1.1 IFT-B proteins

4.3.1.1.1 IFT27, 25 and 22

Rab GTPases are well known for their role in the regulation of various steps of membrane trafficking (Stenmark, 2009). Notably, there are two predicted Rab-like GTPases in the IFT-B complex, namely IFT27 and IFT22 (Figure 4.6). RNAi knockdown of IFT27 in *Chlamydomonas* surprisingly led to cytokinesis defects and prolonged cell division apart from ciliary assembly defects (Qin et al., 2007). However, the role of IFT27 in cell division remains controversial as its depletion in mouse did not lead to any defects in mitosis (Keady et al., 2012). Improved purification of *Chlamydomonas* IFT complexes and *in vitro* pull-down experiments led to the discovery of IFT25 as a direct binding partner of IFT27 (Wang et al., 2009).

To see if this heterodimer is always a part of the IFT complex, sucrose density gradient centrifugation of *Chlamydomonas* flagellar and cytoplasmic fractions was performed and the fractions were subsequently probed by western blotting for the presence of IFT25/27. This revealed that majority of IFT25/27 exists independently of the IFT complex in the cell body but associates with the rest of the IFT complex in flagella. This led to the hypothesis that the association of the IFT25/27 heterodimer with the rest of the IFT complex may constitute a regulatory step in the initiation of IFT (Wang et al., 2009). The crystal structure of human IFT25 determined by the Northeast Structural Genomics Consortium (Ramelot et al., 2008) revealed that IFT25 adopts a jelly-roll fold and binds to Ca^{2+} (Figure 4.6). The stability of IFT27 was shown to depend on IFT25, as depletion of IFT25 in both *Chlamydomonas* and mouse resulted in the loss of IFT27 as well (Keady et al., 2012).

IFT22 is another protein that is predicted to contain a Rab GTPase domain. Sequence comparison of IFT22 with other Rab GTPases revealed that one of the essential GTP binding motifs (G4) is not conserved in IFT22 (Schafer et al., 2006), thus classifying IFT22 as an atypical Rab GTPase (Figure 4.6). Mutations in the IFT22 ortholog of *C.elegans*, IFTA-2, did not have any ciliary morphological defects but surprisingly led to a phenotype of extended life span and dauer formation (Schafer et al., 2006). Interestingly, IFTA-2 with a mutation in the predicted nucleotide-binding pocket was not able to localize to the cilium indicating that nucleotide binding is necessary for the localization of IFT22 to this organelle. In contrast to the role of IFT22 in *C.elegans*, RNAi depletion of the IFT22 ortholog in *Trypanosoma brucei* resulted in short and stumpy cilia with large amounts of accumulated IFT material, consistent with a role in retrograde IFT. This indicates that IFT22 has species specific functions (Adhiambo et al., 2009). Recently, a role for IFT22 in regulating the amounts of cellular pool of IFT

proteins was proposed for *Chlamydomonas* (Silva et al., 2012). It remains to be seen what role the mammalian ortholog of IFT22, RabL5, plays in IFT and ciliogenesis.

4.3.1.1.2 IFT20, 54, 57, 74 and 81

The IFT-B complex contains a number of proteins with predicted coiled-coil structure (Taschner et al., 2012). IFT20 is the smallest and the best studied of all the coiled coil proteins in the IFT complex. Like other IFT proteins, IFT20 was also found to localize to the basal body and the cilium. Interestingly, IFT20 is also shown to localize to the Golgi complex in mammalian cells (Follit et al., 2006). The partial depletion of IFT20 by RNAi led to a decreased transport of the transmembrane protein PC2 into the cilium, indicating that IFT20 may function at the Golgi complex in sorting membrane proteins destined for the cilium (Follit et al., 2009). Consistent with this observation, IFT20 mutations in mouse rod and cone photoreceptor cells led to the accumulation of rhodopsin and opsin near the Golgi complex of the inner segments without any morphological effects on the outer segment and connecting cilium (Keady et al., 2011). Complete depletion of IFT20 in mammalian cells led to severe ciliary assembly defects (Follit et al., 2006). Co-immuno precipitation of flag-tagged IFT20 from cultured mouse kidney cells revealed that it physically interacts with a Golgi protein named GMAP210 (Follit et al., 2008). Further interaction studies showed that it also binds to two other IFT-B coiled coil proteins, namely IFT54 and IFT57 (Keady et al., 2011). Consistent with their physical interaction with IFT20, mutations in both IFT54 and IFT57 led to ciliary transmembrane protein transport defects in addition to ciliary assembly defects (Bacaj et al., 2008; Krock and Perkins, 2008; Kunitomo and Iino, 2008; Omori et al., 2008). In summary, IFT20 along with IFT54 and IFT57 are peripheral IFT-B components that form a hetero-trimeric complex involved in the transport of ciliary membrane proteins (Figure 4.7).

Interestingly, the human ortholog of IFT54, MIP-T3 was shown to interact with tumor necrosis factor receptor associated factor-3 (TRAF-3) (Ling and Goeddel, 2000). MIP-T3 was also shown to directly interact with MTs, tubulin and actin (Guo et al., 2010; Ling and Goeddel, 2000) indicating that it might be involved in cytoskeleton related functions.

Apart from IFT20, IFT54 and IFT57 the IFT-B complex also contains two other proteins, IFT74 and IFT81, with comparatively large predicted C-terminal coiled-coil domains spanning ~500 amino acids. Both IFT74 and IFT81 contain small uncharacterized N-terminal domains of ~100 amino acids (Figure 4.6). Chemical cross-linking and yeast two-hybrid studies revealed that IFT74 and IFT81 interact via their coiled-coil regions (Lucker et al., 2005). In the yeast two-hybrid studies IFT81 was also shown to homo-dimerize. This led to the speculation that IFT74 and IFT81 may form a higher order tetrameric complex containing two copies of each protein. Cross-linking of the purified IFT complex, *E.coli* co-expression and pull-down experiments revealed that the IFT74/81 complex binds to the IFT25/27 heterodimer (Ben F Lucker et al., 2010; Taschner et al., 2011). The purified IFT74/81/25/27 complex showed the stoichiometry of 1:1:1:1. Furthermore, the static light scattering (SLS) profile of this complex did not comply with the speculated tetrameric arrangement of IFT74 and IFT81 (*Unpublished data: Dr. Michael Taschner*). This indicates that the tetrameric arrangement of the IFT74/81 complex suggested by Lucker et al. 2005 might be a false positive result obtained due to the non-specific homo-dimerization of IFT81 in the yeast two-hybrid studies (Figure 4.7) (*Unpublished data: Dr. Michael Taschner, Lucker et al., 2005*). It is proposed that the IFT74/81 complex acts as a platform onto which other components of the IFT-B complex are assembled (Lucker, 2005; Taschner et al., 2011) (Figure 4.7).

Expectedly, mutations in IFT74 or IFT81 orthologs in *C.elegans* sensory neurons resulted in defects in ciliary assembly and IFT (Kobayashi et al., 2007).

4.3.1.1.3 IFT46, 52, 70 and 88

In vitro pull-down and co-expression studies revealed that IFT46, IFT52, IFT70 and IFT88 form a hetero-tetrameric complex (Ben F Lucker et al., 2010; Fan et al., 2010; Taschner et al., 2011). Interestingly, IFT52 was also shown to interact with IFT74/81/25/27 tetramer thus bridging two IFT-B “core” sub-complexes, namely IFT46/52/70/88 and IFT74/81/25/27 (Taschner et al., 2011) (Figure 4.7). While the IFT52 C-terminus binds to other IFT proteins, the N-terminus of IFT52 was predicted to contain a putative carbohydrate binding “GIFT domain” (Beatson and Ponting, 2004; Taschner et al., 2011). However, *in vitro* purified GIFT domain of IFT52 failed to show any carbohydrate binding indicating that this domain may have some other function(s) (Taschner et al., 2011). *Chlamydomonas bld1* mutants defective in the IFT52 gene are devoid of flagella and were shown to contain a completely disrupted IFT-B core complex indicating that IFT52 is critical for IFT-B core stability (Figure 4.7) (Deane et al., 2001; Richey and Qin, 2012). IFT46, another component of the IFT-B “core”, contains no predictable domains. Knockdown of IFT46 orthologs in mouse and zebrafish revealed a role in normal vertebrate development (Gouttenoire et al., 2007). *Chlamydomonas* with an insertional mutation in the IFT46 gene (*ift46*) contain short flagella that lack the dynein arms required for motility (Hou et al., 2007). A partial suppressor mutant expressing the C-terminal fragment of IFT46 rescues the flagellar length phenotype in the *Chlamydomonas ift46* mutant strain but these cells still specifically lack axonemal dynein arms (Hou et al., 2007). This indicates that the IFT46 N-terminus specifically recognizes and transports dynein arms into the cilium, while the C-terminus of IFT46 is needed for stability of the IFT-

B complex (Figure 4.7). Indeed, co-immuno precipitation and *in-vitro* pull-down studies from *Chlamydomonas* flagellar extracts revealed that IFT46 interacts with dynein arms through the adaptor protein ODA16 (Ahmed et al., 2008).

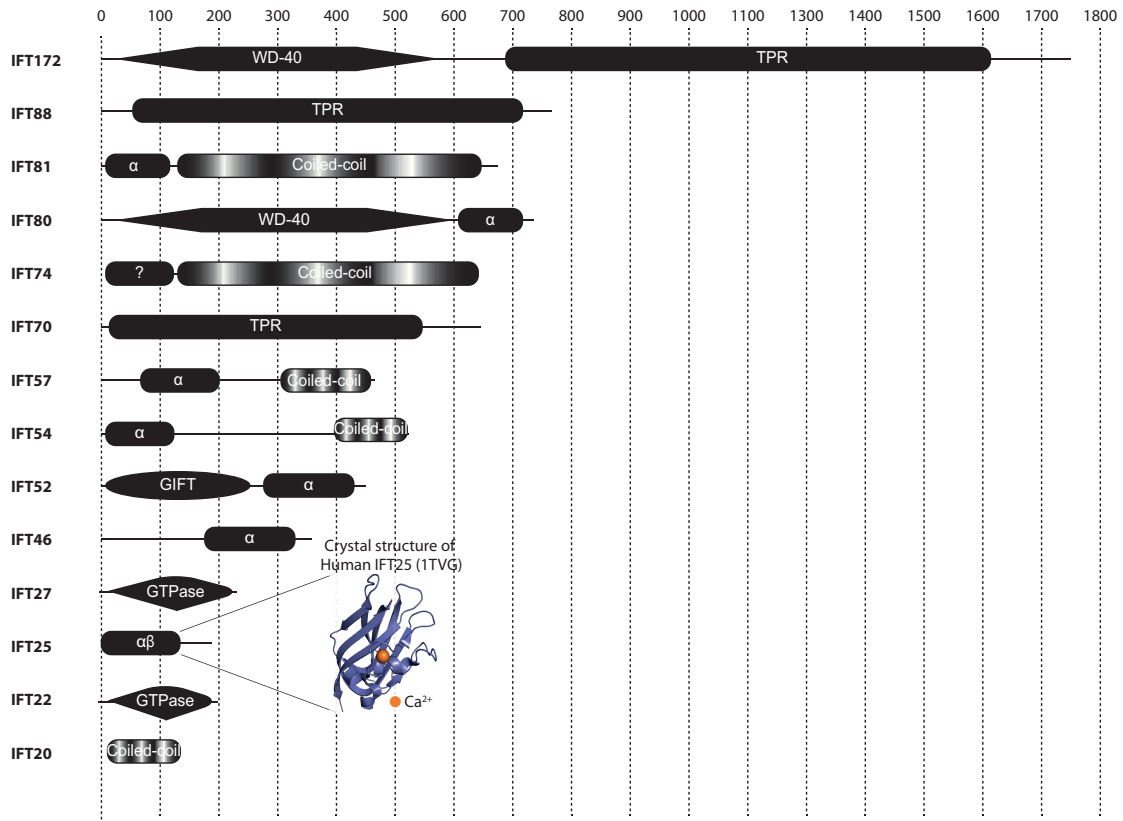


Figure 4.6: Domain architecture of all the IFT- B proteins showing that the majority of the proteins are predicted to contain protein-protein interaction motifs such as coiled-coil, WD-40 repeats and TPRs. The crystal structure of human IFT25 is shown next to its domain architecture cartoon.

IFT70 is a TPR (Tetratricopeptide repeat) domain containing protein that was recently identified as a core component of the IFT-B complex (Fan et al., 2010). The *C.elegans* ortholog, DYF-1, was shown to play a role in the docking of the IFT complex onto the anterograde motor OSM-3 (Ou et al., 2005). Mutations in the zebrafish ortholog of IFT70, *flee*, led to randomization of left-right asymmetry, cystic kidneys, hydrocephalus and defects in photoreceptor rod outer segment

formation, all phenotypes suggestive of severe ciliary assembly defects (Pathak et al., 2007). IFT88 is the largest of the IFT-B “core” proteins and is also a TPR domain containing protein (Figure 4.6). *Chlamydomonas* strains lacking the IFT88 gene are completely devoid of both flagella (Pazour et al., 2000). Whereas the complete knock-out of Tg737, the mouse ortholog of IFT88 causes early embryonic lethality, a hypomorphic mutation in the gene leads to the formation of short primary cilia which allow development but cause death of mice shortly after birth due to the onset of polycystic kidney disease (Pazour et al., 2000). Named as “The Oak Ridge Polycystic Kidney (ORPK) mouse”, this IFT88 mutant mouse exhibits a range of phenotypes that are comparable to many human ciliopathies (Lehman et al., 2008).

4.3.1.1.4 IFT172 and 80

IFT172 is the largest component of the IFT complex and is a peripheral subunit as it dissociates from the IFT-B core at higher ionic strength. It contains an N-terminal WD-40 repeat domain and a C-terminal TPR domain. This domain organization is similar to COP1 and clathrin vesicle coats, indicating an evolutionary relationship between IFT172 and canonical coat proteins (Figure 4.6) (Jékely and Arendt, 2006). At the permissive temperature of 22°C, *Chlamydomonas* strains with a temperature sensitive mutation in the IFT172 gene *FLA11* (*fla11^{ts}*), show normal anterograde and retrograde transport rates but have decreased number of IFT particles leaving the flagellar tip (Iomini et al., 2001). Moreover, co-immuno precipitation analysis revealed that IFT172 interacts with the MT plus end-binding protein EB1. Based on these observations, it was proposed that IFT172 functions at the flagellar tip and facilitates the transition from anterograde transport to retrograde transport (Pedersen et al., 2005). IFT80 is a recently identified peripheral component of the IFT-B complex (Beales et al., 2007; Blacque et al., 2004) and contains a WD40 repeat

domain at the N-terminus and a small α -helical domain at the C-terminus (Taschner et al., 2012). Mutations in IFT80 are associated with two human diseases, Jeune asphyxiating thoracic dystrophy (JATD) and short-rib polydactyly (SRP) (Beales et al., 2007; Cavalcanti et al., 2011). Both of these diseases are associated with abnormal bone formation and cause infant lethality. At the molecular level, mutations in IFT80 are shown to affect bone differentiation by down-regulating hedgehog signaling (Rix et al., 2011; Yang and Wang, 2012).

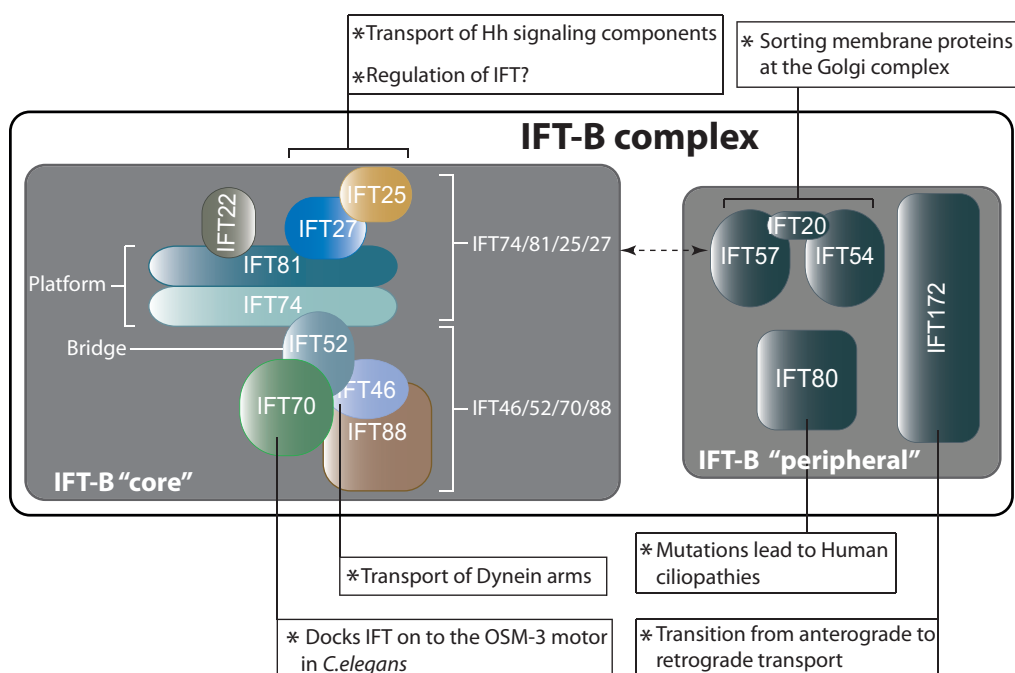


Figure 4.7: The IFT-B complex. The organizational layout of the complex is represented and the known functions of some proteins are indicated.

In summary, most of the IFT-B proteins are predicted to contain multiple domains. Identification of these domains followed by biochemical and structural characterization will give important insights into the function of individual proteins. Studies such as the one by Taschner et al., 2011 aiming at the precise identification of these domain boundaries in IFT-B proteins will be of great importance.

4.3.1.2 IFT-A proteins

The IFT-A complex contains six proteins (IFT144, IFT140, IFT139, IFT122, IFT121 and IFT43) of which five are large proteins with a molecular weight of more than 100kDa. Unlike IFT-B proteins, mutations in IFT-A proteins do not lead to lethality in vertebrates but are one of the main causes of various human ciliopathies (Arts et al., 2011; Davis et al., 2011). Barring IFT139 and IFT43, all the IFT-A proteins have a similar predicted domain architecture and contain a WD40 repeat domain at the N-terminus and a C-terminal TPR domain (Figure 4.8B). This domain architecture is similar to proteins forming clathrin vesicle coats and COPI coats (Jékely and Arendt, 2006). IFT139 is entirely a TPR domain containing protein and IFT43 has no predictable domains (Jékely and Arendt, 2006; Taschner et al., 2012). One of the earliest glimpses into the function of the IFT-A complex came from the identification of an interacting protein, Tubby-like protein 3 (TULP3) (Mukhopadhyay et al., 2010). TULP3 was shown to be associated with the IFT-A complex by co-immunoprecipitation studies performed using extracts from various mammalian cell lines (Mukhopadhyay et al., 2010). In serum starved human RPE-1 cells, siRNA mediated depletion of TULP3 or IFT-A component proteins were shown to affect the localization of a subset of GPCRs to cilia (Mukhopadhyay et al., 2013; 2010). Consistent with this, mutations in IFT-A proteins in mammalian cells were also shown to affect the transport of membrane proteins involved in the hedgehog signaling pathway (Liem et al., 2012).

Largely due to the size of the proteins involved, recombinant expression of IFT-A proteins has been very difficult and the architecture of the IFT-A complex was completely unknown until recently. However, elegant biochemical studies using *Chlamydomonas* strains containing loss of function mutations in IFT121 and IFT122

(*ift121* and *ift122*) revealed some important organizational features of the IFT-A complex (Behal et al., 2012). The authors of this study have isolated IFT-A complexes from *ift121* and *ift122* mutants and analyzed the stability of the IFT-A complex as well as the presence or absence of various subunits. This revealed that IFT122, IFT140 and IFT144 form the core of the IFT-A complex upon which the rest of the subunits are assembled (Figure 4.8A). Akin to the 9-subunit IFT-B “core” complex, this 3-subunit IFT-A complex was termed the IFT-A “core”. *In vitro* expression and pull-down experiments also revealed a direct interaction between IFT43 and IFT121 (Behal et al., 2012). Similar to IFT-B, the lack of structural information on IFT-A complexes and individual components is acting as a deterrent in the precise functional characterization of IFT-A proteins. Further dissection of interactions amongst the IFT-A proteins followed by mutational analysis will be of great importance in understanding the function of IFT-A. The intriguing homology between IFT-A proteins and coat proteins also should be explored further to see if there is any functional similarity between these complexes.

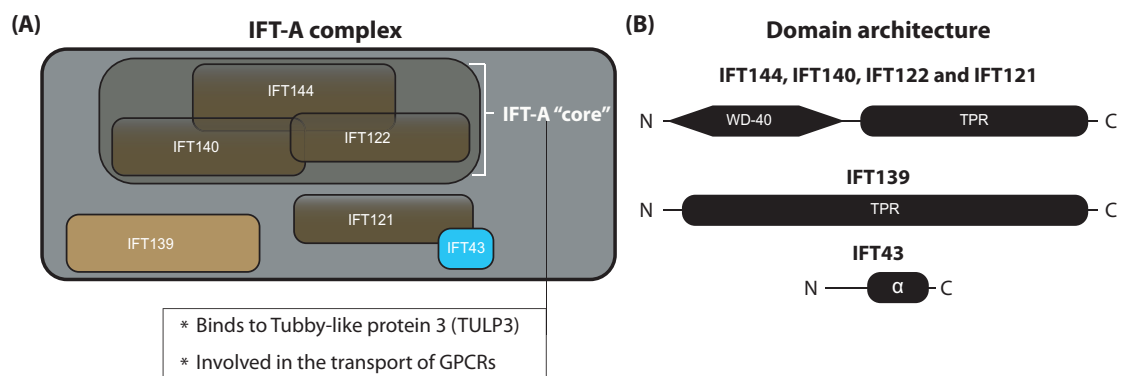


Figure 4.8: *A) IFT-A complex organization. B) Domain architecture of IFT-A proteins show that four out of six IFT-A proteins have similar domain architecture as coat proteins.*

4.4 Ciliary length control

How cell size and the size of cellular organelles are determined is an interesting and largely unresolved question. The cilium represents an ideal organelle to examine such questions as the size of a cilium can be reduced to a function of its length, a one-dimensional parameter. Cilia from various tissues and organisms are of different lengths indicating that regulation of ciliary length is a very important aspect of ciliary function. For motile cilia such as nodal mono cilia and respiratory epithelial cilia, the corresponding functions involve generating hydrodynamic fluid flows by creating specialized ciliary beating motions. Such fluid flows are a direct function of ciliary length and is greatly altered in several flagellar length mutants, leading to various ciliopathies (Ishikawa and Marshall, 2011). Ciliary length was also shown to affect the function of the primary cilium, but the exact mechanism has remained a mystery, largely due to the lack of information on the factors involved in ciliary length regulation.

However, a consensus model addressing the general features of ciliary length control exists and is referred to as the “balance-point” model. This model is largely based on some elegant studies on tubulin turnover and flagellar assembly rate measurements in the biflagellate model organism *Chlamydomonas* (Engel et al., 2009; Marshall and Rosenbaum, 2001b; Marshall et al., 2005). When a *Chlamydomonas* strain expressing HA-tagged tubulin is mated with the wild-type biflagellate strain, the resulting quadriflagellate dikaryon *Chlamydomonas* contains two intact flagella containing HA tagged tubulin and two flagella with unlabeled tubulin. Careful observation of this quadriflagellate revealed that over time, flagella with the untagged tubulin started incorporating the HA tagged tubulin at its distal end, indicating that the tubulin in *Chlamydomonas* flagella is constantly being turned over (Marshall and Rosenbaum,

2001b) (Figure 4.9A). Tubulin turnover failed to occur in *Chlamydomonas* strains with the defective IFT anterograde motor indicating that IFT is responsible for the tubulin turnover (Marshall and Rosenbaum, 2001b). Consistent with this, fluorescently tagged tubulin was shown to undergo IFT like movement inside *C.elegans* sensory cilia (Hao et al., 2011). Since tubulin forms the MT-based backbone of the cilium, regulation of tubulin transport can be a simple and an elegant way of controlling ciliary length. This can be accomplished by fine-tuning either the levels of tubulin or of the IFT complex during ciliogenesis.

Surprisingly, quantification of IFT protein levels in *Chlamydomonas* flagella by immuno fluorescence and western blotting revealed that the IFT protein amounts inside the cilium remain constant during all the stages of ciliary assembly (Marshall and Rosenbaum, 2001b; Marshall et al., 2005). This means that the concentration of IFT proteins decreases as the length of the cilium increases, and IFT proteins have to travel increasingly longer distances to reach the tip as the cilium grows. This makes the ciliary assembly rate implicitly length dependent (negative correlation between cilium length and ciliary assembly) (Figure 4.9B). Indeed, the measured flagellar elongation rate in *Chlamydomonas* decreases as the length of the flagellum increases, with assembly rate being maximum during the initial stages of elongation (Marshall et al., 2005). In contrast to the decelerating assembly rate, the disassembly rate in the resorbing *fla10^{ts}* (defective in IFT) *Chlamydomonas* flagella was shown to be constant, indicating that it is independent of its length (Marshall et al., 2005). Based on these observations the balance-point model proposes that the cilium reaches a steady-state length when the assembly rate (decreases with increasing ciliary length) equals the disassembly rate (constant) (Figure 4.9B). This means that at steady state, the cilium assembles and disassembles at the same rate, thereby maintaining a

constant length. Several predictions of this model, such as constant disassembly rate, decrease in length as number of flagella increase, were tested and found to be in complete agreement with the predictions (Engel et al., 2009; Marshall et al., 2005). However, there are several important questions that still remain to be answered. For example, which factors are responsible for maintaining constant IFT levels during cilia growth? Which components of the IFT machinery are directly involved in the transport of tubulin? What is the identity of the factors responsible for the constant ciliary disassembly rate? Further work is needed to answer these questions and understand the nuances of the balance-point model.

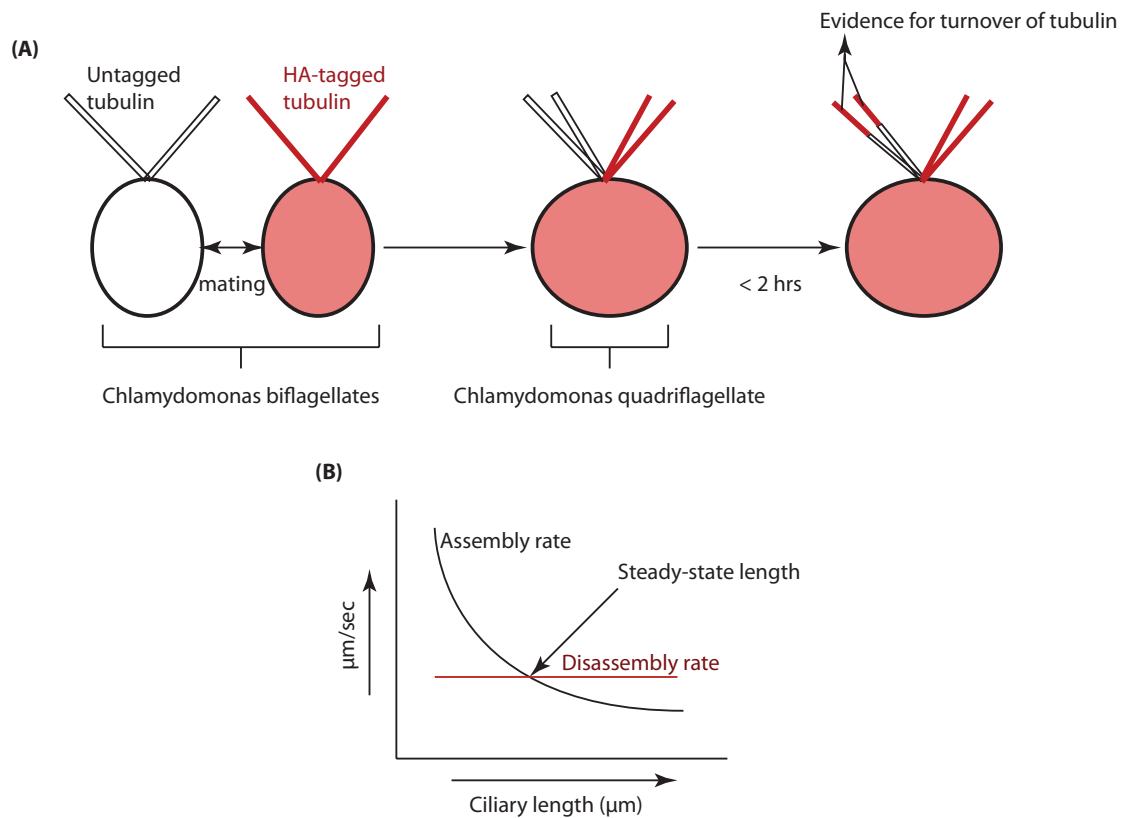


Figure 4.9: Flagellar length control. **A)** Schematic representation of the experiment that showed the constant turnover of tubulin at the ciliary tip (adapted from (Marshall and Rosenbaum, 2001b)) **B)** The 'balance-point model' for the ciliary length control. The cilium reaches a steady-state length when the decelerating assembly rate intersects the constant disassembly rate.

5. Aim of research

Although a great deal of information is available about the function of IFT proteins, mainly from the mutational studies in *Chlamydomonas*, *mouse* and *C.elegans*, the lack of high resolution structural information of these proteins (barring the crystal structure of IFT25) means that all the functional studies done so far involved either knocking down or deleting an entire IFT protein. For most of the IFT-B complex proteins, this always resulted in a common phenotype of a ciliary assembly defect thus blurring out the molecular/specific function(s) of individual subunits. In addition, although the association between ciliary cargo and IFT proteins became evident a long time ago (Qin, 2004), there is no evidence so far of a direct interaction between an IFT protein and a cargo. Having structural information of IFT proteins will enable us to predict their molecular function with more confidence and functional studies can be carried in which the effect of point mutations or domain deletions can be tested instead of disrupting an entire protein. This will enable us to assign specific functions to individual domains/proteins and may also help identify cargo-binding modules in the IFT proteins, eventually leading to the molecular understanding of ciliopathies. To this end, the studies described in this thesis were aimed at identifying and structurally characterizing the domains in some of the IFT-B complex proteins.

6. Results

Chapter I

Crystal structure of the intraflagellar transport complex IFT25/27.

Crystal structure of the intraflagellar transport complex 25/27

Sagar Bhogaraju, Michael Taschner,
Michaela Morawetz, Claire Basquin
and Esben Lorentzen*

Department of Structural Cell Biology, Max-Planck-Institute
of Biochemistry, Martinsried, Germany

The cilium is an important organelle that is found on many eukaryotic cells, where it serves essential functions in motility, sensory reception and signalling. Intraflagellar transport (IFT) is a vital process for the formation and maintenance of cilia. We have determined the crystal structure of *Chlamydomonas reinhardtii* IFT25/27, an IFT sub-complex, at 2.6 Å resolution. IFT25 and IFT27 interact via a conserved interface that we verify biochemically using structure-guided mutagenesis. IFT27 displays the fold of Rab-like small guanosine triphosphate hydrolases (GTPases), binds GTP and GDP with micromolar affinity and has very low intrinsic GTPase activity, suggesting that it likely requires a GTPase-activating protein (GAP) for robust GTP turnover. A patch of conserved surface residues contributed by both IFT25 and IFT27 is found adjacent to the GTP-binding site and could mediate the binding to other IFT proteins as well as to a potential GAP. These results provide the first step towards a high-resolution structural understanding of the IFT complex.

The EMBO Journal (2011) 30, 1907–1918. doi:10.1038/
emboj.2011.110; Published online 19 April 2011

Subject Categories: cell & tissue architecture; structural
biology

Keywords: cilium; crystal structure; intraflagellar transport;
IFT25; IFT27

Introduction

Cilia or flagella (interchangeable terms) are membrane-surrounded microtubule-based structures that protrude from a wide range of eukaryotic cells and serve a number of important functions including cellular motility, sensory reception and signalling (Michaud and Yoder, 2006). The motile cilium enables unicellular organisms such as *Chlamydomonas reinhardtii* (Cr) to move in response to light or other environmental cues (Witman, 2009). In mammals, the motile cilium is found on sperm cells and on cells that line the fallopian tubes and the trachea of the lungs (Satir and Christensen, 2008). As the cilium protrudes from the cell

surface, it is in a perfect position to convey signals between the cell and the environment. Immotile sensory cilia are found on photoreceptor cells in the eye and on olfactory neurons and are thus sensory organelles of smell and sight (Perkins *et al*, 1986; Snell *et al*, 2004). Furthermore, cilia are important to a number of signal transduction pathways such as platelet-derived growth factor receptor α , sonic hedgehog, epidermal growth factor and 5HT₆ serotonin signalling (Brailov *et al*, 2000; Huangfu *et al*, 2003; Haycraft *et al*, 2005; Ma *et al*, 2005; Schneider *et al*, 2005). Both sensory reception and signalling in the cilium are believed to be a result of increased clustering of receptor molecules in the ciliary membrane. Due to the versatility of cilium function, a large number of genetic diseases (collectively known as ciliopathies) and developmental abnormalities are the result of non-functional cilia. In human, these diseases range from blindness, male sterility, ectopic pregnancy and polycystic kidney disease to cognitive impairment and various limb deformities (Snell *et al*, 2004; Tobin and Beales, 2007).

The axoneme, which forms the structural framework of the cilium, is built up of nine doublets of microtubules that grow from a centriole-derived basal body anchored in the cell body at the base of the cilium. The axoneme is surrounded by the ciliary membrane that is contiguous with the plasma membrane, but has a unique composition of lipids and proteins (Emmer *et al*, 2010). Transition-zone fibres are proteinaceous structures that span the distance between the plasma membrane and the microtubules of the basal body (Gibbons and Grimstone, 1960; Craige *et al*, 2010). This prevents random diffusion of macromolecules between the cilium and the cell body and effectively creates a ciliary pore that brings about the necessity of active transport in order to correctly target proteins to the cilium. This transport process was first discovered by Joel Rosenbaum and co-workers and is termed intraflagellar transport (IFT) (Kozminski *et al*, 1993). IFT not only mediates the kinesin-2-dependent targeting of structural proteins and signalling receptors to the cilium (anterograde transport) but is also responsible for the removal of ciliary turnover products in a dynein-1b/2-dependent manner (retrograde transport) (Qin *et al*, 2004). These transport processes rely on a large protein complex, the IFT complex, that is believed to mediate the contacts between ciliary cargo proteins and the motor proteins that facilitate transport (Piperno and Mead, 1997; Cole *et al*, 1998; Piperno *et al*, 1998). The complete IFT complex contains at least 20 different proteins and has been shown to dissociate into two different sub-complexes, namely IFT-A and IFT-B, that are involved in retrograde and anterograde transport, respectively (Piperno and Mead, 1997; Cole *et al*, 1998). To date, six protein subunits of the IFT-A (IFT43, 121, 122, 139, 140 and 144) and 14 of the IFT-B (IFT20, 22, 25, 27, 46, 52, 54, 57, 70, 72/74, 80, 81, 88 and 172) complexes have been identified (Cole *et al*, 1998; Piperno *et al*, 1998; Lucker *et al*, 2005; Follit *et al*, 2009; Lechtreck *et al*, 2009; Wang *et al*, 2009; Fan *et al*, 2010). In addition to the IFT complex, another large macro-

*Corresponding author. Department of Structural Cell Biology, Max-Planck-Institute of Biochemistry, Am Klopferspitz 18, Martinsried 82152, Germany. Tel.: +49 89 578 3479; Fax: +49 89 578 3605; E-mail: lorentze@biochem.mpg.de

Received: 22 November 2010; accepted: 14 March 2011; published
online: 19 April 2011

molecular complex, the BBSome, may participate in IFT (Nachury *et al*, 2007; Lechtreck *et al*, 2009). The BBSome appears to physically bridge the IFT-A and -B complexes in *Caenorhabditis elegans* (Ou *et al*, 2005) and has been suggested to function as a coat for the sorting of membrane proteins to cilia (Jin *et al*, 2010). IFT appears to be a universal process as genes encoding IFT subunits are conserved in almost all ciliated eukaryotic organisms ranging from single-celled algae to humans (Jekely and Arendt, 2006). The importance of the IFT complex is illustrated by the fact that mutations in IFT genes lead to perturbation of cilium formation in organisms as diverse as green alga, nematodes, fruitfly, zebrafish, mouse and human (Cole *et al*, 1998; Murcia *et al*, 2000; Pazour *et al*, 2000; Han *et al*, 2003; Sun *et al*, 2004; Tsujikawa and Malicki, 2004; Pedersen *et al*, 2005; Beales *et al*, 2007). Furthermore, knockouts of the IFT core proteins IFT88 and IFT172 in mice are embryonically lethal, which demonstrates that the IFT process is essential for development (Murcia *et al*, 2000; Huangfu *et al*, 2003).

Based on primary sequence information, most subunits of the IFT complex appear to contain protein–protein interaction domains such as tetratricopeptide repeats, β -propeller or coiled-coil domains that likely mediate contacts within the IFT complex as well as contacts to cargo and motor proteins (Jekely and Arendt, 2006). However, two of the IFT-B core subunits (IFT22 and IFT27) show significant sequence identity to members of the small guanosine triphosphate hydrolyase (GTPase) superfamily and may well serve regulatory roles in IFT. IFT27 was predicted to be an Rab-like GTPase and shown to bind GTP in a previous study (Qin *et al*, 2007). A complete knockdown of CrIFT27 with siRNA is lethal, whereas a partial depletion of IFT27 leads to shorter flagella (Qin *et al*, 2007). Recently, IFT25 was identified as a component of the IFT-B complex in *Chlamydomonas* (Lechtreck *et al*, 2009; Wang *et al*, 2009) as well as in mouse (Follit *et al*, 2009) and has been demonstrated to interact with IFT27 in *Chlamydomonas* (Wang *et al*, 2009), mouse (Follit *et al*, 2009) and human (Rual *et al*, 2005). IFT25 and IFT27 are conserved in many ciliated organisms with the notable exception of *C. elegans* and *Drosophila melanogaster* (Lechtreck *et al*, 2009). Another interesting exception is *Tetrahymena thermophila* that appears to have lost IFT25, but retained IFT27 (Shida *et al*, 2010). Although IFT-B complexes are known to pre-assemble in the cell body before entering the cilium, sedimentation experiments have shown that IFT-B from the cell body contains sub-stoichiometric amounts of IFT25/27 (Wang *et al*, 2009). A significant portion of IFT25 and IFT27 is pre-assembled in an IFT25/27 sub-complex that appears to associate with the rest of the IFT-B complex only upon entrance into the flagellum. These observations have led to the suggestion that IFT25/27 could be involved in the regulation of IFT initiation at the base of the cilium (Wang *et al*, 2009).

Electron tomographic reconstructions of the *Chlamydomonas* flagellum represent the most detailed structural study of IFT complexes to date (Pigino *et al*, 2009). Although these reconstructions provide a first view of how IFT complexes assemble into larger particles (so-called IFT-trains), the resolution is not sufficiently high to model individual IFT proteins. There is thus a paucity of knowledge about the molecular basis for IFT in ciliary assembly and function. To this end, we have determined the crystal

structure of the IFT25/27 sub-complex. The structure reveals a conserved interaction interface between the two components as well as a calcium-binding site in IFT25 and a GTP-binding site in IFT27. We show that IFT27 has very low intrinsic GTPase activity and displays micromolar affinity for GDP and GTP. Additionally, by mapping the degree of surface conservation onto the complex structure, we identify a surface patch that likely mediates the interaction to a putative GTPase-activating protein (GAP) and/or to other proteins of the IFT complex.

Results

IFT25/27 structure characterization

Initial recombinant expression and purifications of full-length CrIFT25 and CrIFT27 from *Escherichia coli* showed that CrIFT25 can be purified as a soluble protein, but CrIFT27 has a tendency to aggregate and is lost during the purification. However, CrIFT27 is significantly stabilized upon co-expression with CrIFT25. We thus co-expressed and purified the full-length CrIFT25/27 complex (Supplementary Figure S1A), but did not obtain any crystals. CrIFT25 contains an approximately 55 residue long C-terminal glycine-rich tail that is predicted to be disordered (DRIPPRED server, <http://www.sbc.su.se/~maccallr/disorder/>). This C-terminal extension of IFT25 appears to be unique to the *Chlamydomonas* protein and is not conserved in other IFT25 orthologues (Supplementary Figure S2). Consequently, a truncated version of CrIFT25 (IFT25 Δ C, residues 1–135) was co-expressed with CrIFT27 and the CrIFT25 Δ C/27 complex was purified and crystallized (Supplementary Figure S1B). The structure of the complex was determined from two different crystal forms at resolutions of 2.6 and 2.8 Å, respectively. Both crystal forms show a heterodimer of the CrIFT25 Δ C/27 complex (Figure 1), which is in accordance with the molecular weight of the complex in solution, estimated as 37 kDa using static light scattering. The structures from the two different crystal forms are very similar as they superpose with a root mean square deviation (r.m.s.d.) of 0.6 Å over all C α atoms. As typically seen in small GTPases crystallized in the absence of nucleotide, the switch I region (residues 39–55) and part of the G4 region (residues 138–140) of IFT27 did not have any interpretable electron density and were not included in the model. Further data collection and refinement statistics are given in Table I.

IFT25 is a calcium-binding protein with a jelly-roll fold

IFT25 displays a jelly-roll fold consisting of nine β -strands that are organized into two anti-parallel sheets stacked on top of each other (Figure 1). The CrIFT25 structure is similar to a previously determined structure of human IFT25 (Ramelot *et al*, 2009) as they superpose with an r.m.s.d. of 0.7 Å over 95% of the C α atoms (Supplementary Figure S3A). When compared with all structures in the protein data bank (pdb) using the DALI server (Holm and Sander, 1993), the IFT25 structures are most similar to the galactose-binding domain of bacterial sialidases, superposing with an r.m.s.d. of 1.6 Å over >90% of the C α atoms (Gaskell *et al*, 1995; Boraston *et al*, 2007). Although IFT25 shares a conserved calcium-binding site with sialidases, the putative galactose-binding site is poorly conserved in IFT25. Indeed, the IFT25/27 complex structure is incompatible with galactose binding as

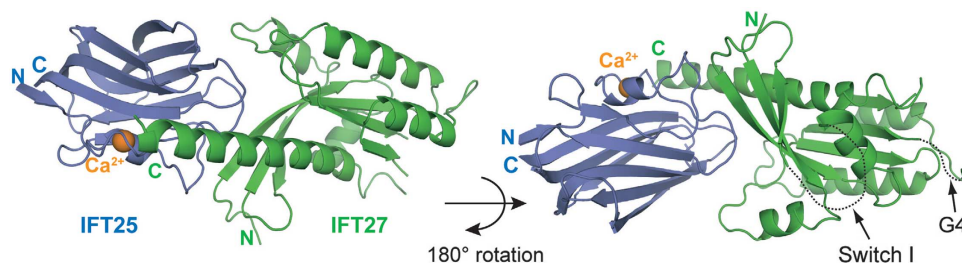


Figure 1 Structure of the IFT25 Δ C/27 complex. Cartoon representation of the overall structure of IFT25 Δ C/27 with IFT27 and IFT25 shown in green and slate, respectively. The calcium ion bound to IFT25 is shown as an orange ball. The two views of the complex are related by a 180-degree rotation around the horizontal axis. The switch I and G4 regions of IFT27 are disordered in the structure and represented with dotted lines in the figure. The N- and C-termini of both proteins are indicated.

Table I Data collection and refinement statistics

<i>C. reinhardtii</i> IFT25 Δ C-IFT27	Native 1	Native 2
<i>Data collection</i>		
Wavelength (Å)	0.973	0.973
Space group	P2 ₁	P2 ₁
<i>Cell dimensions</i>		
a, b, c (Å)	44.1, 96.2, 66.9	50.0, 68.3, 93.8
α , β , γ (deg)	90.0	92.4
Resolution (Å)	50–2.59 (2.59–2.74)	50–2.8 (3.00–2.80)
R_{sym}	0.090 (0.56)	0.099 (0.65)
$I/\sigma I$	12.6 (2.2)	14.3 (2.5)
Completeness (%)	0.973 (0.848)	0.993 (0.920)
<i>Refinement</i>		
Resolution (Å)	50–2.59	50–2.80
No. reflections	16992	15717
$R_{\text{work}}/R_{\text{free}}$	0.212/0.269	0.236/0.317
<i>No. atoms</i>		
Protein	4310	4689
Ligand/ion	2 Ca ⁺⁺	1 Cl ⁻ and 2 Ca ⁺⁺
Water	32	27
<i>B-factors</i>		
Protein	35	47
Water	36	40
<i>r.m.s. deviations</i>		
Bond lengths (Å)	0.011	0.007
Bond angles (deg)	1.5	1.2

Highest resolution shell is shown in parenthesis.

the C-terminal helix of IFT27 occupies the putative galactose-binding site (Supplementary Figure S3B). It thus appears that, although IFT25 and sialidases are clearly evolutionarily related, they have diverged in function. The calcium ion bound to CrIFT25 is coordinated by the side chains of amino acids D30, T35 as well as by several main-chain carbonyls (Figure 2A). These calcium-binding residues are completely conserved in IFT25 orthologues and it is thus very likely that IFT25 proteins from other species also bind calcium (Supplementary Figure S2).

Prior to its characterization as an IFT complex protein, IFT25 was classified as a member of the family of small heat shock proteins (sHSPs) of the α -crystallin fold and named Hsp16.2 (Bellyei *et al*, 2007) or HSPB11 (Kampinga *et al*, 2009). IFT25 could thus have a chaperone function in preventing ciliary proteins or turnover products from aggregating.

Indeed, we observe that CrIFT25 increases the solubility of IFT27 when co-expressed in *E. coli*. However, when the IFT25 structure is compared with all structures in the pdb, no significant similarity with structures of the sHSPs family is found. Furthermore, the α -crystallin fold, which is a defining feature of sHSPs (Kappe *et al*, 2010), and the jelly-roll fold of IFT25 have only a superficial resemblance and do not share a common topology. This is also reflected by the low sequence identity of 6–15% between IFT25 and sHSPs. sHSPs are known to assemble into large oligomers required for their chaperone activity (Bagneris *et al*, 2009). In agreement with Ramelot *et al* (2009), we find that full-length CrIFT25 (Supplementary Figure S1A), truncated CrIFT25 Δ C (Supplementary Figure S1B) as well as full-length human IFT25 (data not shown) all behave as monomers in solution during size exclusion chromatography (SEC) experiments. Thus, as previously pointed out by de Jong and co-workers, IFT25 should not be classified as a member of the family of sHSPs containing the α -crystallin fold (Kappe *et al*, 2010).

IFT27 is structurally similar to Rab8 and Rab11 but has no prenylation site

IFT27 adopts the classical fold of an Ras-like small GTPase that catalyses the hydrolysis of GTP to GDP and inorganic phosphate. GTPases are switch molecules that exist in an active GTP-bound form or an inactive GDP-bound form. The active form can bind downstream effectors, whereas the inactive form cannot. The regulation of the two forms is achieved by specific GAPs and guanine-nucleotide exchange factors (GEFs) (Vetter and Wittinghofer, 2001). In this way, GTPases can regulate a number of important cellular processes including cell-cycle control, transport processes and sensory reception. The overall structure of IFT27, when compared with all the structures in the pdb, most closely resembles structures of the Rab family of small GTPases. Rab proteins constitute the largest sub-family within the super-family of small GTPases with >60 members in human and have important roles in membrane trafficking (Stenmark, 2009). It is noteworthy that the five sequence signatures of Rab proteins are relatively well conserved in IFT27 proteins (denoted RabF1–F5 in Figure 3). Of all the Rab structures determined to date, the CrIFT27 structure is most similar to that of Rab8 (r.m.s.d. of 2.6 Å for 84% of the C α atoms) and Rab11 (r.m.s.d. of 2.4 Å for 71% of the C α atoms). Interestingly, both Rab8 and Rab11 are known to be involved in ciliogenesis (Nachury *et al*, 2007; Knodler *et al*, 2010). This suggests that ciliary Rabs could have arisen by gene

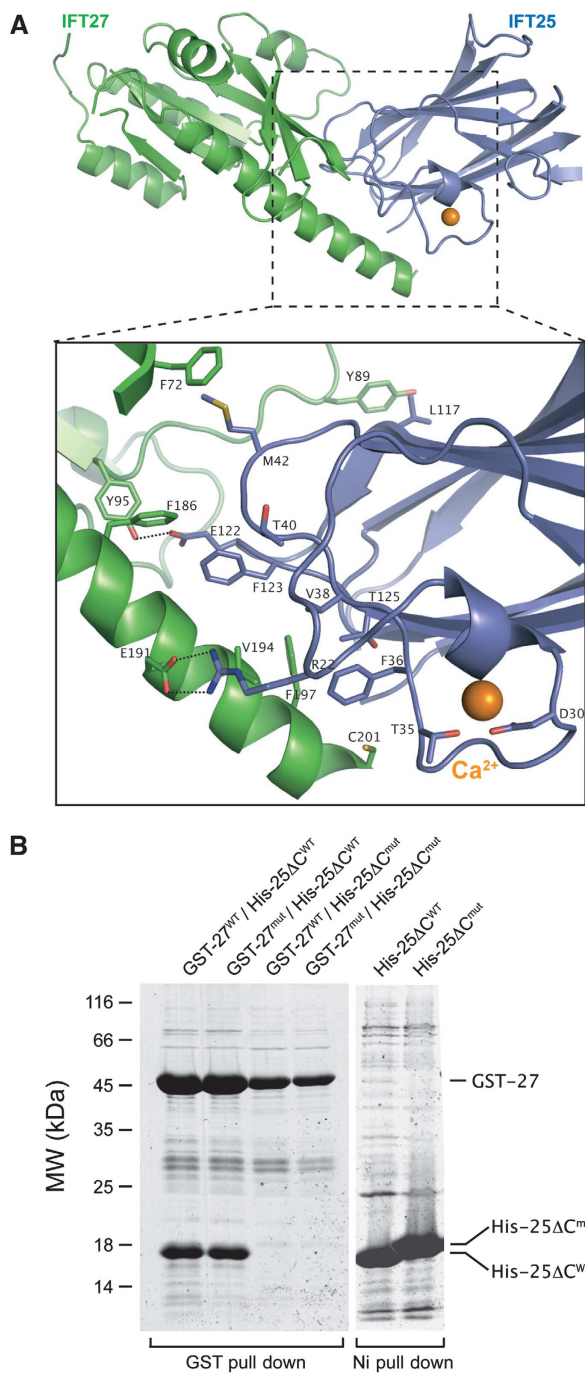


Figure 2 Structural characterization of the IFT25 Δ C/27 interface. (A) Close-up view of the protein-protein interface of the IFT25/27 complex. IFT27 secondary structure elements that do not engage in interactions with IFT25 but hinder the view of the interface have been removed for better visualization. Residues involved in calcium coordination (D30 and T35) or forming the interaction interface between the two proteins are shown in a stick representation and labelled. The salt bridge between R22_{IFT25} and E191_{IFT27} and the hydrogen bond between E122_{IFT25} and Y95_{IFT27} are indicated with dashed lines. (B) Pull-down experiments with interface mutants. GST-tagged wild-type IFT27 (GST-27^{WT}) or mutant IFT27 (GST-27^{mut}, V194R) was co-expressed with C-terminally truncated but otherwise wild-type IFT25 (25 Δ C^{WT}) or mutant IFT25 (25 Δ C^{mut}, V38R, T40R and T125E triple mutant) and pulled down using GSH beads. Whereas both GST-27^{WT} and GST-27^{mut} effectively pull down 25 Δ C^{WT}, they do not pull down 25 Δ C^{mut}, demonstrating that the interface between the two proteins has been disrupted. To ensure that 25 Δ C^{mut} is expressed and soluble, the protein was pulled down separately using the His-affinity tag on IFT25 (right panel).

duplication from an ancestral ciliary Rab-like GTPase. However, despite the large degree of overall structural similarity between IFT27, Rab8 and Rab11, the C-termini of the proteins are highly divergent. A typical hallmark of Rab proteins is the presence of a C-terminal prenylation motif consisting of one or, typically, more cysteines that upon modification allows for membrane association. Such a prenylation site can be found in both Rab8 and Rab11, but as previously noted (Qin *et al*, 2007) is not present in IFT27 (Figure 3). Interestingly, the other identified Rab-like GTPase of the IFT complex, IFT22 (also known as RABL5 or IFTA-2), is also missing a prenylation motif (Figure 3) (Adhiambo *et al*, 2009).

Structural organization of the IFT25/27 complex

The IFT25 Δ C/27 structure displays an elongated shape with dimensions of 80 Å × 40 Å × 25 Å. The complex has a mixed hydrophobic/hydrophilic interface with a buried surface area of 1070 Å². Nine residues from IFT25, contributed from two loop regions (residues 36–42 and 117–125; Figure 2A), mediate binding to IFT27 (Figure 2A). These two loops are very well conserved among IFT25 orthologues and are thus likely to mediate IFT27 interactions in other species. The calcium-binding loop of IFT25 (residues 30–35) precedes the first of the two IFT27-interacting loops and is in close proximity to the interaction interface (Figure 2A). Calcium signalling is known to occur in the cilium and recent findings show that the levels of calcium influence anterograde IFT (Besschetnova *et al*, 2010). One possibility is that calcium directly regulates IFT via the calcium-binding site of IFT25. To assess the effect of calcium in complex stability, IFT25/27 was treated with a large excess of the calcium chelator EGTA and subjected to SEC. The results show that calcium binding does not have any apparent effect on the stability of the IFT25/27 complex (Supplementary Figure S4B). Consistently, neither the D30A nor the T35A single point mutations affect IFT25/27 complex formation in pull-down experiments (data not shown). However, it cannot be ruled out that calcium levels have an effect on the IFT25/27 complex *in vivo*.

IFT27 contributes residues from several different regions to the IFT25-binding surface. The residues involved in complex formation are in general better conserved among IFT25 orthologues than IFT27 orthologues. More specifically, CrIFT27 residues from β -strand β 3 (F72), the C-terminal α -helix α 5 (F186, E191, V194, F197 and C201) as well as the loop connecting α 2 and β 4 (Y89 and Y95) contribute to the protein complex interface (Figures 2 and 3). A substantial part of the interaction is thus mediated by the C-terminal α -helical extension of IFT27 that is not typically found in the GTPase core domain. Interestingly, this C-terminal α -helical extension is conserved in IFT27 orthologues, where IFT25 is conserved but not in *T. thermophila*, where IFT25 is lost, indicating that α 5 of IFT27 could be specific for the interaction with IFT25 (Figure 3). Notably, of the eight CrIFT27 residues that interact with IFT25, five are aromatic and engage in hydrophobic as well as stacking interactions with residues from IFT25. The two tyrosines Y89 and Y95 are located towards the end of the switch II region (Figure 3), indicating that IFT25/27 complex formation could depend on the nucleotide state of IFT27. To test this possibility, we carried out pull-down experiments with different nucleotide states of IFT27 (Supplementary Figure S5A). The conclusion

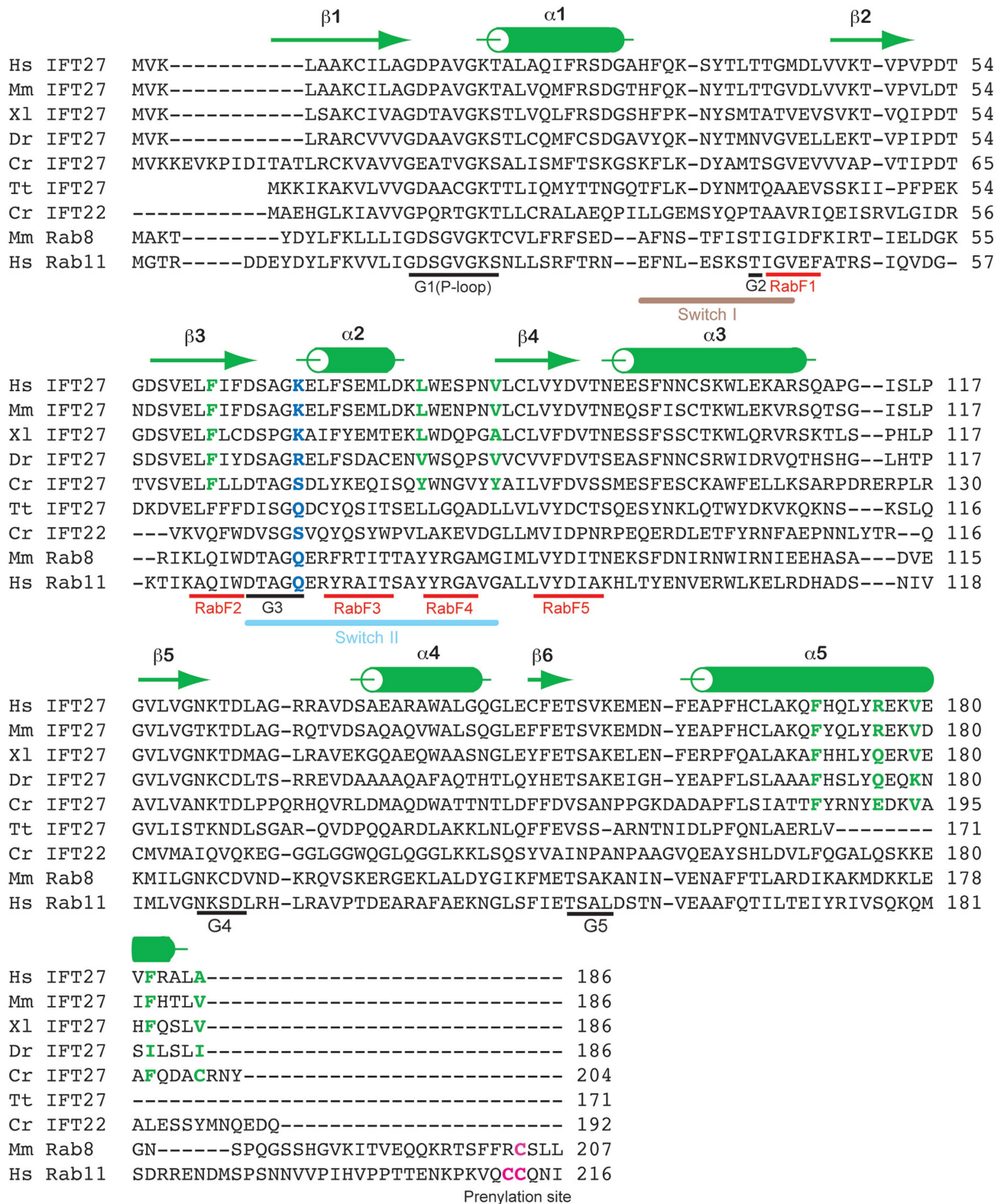


Figure 3 Conserved sequence motifs and IFT25-interacting residues of IFT27. Multiple sequence alignment of IFT27 proteins from different species with CrIFT22 and the GTPases Rab11 and Rab8. The secondary structure derived from the IFT27 structure presented here is indicated above the sequences. Important sequence motifs of small GTPases such as switch regions, G-protein-specific sequences (G1-5) as well as Rab-specific residues (RabF1-5) are marked below the sequence. IFT27 residues that interact directly with residues from IFT25 are coloured green. The catalytic glutamine conserved in most GTPases, but not in IFT27 or IFT22, is coloured in blue and the prenylation sites at the C-termini of Rab8 and Rab11 are shown in pink. Hs: *Homo sapiens*, Mm: *Mus musculus*, Xl: *Xenopus laevis*, Dr: *Danio rerio*, Cr: *Chlamydomonas reinhardtii*, Tt: *Tetrahymena thermophila*.

from this experiment is that IFT27 can interact with IFT25 irrespectively of nucleotide state. This is consistent with the fact that Y89 and Y95 are not well conserved among IFT27 orthologues, indicating that they are not crucial for IFT25 interaction. The three phenylalanine residues of CrIFT27 (F72, F186 and F197) that are engaged in IFT25 binding are well conserved among IFT27 proteins from different species but not conserved in Rab8 or Rab11 sequences (Figure 3). This suggests that these residues are specific for the IFT25/27 interaction. In summary, the conservation of interface residues across species makes it highly probable that the structure of the CrIFT25 Δ C/27 complex reported here can serve as a model for IFT25/27 complexes from other species.

From the structure of the IFT25/27 complex presented here, it should be possible to introduce structure-based mutations of interface residues to break up the complex and verify the interaction biochemically. To this end, we introduced several point mutations of interface residues in both IFT25 and IFT27 and tested for complex formation in pull-down experiments with co-expressed proteins (Figure 2B). The pull-down experiments were performed using either GST-tagged IFT27 (Figure 2B) or CBP-tagged IFT25 (Supplementary Figure S5B) and carried out using co-expressed rather than purified proteins because of the low solubility of IFT27 when expressed in the absence of IFT25. Several single point mutations were introduced in both IFT27 (V194R, GST-27^{mut} in Figure 2B) and IFT25 Δ C (V38R or T40R, data not shown) but did not prevent complex formation in the pull-down experiment. Consequently, an IFT25 Δ C mutant protein was tested where three small non-charged residues were mutated to large charged residues (IFT25 Δ C^{mut} in Figure 2B, V38R, T40R and T125E triple point mutant). IFT25 Δ C^{mut} is well expressed and soluble (see Ni pull down in Figure 2B) but does not form a complex with IFT27 demonstrating that the interface has been effectively disrupted. This is also the case in the reciprocal pull down using CBP-tagged IFT25 to precipitate IFT27 (Supplementary Figure S5B). These data provide a biochemical verification of the structural organization of the IFT25/27 complex.

IFT27 binds GTP/GDP with micromolar affinity and has very low intrinsic GTPase activity

The crystal structure of the IFT25 Δ C/27 complex presented here allows us to analyse and compare the active site configuration of IFT27 to that of well-studied GTPases such as Ras (Figure 4A). As the IFT25 Δ C/27 crystals represent the nucleotide-free state of IFT27, the switch I region is disordered and not modelled. However, the positions of the phosphate-binding P-loop as well as the α -helix (α 1) preceding switch I are well conserved in the structure (Figure 4A). Additionally, the mapping of sequence conservation onto the surface of the IFT25 Δ C/IFT27 structure reveals a conserved surface area at the GTP-binding pocket (Figure 5). Important nucleotide-binding motifs such as N/TKXD (G4), DXXG (G3) and GXXXXGKS/T of the P-loop are completely conserved in IFT27 (Figure 3). Specificity for guanine versus adenine is provided by the NXXD motif of G4 (Espinosa *et al*, 2009), which is conserved in IFT27 orthologues (see Figure 3), indicating that IFT27 binds GTP but not ATP (confirmed experimentally; Figure 4C; Supplementary Figure S6). The sequence and structure of IFT27 are thus compatible with

a competent GTP-binding site. Interestingly, the other Rab-like protein of the IFT complex B (IFT22/RabL5) does not have G4 conserved (as previously noted by Adhiambo *et al* (2009)) and may not be specific for GTP.

GTP hydrolysis by GTPases relies on the coordination of a water molecule for the in-line attack on the γ -phosphate (Pai *et al*, 1990). Different families of GTPases utilize different catalytic residues to achieve GTP hydrolysis. In case of the Ras, Rho and Ran GTPases, a conserved glutamine in the switch II region (Q61 in human Ras; Figure 4A) was found to coordinate the nucleophilic water molecule (Pai *et al*, 1990; Rittinger *et al*, 1997; Seewald *et al*, 2002). Mutation of Q61 is oncogenic in Ras and lowers the intrinsic GTPase activity by 8–10-fold (Der *et al*, 1986). Other GTPases such as Sar1 (Bi *et al*, 2002) and elongation factors Tu (Voorhees *et al*, 2010) utilize a catalytic histidine for the purpose of orienting a nucleophilic water molecule. The catalytic glutamine of Ras is conserved in most Rab proteins but appears to be involved in GAP binding rather than catalysis as demonstrated for Rab33, where the catalytic glutamine is instead provided *in trans* by the Rab-GAP (Pan *et al*, 2006). In Rap proteins, the Q61 residue is replaced by a threonine that is involved in Rap-GAP binding and not in catalysis (Chakrabarti *et al*, 2007). For Rap proteins, the water molecule needed for hydrolysis is instead coordinated by an Asn-thumb coming from the Rap-GAP (Daumke *et al*, 2004; Scrima *et al*, 2008). Despite a conserved fold and GTP-binding motifs, GTPases thus have different ways of achieving GTP hydrolysis. The catalytic glutamine of Ras is poorly conserved in IFT27 orthologues and is found to be a serine in the case of CrIFT27 (S79; Figures 3 and 4A). The other GTPase of the IFT complex B, IFT22, also has a serine (S67; Figure 3) at the position of the catalytic Q61 of Ras. Since the switch regions of IFT27 are likely to undergo significant conformational changes upon nucleotide binding, it is currently not clear if S79 could participate in the positioning of a nucleophilic water molecule. It is noteworthy that the IFT25 protein is located >10 Å from the nucleotide-binding pocket of IFT27 and is thus unlikely to contribute any nucleotide binding or catalytic residues.

To test if IFT27 can bind and hydrolyse GTP, we carried out GTP binding and hydrolysis assays using purified CrIFT25 Δ C/27. To measure the intrinsic GTP hydrolysis activity of IFT27, the release of inorganic phosphate upon conversion of GTP to GDP was followed (Figure 4B). This experiment shows that IFT25 Δ C/27 has very low but measurable intrinsic GTPase activity. The reaction rate under the conditions of the assay is $2.1 \times 10^{-3} \text{ min}^{-1} \pm 2.9 \times 10^{-5} \text{ min}^{-1}$, which is very low but comparable with the intrinsic rate of other small GTPases (Simon *et al*, 1996; Scheffzek and Ahmadian, 2005). As a positive control, the interferon-induced large GTPase IIGP1 with a reaction rate of 2 min^{-1} was used in the GTPase assay (Uthaiyah *et al*, 2003; Ghosh *et al*, 2004). As for most large GTPases, IIGP1 has robust GTPase activity without the assistance of a GAP (Ghosh *et al*, 2004). The GTP hydrolysis can be attributed to the GTPase site of IFT27 as mutations known to affect GTP binding or catalysis significantly change the reaction rate of the IFT25 Δ C/27 complex. The CrIFT25 Δ C/27(S30N) mutant, where GTP binding is impaired, displays a significantly lower reaction rate ($1.5 \times 10^{-3} \text{ min}^{-1} \pm 1.5 \times 10^{-4} \text{ min}^{-1}$) than wild-type (WT) complex (Figure 4B). CrIFT27 has a

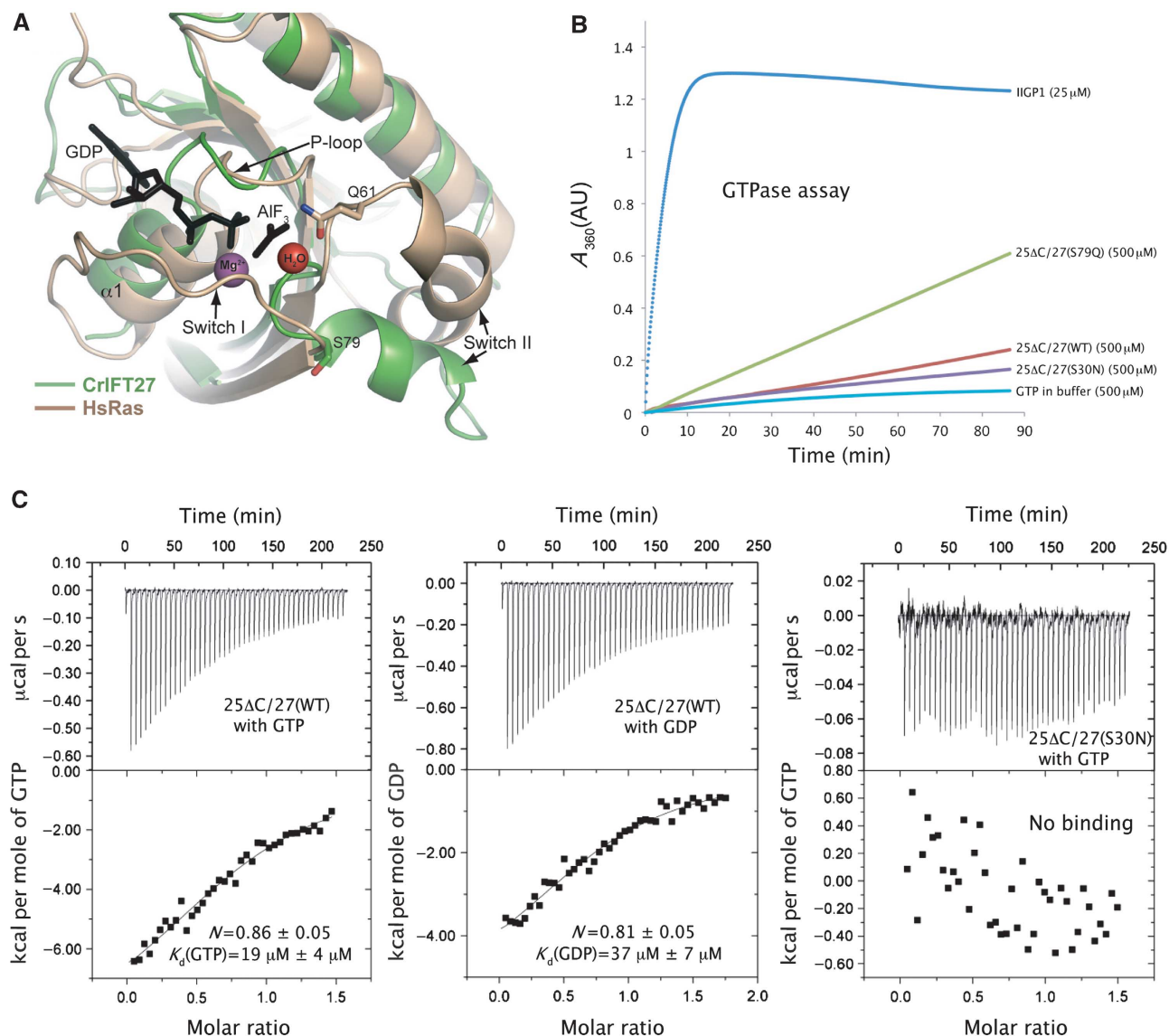


Figure 4 IFT27 is lacking a catalytic glutamine residue. **(A)** Comparison of the GTPase sites of GDP-AIF₃-bound Ras (pdb code 1WQ1) and nucleotide-free IFT27. IFT27 is coloured green, Ras light brown and the bound nucleotide is shown as black sticks. The magnesium ion and the catalytic water are shown as a purple and red ball, respectively. The catalytic Q61 of Ras and equivalent residue of IFT27 (S79) are shown as sticks and labelled. Switch regions and the P-loop are also labelled. **(B)** GTPase assay. The release of inorganic phosphate upon GTP hydrolysis is followed using the EnzCheck Phosphate kit (Invitrogen) by absorbance measurements at 360 nm. Uncatalysed GTP hydrolysis in buffer as well as catalysed reactions using 500 μM of WT or mutant IFT25ΔC/27 complex over a time course of 90 min are shown. The concentration of GTP is in all cases 500 μM. As a positive control, 25 μM of the large GTPase IIGP1 is seen to hydrolyse all of the GTP in approximately 10 min. Whereas the GTP-binding mutant S30N is seen to reduce the GTPase activity, introduction of a glutamine at the position of S79 of IFT27 increases the activity significantly. Each of the curves representing WT or mutant IFT25ΔC/27 catalysed GTP turnover is the average of two independent experiments. **(C)** ITC measurements. ITC was used to measure the affinity of IFT25ΔC/27 for GDP and GTP nucleotides. WT IFT25ΔC/27 is seen to bind both GTP and GDP with micromolar affinities. The occupancies are close to one, demonstrating that only one nucleotide-binding site is present in the complex. The nucleotide binding can be attributed to the GTPase site of IFT27 since a point mutation (S30N) in the P-loop of IFT27 abolishes binding to GTP (right panel).

serine (S79) at the position of the catalytic glutamine (Q61) that in the Ras protein coordinates a water molecule for the nucleophilic attack on the γ -phosphate of GTP. To explore if the residue at this position is also important for the catalytic activity of IFT27 we introduced an S79Q mutation and tested the CrIFT25ΔC/27(S79Q) mutant complex in GTPase assays. As seen from Figure 4B, the S79Q mutant has significantly higher activity (reaction rate of $5.4 \times 10^{-3} \text{ min}^{-1} \pm 5.4 \times 10^{-4} \text{ min}^{-1}$) than WT protein, indicating that glutamine at position 79 in CrIFT27 is better suited to coordinate the

catalytic water than serine is. To summarize, CrIFT25ΔC/27 has very low but measurable intrinsic GTPase activity suggesting that if the cellular function of IFT27 requires GTP hydrolysis, a yet unidentified GAP is likely to be involved.

To measure the affinities of CrIFT25ΔC/27 for GDP and GTP nucleotides, isothermal titration calorimetry (ITC) was carried out. The results of these experiments show that the complex binds GTP with a K_d of 19 μM and GDP with a K_d of 37 μM (Figure 4C). The observed nucleotide binding is specific for the GTPase site of IFT27 as the S30N mutant

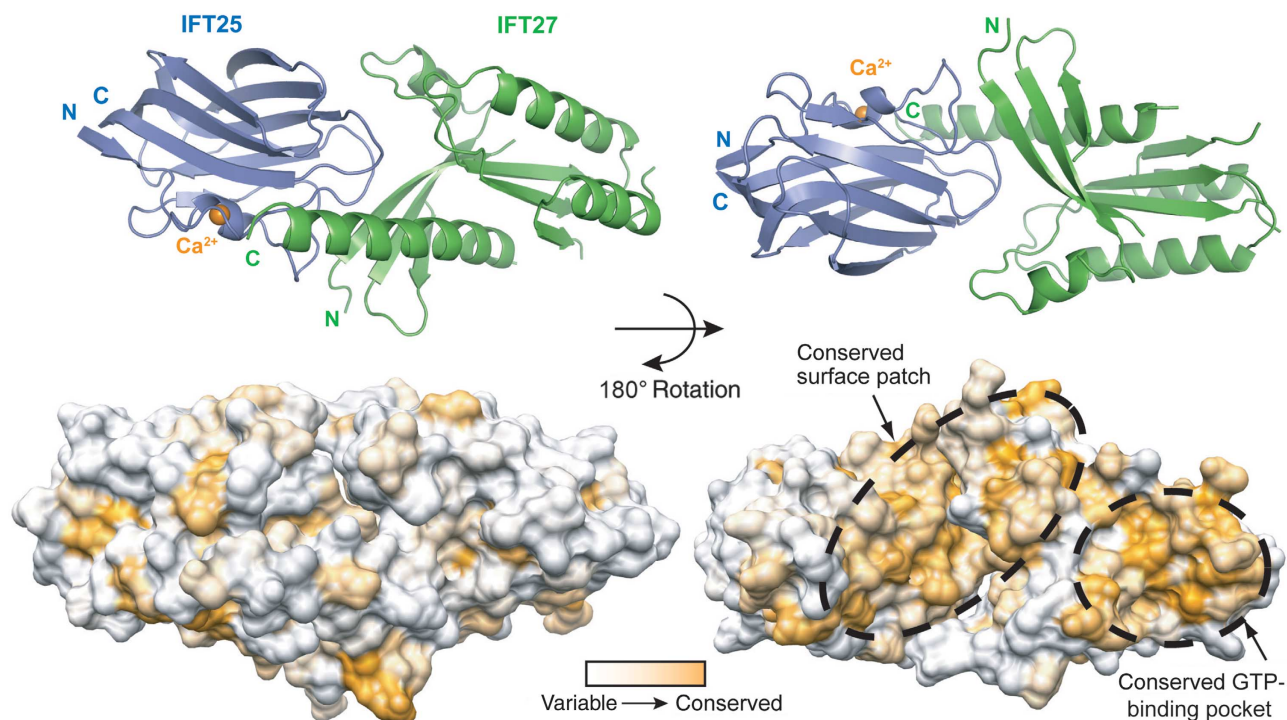


Figure 5 Surface conservation of the IFT25/27 structure. (Top) Cartoon representation of the IFT25 Δ C/27 complex in a similar orientation as for Figure 1. Residues 24–38 of IFT27 that partly block the view of the GTP-binding pocket have been omitted from the figure for better visualization. (Bottom) Surface representation of the IFT25 Δ C/27 complex in a similar orientation as for Figure 1. The sequence conservation between different species of IFT27 and IFT25 (same species as for the alignment in Figure 3; Supplementary Figure S2) are mapped onto the surface of the IFT25/27 heterodimeric structure. Variable residues are coloured white, whereas conserved residues are shown in orange according to the colour bar. In addition to a highly conserved GTP-binding pocket of IFT27, a neighbouring surface patch, extending across the IFT25/27 dimer, is highly conserved and likely to mediate protein–protein interactions.

does not display any GTP binding in our ITC experiment (Figure 4C). This micromolar affinity for GDP/GTP is much weaker than what is observed for other small GTPases of the Ras superfamily that typically display picomolar to nanomolar affinities for nucleotides (Simon *et al*, 1996; Esters *et al*, 2001). Interestingly, large GTPases that also have K_d 's for GDP in the μ M range typically do not have an identified GEF and may well function without exchange factors (Uthaiyah *et al*, 2003). Given the low affinity of IFT27 for GDP, it is plausible that IFT27 could fulfil its biological role without a cellular GEF. The conclusions from the biochemical analyses are that IFT27 binds GTP/GDP with micromolar affinity and has very low intrinsic GTPase activity.

Discussion

The IFT25/27 structure displays a conserved surface patch that could mediate protein–protein interactions

IFT25/27 is a sub-complex of the larger 14-subunit IFT-B complex and was found to associate with a core of IFT-B proteins after washing away salt labile subunits with 300 mM NaCl (Lucker *et al*, 2005). In addition to IFT27, this IFT-B core was originally shown to contain IFT subunits IFT46, 52, 72/74, 81 and 88 (Lucker *et al*, 2005). IFT25 was not identified as an IFT subunit in the Lucker *et al* (2005) study, but was recently shown to belong to the IFT-B and not the IFT-A complex in co-immunoprecipitation and co-sedimentation experiments, consistent with its direct interaction with IFT27 (Follit *et al*, 2009; Lechtreck *et al*, 2009; Wang *et al*,

2009). As we find that IFT25 Δ C/27 forms a stable complex in the presence of 300 mM NaCl (Supplementary Figure S4C), IFT25 should also be counted as part of this IFT-B core complex. It follows that the IFT25/27 complex must present a surface interface mediating the association with other IFT-B core subunits. Although there is limited data available on how IFT25/27 associates with the rest of the IFT-B core, chemical cross-linking and MALDI-TOF analysis have indicated a possible interaction between IFT27 and IFT81 (Lucker *et al*, 2010).

To explore which part of the IFT25/27 complex could potentially be responsible for IFT-B core binding, we mapped the degree of sequence conservation of IFT25 and IFT27 orthologues onto the surface of the IFT25 Δ C/27 crystal structure (Figure 5) (Landau *et al*, 2005). This method assumes that surface residues engaged in protein–protein interactions will show a higher degree of conservation than residues that are not. Two surface areas of the IFT25 Δ C/27 structure, located on the same side of the complex, show a high degree of conservation (encircled in Figure 5). One of these areas maps solely to IFT27 and overlaps with the GTP-binding site. Adjacent to this, a second, somewhat larger patch is found to display a surface of highly conserved residues. This surface area has residues contributed by both IFT25 and IFT27 and is a good candidate for a protein–protein interaction surface. Part of this conserved surface overlaps with the Rab-GAP-binding site as seen in an Rab33-Rab-GAP crystal structure and could thus be conserved for the purpose of Rab-GAP binding (see Figure 6 and the following section).

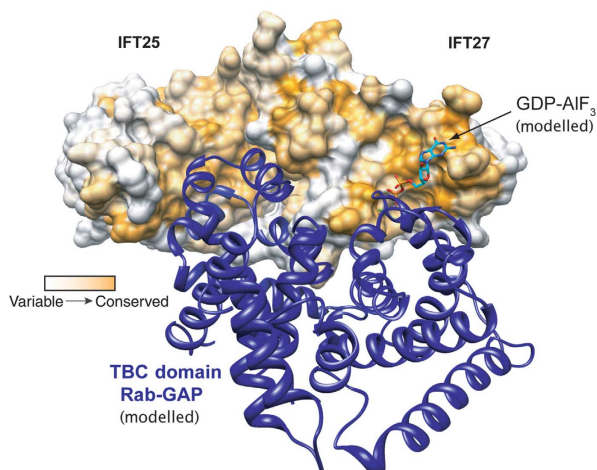


Figure 6 Model of putative Rab-GAP binding to IFT25/27. Surface representation of the IFT25/27 heterodimer with the sequence conservation mapped onto the surface as for Figure 5. The model for the putative binding of Rab-GAP to the IFT25/27 complex is shown in blue as ribbon. The model has been derived by superimposing a transition-state structure of Rab33 (the Rab33-GDP-AIF₃-Rab-GAP complex) (pdb code 2G77) onto IFT27 of the IFT25/27 complex. GDP-AIF₃ from the Rab33 structure is displayed as sticks. Both the GDP-AIF₃ and the Rab-GAP binding to IFT25/27 represent models and are not experimentally determined structures.

However, a significant portion of the surface area is not predicted to be involved in Rab-GAP binding and could thus mediate interactions between IFT25/27 and the IFT-B core complex, although additional biochemical and structural data are required to verify this prediction.

Is IFT27 GTP hydrolysis activated by a Tre-2, Bub2 and Cdc16 domain containing GAP?

Small Ras-like GTPases are known to function as switch molecules cycling between an active GTP-bound form and an inactive GDP-bound form. Small GTPases in general have low intrinsic GTP hydrolytic activity and thus usually require the activation by a GAP for robust GTP turnover. Once GTP is hydrolysed, typical affinities for GDP in the picomolar to nanomolar range mean that the GDP-bound form of the GTPase requires the assistance of a GEF to exchange the GDP for GTP (Simon *et al*, 1996; Esters *et al*, 2001). IFT27 appears to be an unusual small GTPase in the sense that it exhibits micromolar affinity rather than sub-nanomolar affinity for GDP (Figure 4C). In this respect, IFT27 more closely resembles large GTPases like IIGP1 that also exhibit micromolar affinities for GDP/GTP (Uthaiyah *et al*, 2003; Ghosh *et al*, 2004). Since many large GTPases, such as IIGP1, appear to function without a GEF, it is possible that the low affinity of IFT27 for GDP allows this small GTPase to efficiently exchange GDP for GTP without the assistance of a GEF.

Although IFT27 may function without a GEF, its very low intrinsic GTPase activity indicates that a GAP is needed for robust GTP turnover. Different families of GAPs serve as activators for the different families of GTPases (Scheffzek and Ahmadian, 2005). Although the details of GAP-mediated activation appear to differ between different GAPs, the insertion of one or more residues into the GTPase active site seems to be a common feature to facilitate hydrolysis (Scheffzek and Ahmadian, 2005). In the case of Ras, Ras-GAP contributes

a so-called arginine finger to the GTPase site, thereby increasing the rate of hydrolysis by several orders of magnitude (Scheffzek *et al*, 1997). Of the different Ras-like GTPase families, the sequence and structure of IFT27 most closely resembles that of Rabs. Rab-like GTPases appear to rely on GAPs that possess a Tre-2, Bub2 and Cdc16 (TBC) domain for efficient GTP hydrolysis (Pan *et al*, 2006). The mechanism of activation by TBC domain containing Rab-GAPs was elucidated by the crystal structure of a trapped GDP-AIF₃ transition-state intermediate of Rab33 in complex with the Rab-GAP Gyp1p (Pan *et al*, 2006). This study demonstrates that Gyp1p functions via a dual-finger mechanism where, in addition to the classical arginine finger, a glutamine is inserted *in trans* into the active site of Rab33 (Pan *et al*, 2006). Since IFT27 does not have the catalytic glutamine conserved, it is thus conceivable that it is also activated by a TBC domain containing GAP that provides the missing catalytic glutamine *in trans*. To test if the IFT25ΔC/27 structure is compatible with Rab-GAP binding, the Rab33-Gyp1p structure was superimposed on the IFT25ΔC/27 structure (Figure 6). This superposition shows that the TBC domain containing GAP complements the surface of the IFT25ΔC/27 structure without any major clashes. It is also noteworthy that the predicted GAP-binding surface partly overlaps with the highly conserved surface patch and covers both IFT27 and IFT25. BLAST searches with Gyp1p against the *Chlamydomonas* genome reveal the presence of seven TBC domain containing GAPs (*E*-value < 10⁻³) that could be possible candidates for an IFT27 GAP (Supplementary Table S1). Of the seven candidates, one candidate (gene accession code XP_001699577.1) was shown to localize to the cilium (Pazour *et al*, 2005) but, curiously, does not contain the usual Rab-GAP catalytic motifs (see Supplementary Table S1). Further research is thus required to identify the potential GAP specific for IFT27. The cellular localization of such a GAP will likely provide important insights into the function of IFT25/27 in IFT.

Materials and methods

Preparation and crystallization of the CrIFT25/27 complex

IFT25ΔC and IFT27 were co-expressed in the *E. coli* BL21 (DE3) Gold pLysS strain with TEV protease cleavable GST and His tags, respectively. The complex was purified by Ni²⁺ and glutathione sepharose (GSH)-affinity chromatography followed by TEV cleavage of the tags and further purification by anion exchange chromatography (MonoQ, GE healthcare). As a last step, SEC (Superdex 75, GE Healthcare) was performed in a buffer containing 10 mM Tris pH 7.5, 150 mM NaCl, 5 mM MgSO₄, 1 mM CaCl₂ and 1 mM DTT to separate excess IFT25ΔC from the IFT25ΔC-IFT27 complex. All mutant constructs of IFT25 and IFT27 were generated using the QuickChange site-directed mutagenesis method from Stratagene and the proteins purified using the same protocol as for the WT complex. Crystals of IFT25ΔC/27 at 30 mg ml⁻¹ were obtained by sitting drop vapour diffusion at 18°C by mixing the complex with an equal volume of 20% PEG 3350 buffered with 50 mM MES pH 6.0.

Data collection and structure determination

Crystals were cryo protected using mother liquor supplemented with 35% PEG3350 before flash cooling at 100 K. Diffraction data were collected at the Swiss Light Source (SLS, Villigen, Switzerland) and processed with XDS (Kabsch, 1993). Phase information was obtained for the 2.8-Å resolution data set by molecular replacement using the coordinates of the human IFT25 structure (pdb code 1TVG) and an ensemble of four different Rab GTPase structures that were superimposed (pdb codes 2O52, 1Y2K, 2AED and 1N6H) as

search models in the program PHASER (Storoni *et al*, 2004). The model was completed by iterative cycles of model building in COOT (Emsley and Cowtan, 2004) and refinement in PHENIX (Adams *et al*, 2010). The structure from the second crystal form (2.6 Å resolution data set) was determined by molecular replacement using the model obtained from the 2.8-Å resolution data.

ITC and GTPase assay

ITC was carried out at 25°C using a VP-ITC Microcalorimeter (Microcal, GE healthcare). Proteins and nucleotides were buffered with 10 mM Tris, 150 mM NaCl, 1 mM CaCl₂ and 5 mM MgSO₄ pH 7.5. A volume of 1.44 ml of protein was titrated with nucleotide in 45 injections of 5 µl each with 5 min intervals between injections. CrIFT25ΔC/27 (WT or S30N mutant) were at a concentration of 50 µM for the GTP and ATP titration and at 95 µM concentration for the GDP titration. The nucleotides were in all cases 10× the concentration of protein in the cell. For each ITC curve, a background curve consisting of the titration of nucleotide into buffer without protein was subtracted to account for heat dilution. The ITC data were analysed using the program Origin version 7 provided by Microcal.

The GTPase activity of CrIFT25ΔC/27 was measured using the EnzCheck Phosphate kit (Invitrogen) at 20°C. For each assay, 500 µM GTP was added to the solutions provided in the assay kit according to the manufacturer's recommendations. The reaction was initiated by the addition of 500 µM CrIFT25ΔC/27 and the release of phosphate upon GTP hydrolysis monitored by following the enzymatic conversion of inorganic phosphate and 2-amino-6-mercapto-7-methylpurine riboside into ribose 1-phosphate and 2-amino-6-mercapto-7-methyl-purine by absorbance measurements at 360 nm. Absorbance measurements were taken every 6 s for a total duration of 90 min, and each curve in Figure 4B represents the average of two independent experiments. For the positive control, 25 µM of the GTPase IIGP1 was found to hydrolyse 500 µM GTP in approximately 10 m in agreement with its reported reaction rate of 2 min⁻¹ (Uthaiyah *et al*, 2003). As a negative control, the intrinsic hydrolysis of GTP in buffer (without the addition of any protein) was measured.

Pull-down experiments

His-tagged CrIFT25ΔC and GST-tagged CrIFT27 were co-expressed in *E. coli* BL21 (DE3) Gold pLysS cells. Cells were lysed in lysis buffer containing 50 mM Tris pH 7.5, 150 mM NaCl, 5 mM MgSO₄ and 1 mM CaCl₂ and the supernatants after centrifugation were incubated with pre-blocked GSH beads to pull down GST-CrIFT27 from the lysate. Beads were washed extensively using the lysis

buffer to remove contaminants and the bound protein was eluted from the beads using lysis buffer supplemented with 30 mM glutathione. For the Ni-NTA pull downs of IFT25, lysed cells expressing the proteins were centrifuged and the supernatant incubated with Ni-NTA beads followed by extensive washing with lysis buffer before eluting with 500 mM imidazole. For the CBP pull downs shown in Supplementary Figure S5B, pre-blocked calmodulin beads were incubated with the supernatant from cells where CBP-IFT25ΔC and IFT27 were co-expressed. After extensive washing, proteins were eluted from the calmodulin beads using a buffer containing 20 mM EGTA. In all cases, the eluted proteins were analysed using SDS-PAGE.

Accession codes

The coordinates and structure factors have been deposited in the pdb under the accession codes 2yc2 and 2yc4.

Supplementary data

Supplementary data are available at *The EMBO Journal* Online (<http://www.embojournal.org>).

Acknowledgements

We thank Fabien Bonneau for advice on the GTPase hydrolysis assays. Atlanta Cook, Elena Conti, Sutapa Chakrabarti and AA Jeyaprakash are thanked for carefully reading this manuscript and Gaspar Jekely, Melanie Vetter and Kristina Weber for many valuable discussions. Eva Wolf and Christian Herrmann are thanked for the kind gift of the IIPG1 expression plasmid. The staff at SLS is acknowledged for excellent assistance with X-ray crystallographic data collection. Furthermore, we thank the crystallization facility of the Max-Planck-Institute of Biochemistry (Munich) for access to crystallization screening. This work was supported by a grant from the Emmy Noether-program (DFG) to EL.

Author contributions: SB did the protein expression, purification, crystal structure determination and biochemistry under the supervision of EL. The ITC experiments shown in and Supplementary Figure S6 were done by SB under the supervision of CB. MM cloned the IFT25 and IFT27 constructs. MT assisted with purification and pull-down experiments and made Figures 4–6. SB, MT and EL wrote the paper.

Conflict of interest

The authors declare that they have no conflict of interest.

References

- Adams PD, Afonine PV, Bunkoczi G, Chen VB, Davis IW, Echols N, Headd JJ, Hung LW, Kapral GJ, Grosse-Kunstleve RW, McCoy AJ, Moriarty NW, Oeffner R, Read RJ, Richardson JS, Richardson JS, Terwilliger TC, Zwart PH (2010) PHENIX: a comprehensive python-based system for macromolecular structure solution. *Acta Crystallogr D Biol Crystallogr* **66**(Part 2): 213–221
- Adhiambo C, Blisnick T, Toutirais G, Delannoy E, Bastin P (2009) A novel function for the atypical small G protein Rab-like 5 in the assembly of the trypanosome flagellum. *J Cell Sci* **122**(Part 6): 834–841
- Bagneris C, Bateman OA, Naylor CE, Cronin N, Boelens WC, Keep NH, Slingsby C (2009) Crystal structures of alpha-crystallin domain dimers of alphaB-crystallin and Hsp20. *J Mol Biol* **392** (5): 1242–1252
- Beales PL, Bland E, Tobin JL, Bacchelli C, Tuysuz B, Hill J, Rix S, Pearson CG, Kai M, Hartley J, Johnson C, Irving M, Elcioglu N, Winey M, Tada M, Scambler PJ (2007) IFT80, which encodes a conserved intraflagellar transport protein, is mutated in Jeune asphyxiating thoracic dystrophy. *Nat Genet* **39** (6): 727–729
- Bellyei S, Szigeti A, Pozsgai E, Boronkai A, Gomori E, Hocsak E, Farkas R, Sumegi B, Gallyas Jr F (2007) Preventing apoptotic cell death by a novel small heat shock protein. *Eur J Cell Biol* **86**: 161–171
- Besschetnova TY, Kolpakova-Hart E, Guan Y, Zhou J, Olsen BR, Shah JV (2010) Identification of signaling pathways regulating primary cilium length and flow-mediated adaptation. *Curr Biol* **20**: 182–187
- Bi X, Corpina RA, Goldberg J (2002) Structure of the Sec23/24-Sar1 pre-budding complex of the COPII vesicle coat. *Nature* **419**: 271–277
- Boraston AB, Ficko-Blean E, Healey M (2007) Carbohydrate recognition by a large sialidase toxin from *Clostridium perfringens*. *Biochemistry* **46**: 11352–11360
- Braïlov I, Bancila M, Brisorgueil MJ, Miquel MC, Hamon M, Verge D (2000) Localization of 5-HT(6) receptors at the plasma membrane of neuronal cilia in the rat brain. *Brain Res* **872**: 271–275
- Chakrabarti PP, Daumke O, Suveyzdis Y, Kotting C, Gerwert K, Wittinghofer A (2007) Insight into catalysis of a unique GTPase reaction by a combined biochemical and FTIR approach. *J Mol Biol* **367**: 983–995
- Cole DG, Diener DR, Himelblau AL, Beech PL, Fuster JC, Rosenbaum JL (1998) Chlamydomonas kinesin-II-dependent intraflagellar transport (IFT): IFT particles contain proteins required for ciliary assembly in *Caenorhabditis elegans* sensory neurons. *J Cell Biol* **141**: 993–1008
- Craige B, Tsao CC, Diener DR, Hou Y, Lehtreck KF, Rosenbaum JL, Witman GB (2010) CEP290 tethers flagellar transition zone microtubules to the membrane and regulates flagellar protein content. *J Cell Biol* **190**: 927–940
- Daumke O, Weyand M, Chakrabarti PP, Vetter IR, Wittinghofer A (2004) The GTPase-activating protein Rap1GAP uses a catalytic asparagine. *Nature* **429**: 197–201

- Der CJ, Finkel T, Cooper GM (1986) Biological and biochemical properties of human rasH genes mutated at codon 61. *Cell* **44**: 167–176
- Emmer BT, Maric D, Engman DM (2010) Molecular mechanisms of protein and lipid targeting to ciliary membranes. *J Cell Sci* **123**(Part 4): 529–536
- Emsley P, Cowtan K (2004) Coot: model-building tools for molecular graphics. *Acta Crystallogr D Biol Crystallogr* **60** (Part 12 Part 1): 2126–2132
- Espinosa EJ, Calero M, Sridevi K, Pfeffer SR (2009) RhoBTB3: a Rho GTPase-family ATPase required for endosome to Golgi transport. *Cell* **137**: 938–948
- Esters H, Alexandrov K, Iakovenko A, Ivanova T, Thoma N, Rybin V, Zerial M, Scheidig AJ, Goody RS (2001) Vps9, Rabex-5 and DSS4: proteins with weak but distinct nucleotide-exchange activities for Rab proteins. *J Mol Biol* **310**: 141–156
- Fan ZC, Behal RH, Geimer S, Wang Z, Williamson SM, Zhang H, Cole DG, Qin H (2010) Chlamydomonas IFT70/CrDyf-1 is a core component of IFT particle complex B and is required for flagellar assembly. *Mol Biol Cell* **21**: 2696–2706
- Follit JA, Xu F, Keady BT, Pazour GJ (2009) Characterization of mouse IFT complex B. *Cell Motil Cytoskeleton* **66**: 457–468
- Gaskell A, Crennell S, Taylor G (1995) The three domains of a bacterial sialidase: a beta-propeller, an immunoglobulin module and a galactose-binding jelly-roll. *Structure* **3**: 1197–1205
- Ghosh A, Uthaiar R, Howard J, Herrmann C, Wolf E (2004) Crystal structure of IIGP1: a paradigm for interferon-inducible p47 resistance GTPases. *Mol Cell* **15**: 727–739
- Gibbons IR, Grimstone AV (1960) On flagellar structure in certain flagellates. *J Biophys Biochem Cytol* **7**: 697–716
- Han YG, Kwok BH, Kernan MJ (2003) Intraflagellar transport is required in *Drosophila* to differentiate sensory cilia but not sperm. *Curr Biol* **13**: 1679–1686
- Haycraft CJ, Banizs B, Aydin-Son Y, Zhang Q, Michaud EJ, Yoder BK (2005) Gli2 and Gli3 localize to cilia and require the intraflagellar transport protein polaris for processing and function. *PLoS Genet* **1**: e53
- Holm L, Sander C (1993) Protein structure comparison by alignment of distance matrices. *J Mol Biol* **233**: 123–138
- Huangfu D, Liu A, Rakeman AS, Murcia NS, Niswander L, Anderson KV (2003) Hedgehog signalling in the mouse requires intraflagellar transport proteins. *Nature* **426**: 83–87
- Jekely G, Arendt D (2006) Evolution of intraflagellar transport from coated vesicles and autogenous origin of the eukaryotic cilium. *Bioessays* **28**: 191–198
- Jin H, White SR, Shida T, Schulz S, Aguiar M, Gygi SP, Bazan JF, Nachury MV (2010) The conserved Bardet-Biedl syndrome proteins assemble a coat that traffics membrane proteins to cilia. *Cell* **141**: 1208–1219
- Kabsch W (1993) Automatic processing of rotation diffraction data from crystals of initially unknown symmetry and cell constants. *J Appl Crystallog* **26**: 795–800
- Kampinga HH, Hageman J, Vos MJ, Kubota H, Tanguay RM, Bruford EA, Cheetham ME, Chen B, Hightower LE (2009) Guidelines for the nomenclature of the human heat shock proteins. *Cell Stress Chaperones* **14**: 105–111
- Kappe G, Boelens WC, de Jong WW (2010) Why proteins without an alpha-crystallin domain should not be included in the human small heat shock protein family HSPB. *Cell Stress Chaperones* **15**: 457–461
- Knodler A, Feng S, Zhang J, Zhang X, Das A, Peranen J, Guo W (2010) Coordination of Rab8 and Rab11 in primary ciliogenesis. *Proc Natl Acad Sci USA* **107**: 6346–6351
- Kozminski KG, Johnson KA, Forscher P, Rosenbaum JL (1993) A motility in the eukaryotic flagellum unrelated to flagellar beating. *Proc Natl Acad Sci USA* **90**: 5519–5523
- Landau M, Mayrose I, Rosenberg Y, Glaser F, Martz E, Pupko T, Ben-Tal N (2005) ConSurf 2005: the projection of evolutionary conservation scores of residues on protein structures. *Nucleic Acids Res* **33** (Web Server issue): W299–W302
- Lehtreck KF, Luro S, Awata J, Witman GB (2009) HA-tagging of putative flagellar proteins in *Chlamydomonas reinhardtii* identifies a novel protein of intraflagellar transport complex B. *Cell Motil Cytoskeleton* **66**: 469–482
- Lucker BF, Behal RH, Qin H, Siron LC, Taggart WD, Rosenbaum JL, Cole DG (2005) Characterization of the intraflagellar transport complex B core: direct interaction of the IFT81 and IFT74/72 subunits. *J Biol Chem* **280**: 27688–27696
- Lucker BF, Miller MS, Dziedzic SA, Blackmarr PT, Cole DG (2010) Direct interactions of intraflagellar transport complex B proteins IFT88, IFT52, and IFT46. *J Biol Chem* **285**: 21508–21518
- Ma R, Li WP, Rundle D, Kong J, Akbarali HI, Tsiokas L (2005) PKD2 functions as an epidermal growth factor-activated plasma membrane channel. *Mol Cell Biol* **25**: 8285–8298
- Michaud EJ, Yoder BK (2006) The primary cilium in cell signaling and cancer. *Cancer Res* **66**: 6463–6467
- Murcia NS, Richards WG, Yoder BK, Mucenski ML, Dunlap JR, Woychik RP (2000) The Oak Ridge Polycystic Kidney (orpk) disease gene is required for left-right axis determination. *Development* **127**: 2347–2355
- Nachury MV, Loktev AV, Zhang Q, Westlake CJ, Peranen J, Merdes A, Slusarski DC, Scheller RH, Bazan JF, Sheffield VC, Jackson PK (2007) A core complex of BBS proteins cooperates with the GTPase Rab8 to promote ciliary membrane biogenesis. *Cell* **129**: 1201–1213
- Ou G, Blacque OE, Snow JJ, Leroux MR, Scholey JM (2005) Functional coordination of intraflagellar transport motors. *Nature* **436**: 583–587
- Pai EF, Krenzel U, Petsko GA, Goody RS, Kabsch W, Wittinghofer A (1990) Refined crystal structure of the triphosphate conformation of H-ras p21 at 1.35 Å resolution: implications for the mechanism of GTP hydrolysis. *EMBO J* **9**: 2351–2359
- Pan X, Eathiraj S, Munson M, Lambright DG (2006) TBC-domain GTPases accelerate GTP hydrolysis by a dual-finger mechanism. *Nature* **442**: 303–306
- Pazour GJ, Agrin N, Leszyk J, Witman GB (2005) Proteomic analysis of a eukaryotic cilium. *J Cell Biol* **170**: 103–113
- Pazour GJ, Dickert BL, Vucica Y, Seeley ES, Rosenbaum JL, Witman GB, Cole DG (2000) Chlamydomonas IFT88 and its mouse homologue, polycystic kidney disease gene tg737, are required for assembly of cilia and flagella. *J Cell Biol* **151**: 709–718
- Pedersen LB, Miller MS, Geimer S, Leitch JM, Rosenbaum JL, Cole DG (2005) Chlamydomonas IFT172 is encoded by FLA11, interacts with CrEB1, and regulates IFT at the flagellar tip. *Curr Biol* **15**: 262–266
- Perkins LA, Hedgecock EM, Thomson JN, Culotti JG (1986) Mutant sensory cilia in the nematode *Caenorhabditis elegans*. *Dev Biol* **117**: 456–487
- Pigino G, Geimer S, Lanzavecchia S, Paccagnini E, Cantele F, Diener DR, Rosenbaum JL, Lupetti P (2009) Electron-tomographic analysis of intraflagellar transport particle trains *in situ*. *J Cell Biol* **187**: 135–148
- Piperno G, Mead K (1997) Transport of a novel complex in the cytoplasmic matrix of *Chlamydomonas* flagella. *Proc Natl Acad Sci USA* **94**: 4457–4462
- Piperno G, Siuda E, Henderson S, Segil M, Vaananen H, Sassaroli M (1998) Distinct mutants of retrograde intraflagellar transport (IFT) share similar morphological and molecular defects. *J Cell Biol* **143**: 1591–1601
- Qin H, Diener DR, Geimer S, Cole DG, Rosenbaum JL (2004) Intraflagellar transport (IFT) cargo: IFT transports flagellar precursors to the tip and turnover products to the cell body. *J Cell Biol* **164**: 255–266
- Qin H, Wang Z, Diener D, Rosenbaum J (2007) Intraflagellar transport protein 27 is a small G protein involved in cell-cycle control. *Curr Biol* **17**: 193–202
- Ramelot TA, Raman S, Kuzin AP, Xiao R, Ma LC, Acton TB, Hunt JF, Montelione GT, Baker D, Kennedy MA (2009) Improving NMR protein structure quality by Rosetta refinement: a molecular replacement study. *Proteins* **75**: 147–167
- Rittinger K, Walker PA, Eccleston JF, Smerdon SJ, Gamblin SJ (1997) Structure at 1.65 Å of RhoA and its GTPase-activating protein in complex with a transition-state analogue. *Nature* **389**: 758–762
- Rual JF, Venkatesan K, Hao T, Hirozane-Kishikawa T, Dricot A, Li N, Berriz GF, Gibbons FD, Dreze M, Ayivi-Guedehoussou N, Klitgord N, Simon C, Boxem M, Milstein S, Rosenberg J, Goldberg DS, Zhang LV, Wong SL, Franklin G, Li S et al (2005) Towards a proteome-scale map of the human protein-protein interaction network. *Nature* **437**: 1173–1178
- Satir P, Christensen ST (2008) Structure and function of mammalian cilia. *Histochem Cell Biol* **129**: 687–693

- Scheffzek K, Ahmadian MR (2005) GTPase activating proteins: structural and functional insights 18 years after discovery. *Cell Mol Life Sci* **62**: 3014–3038
- Scheffzek K, Ahmadian MR, Kabsch W, Wiesmuller L, Lautwein A, Schmitz F, Wittinghofer A (1997) The Ras-RasGAP complex: structural basis for GTPase activation and its loss in oncogenic Ras mutants. *Science* **277**: 333–338
- Schneider L, Clement CA, Teilmann SC, Pazour GJ, Hoffmann EK, Satir P, Christensen ST (2005) PDGFRalpha signaling is regulated through the primary cilium in fibroblasts. *Curr Biol* **15**: 1861–1866
- Scrima A, Thomas C, Deaconescu D, Wittinghofer A (2008) The Rap-RapGAP complex: GTP hydrolysis without catalytic glutamine and arginine residues. *EMBO J* **27**: 1145–1153
- Seewald MJ, Korner C, Wittinghofer A, Vetter IR (2002) RanGAP mediates GTP hydrolysis without an arginine finger. *Nature* **415**: 662–666
- Shida T, Cueva JG, Xu Z, Goodman MB, Nachury MV (2010) The major {alpha}-tubulin K40 acetyltransferase {alpha}. *Proc Natl Acad Sci USA* **107**: 21517–21522
- Simon I, Zerial M, Goody RS (1996) Kinetics of interaction of Rab5 and Rab7 with nucleotides and magnesium ions. *J Biol Chem* **271**: 20470–20478
- Snell WJ, Pan J, Wang Q (2004) Cilia and flagella revealed: from flagellar assembly in *Chlamydomonas* to human obesity disorders. *Cell* **117**: 693–697
- Stenmark H (2009) Rab GTPases as coordinators of vesicle traffic. *Nat Rev Mol Cell Biol* **10**: 513–525
- Storoni LC, McCoy AJ, Read RJ (2004) Likelihood-enhanced fast rotation functions. *Acta Crystallogr D Biol Crystallogr* **60**(Part 3): 432–438
- Sun Z, Amsterdam A, Pazour GJ, Cole DG, Miller MS, Hopkins N (2004) A genetic screen in zebrafish identifies cilia genes as a principal cause of cystic kidney. *Development* **131**: 4085–4093
- Tobin JL, Beales PL (2007) Bardet-Biedl syndrome: beyond the cilium. *Pediatr Nephrol* **22**: 926–936
- Tsujikawa M, Malicki J (2004) Intraflagellar transport genes are essential for differentiation and survival of vertebrate sensory neurons. *Neuron* **42**: 703–716
- Uthaiyah RC, Praefcke GJ, Howard JC, Herrmann C (2003) IIGP1, an interferon-gamma-inducible 47-kDa GTPase of the mouse, showing cooperative enzymatic activity and GTP-dependent multimerization. *J Biol Chem* **278**: 29336–29343
- Vetter IR, Wittinghofer A (2001) The guanine nucleotide-binding switch in three dimensions. *Science* **294**: 1299–1304
- Voorhees RM, Schmeing TM, Kelley AC, Ramakrishnan V (2010) The mechanism for activation of GTP hydrolysis on the ribosome. *Science* **330**: 835–838
- Wang Z, Fan ZC, Williamson SM, Qin H (2009) Intraflagellar transport (IFT) protein IFT25 is a phosphoprotein component of IFT complex B and physically interacts with IFT27 in *Chlamydomonas*. *PLoS One* **4**: e5384
- Witman GB (2009) *The Chlamydomonas Sourcebook*, Vol 3. Burlington, MA: Academic Press

Supplemental data

Supplemental figures

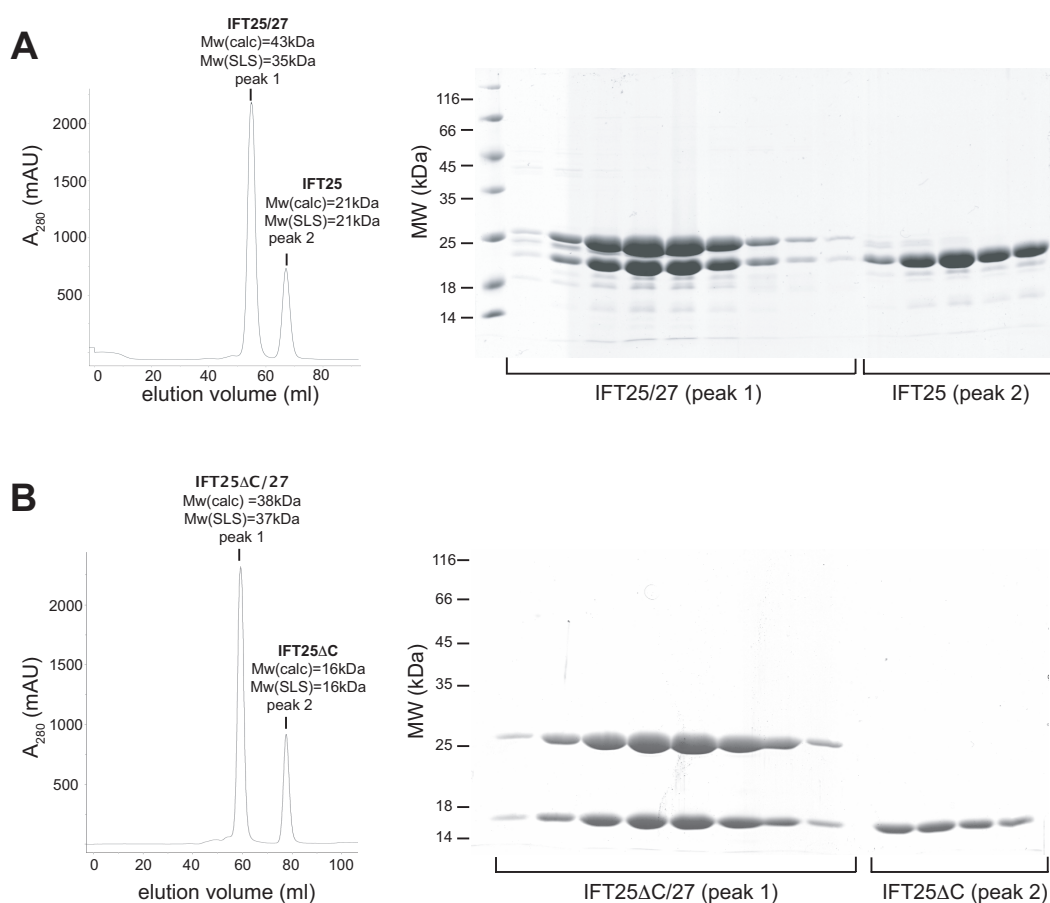


Figure S1 Purification of full-length CrIFT25/27 and truncated CrIFT25DC/27

(A) The left panel shows the elution profile of CrIFT25/27 from a Superdex 75 size exclusion column. The IFT25/27 complex is seen to elute as a heterodimer whereas excess monomeric IFT25 elutes later. The calculated molecular weights (Mw) based on the amino acid sequences as well as experimentally determined values by static light scattering (SLS) are indicated. The somewhat lower Mw(SLS) value of 35 kDa vs. a Mw(calc) of 43 kDa for full length IFT25/27 could be due to the presence of degradation fragments. The right panel shows an SDS PAGE gel of the two peaks from the SEC experiment. (B). As (A) but with the CrIFT25DC/27 truncated complex.

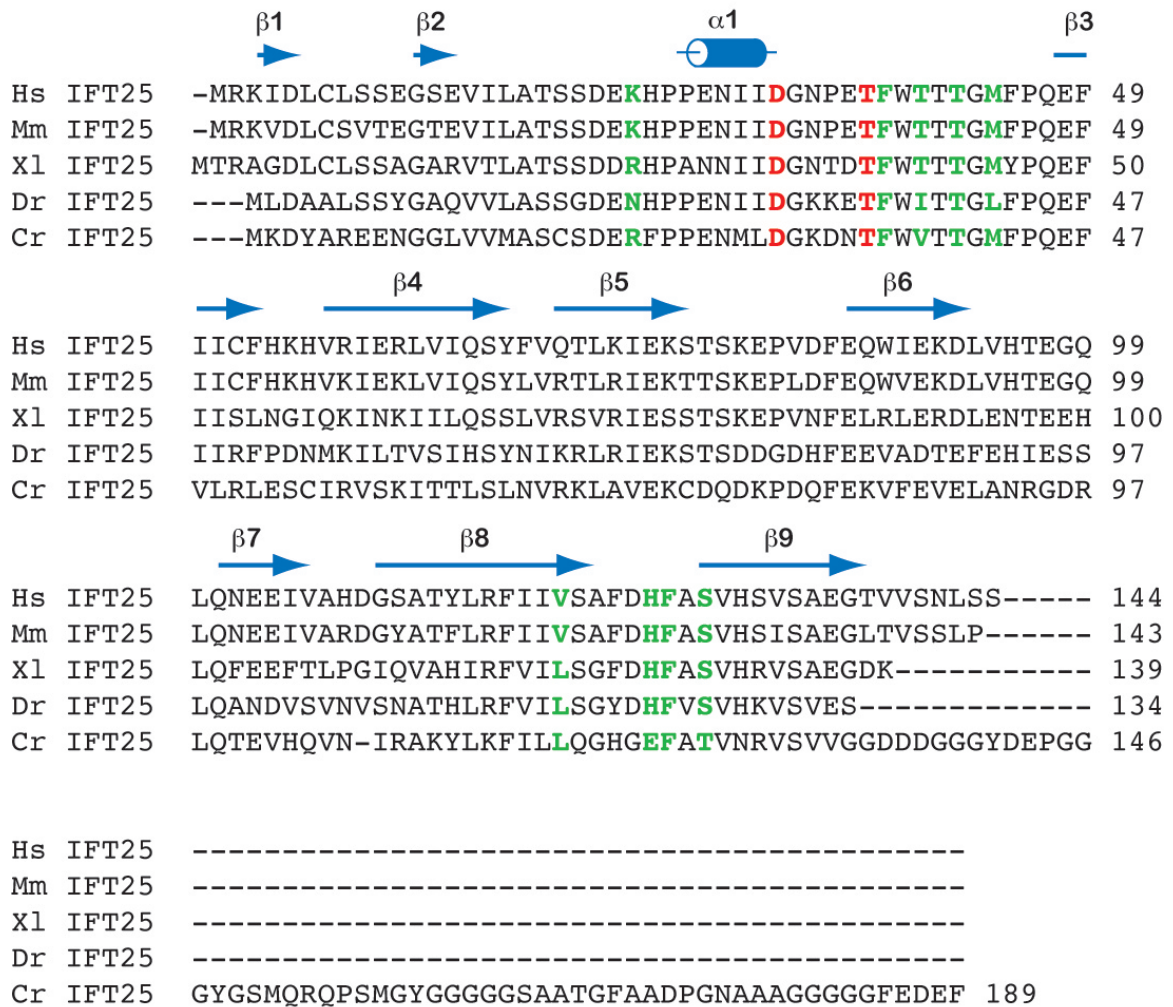


Figure S2 Multiple sequence alignment of IFT25

Secondary structure elements derived from the CrIFT25 structure are indicated above the sequences. IFT25 residues that interact directly with residues from IFT27 are colored green and the calcium-ion coordinating residues are red. CrIFT25 is seen to have a long glycine-rich C-terminal extension not found in other IFT25 orthologues. Hs: Homo sapiens, Mm: Mus musculus, Xl: Xenopus laevis, Dr: Danio rerio, Cr: Chlamydomonas reinhardtii.

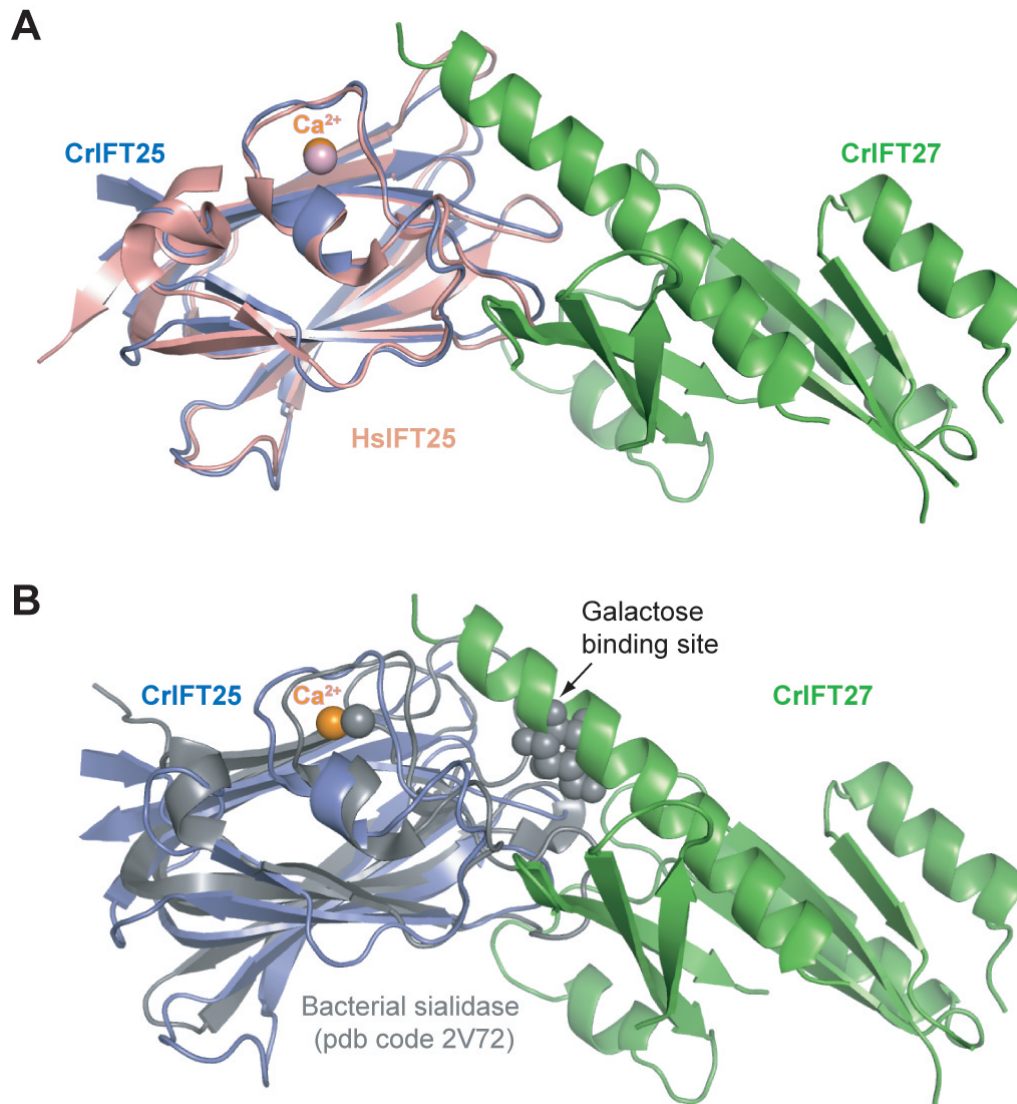


Figure S3 Structural comparison with HsIFT25 and sialidases

(A) The structure of human IFT25 (in salmon) has been superimposed on the *Chlamydomonas* IFT25/27 complex. HsIFT25 and CrIFT25 show high structural similarity and share a conserved calcium-binding site. (B) Structural comparison of a bacterial sialidase with the IFT25/27 complex. The overall structure of the sialidase is similar to IFT25 and the two proteins share a common calcium-binding site. However, the galactose-binding site of sialidases is not conserved in IFT25 and is seen to overlap with the C-terminal helix of IFT27 in the IFT25/27 complex structure.

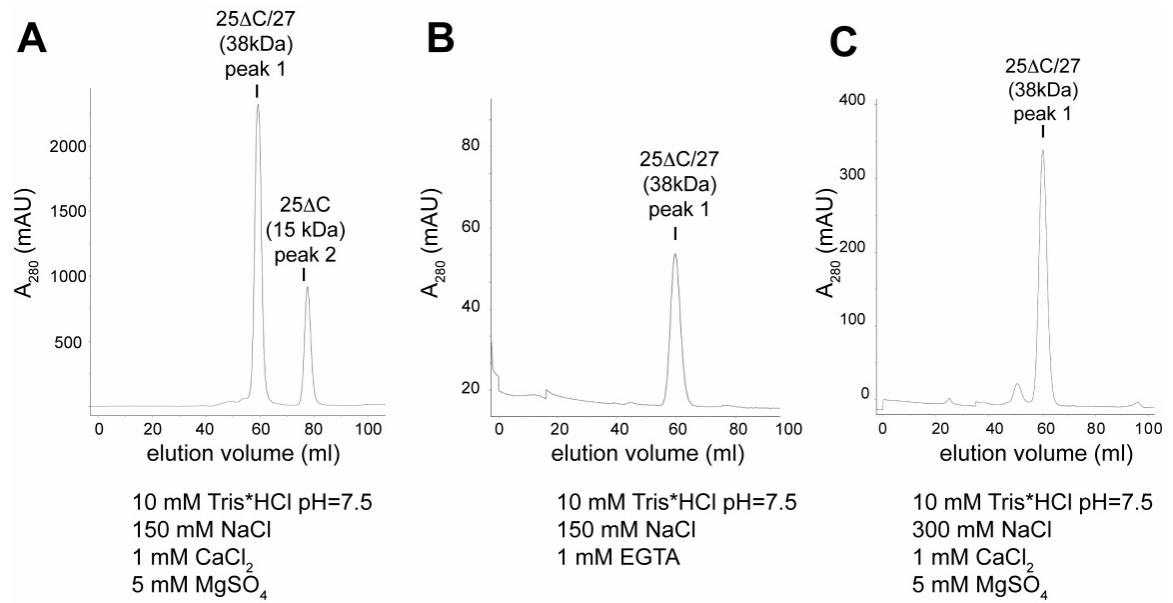


Figure S4 Effect of different buffer conditions on the IFT25DC/27 complex

(A) SEC profile of a standard IFT25DC/27 purification using a Superdex 75 column. The IFT25DC/27 complex is seen to elute around 60 mL whereas excess 25DC elutes at around 80 mL. (B) The SEC purified IFT25DC/27 complex (peak 1 from panel (A)) was incubated with 10 mM of the strong calcium chelator EGTA for 30 min at 20°C and subjected to another round of SEC where 1 mM of EGTA (and no divalent metal ions) was included in the buffer to assess the role of calcium in complex formation. The IFT25DC/27 complex is not disrupted indicating that calcium-binding is not a requirement for complex stability. (C) The effect of salt on IFT25DC/27 complex stability. SEC purified IFT25DC/27 complex (peak 1 from panel (A)) was incubated with a buffer containing 300 mM NaCl for 30 min at 20°C and subjected to SEC run in a 300 mM NaCl-containing buffer. The higher salt concentration does not have any apparent effect on the IFT25DC/27 complex stability.

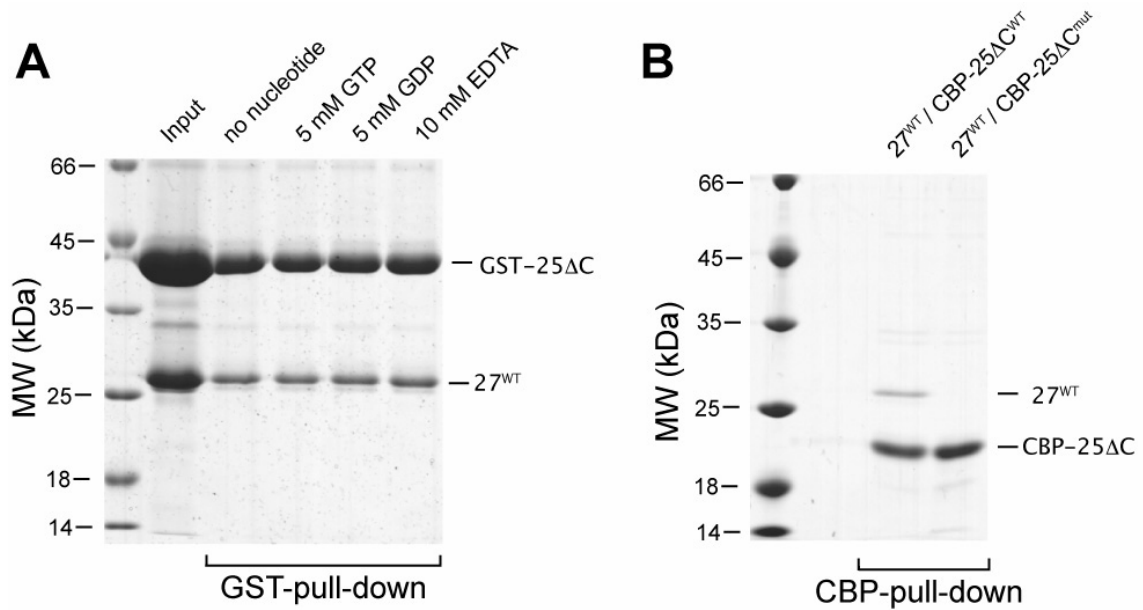


Figure S5 IFT27 binds IFT25 regardless of its nucleotide state

(A) The effect of the nucleotide bound to IFT27 on the ability to bind IFT25 was tested experimentally in pull-down assays. GST-tagged IFT25DC can pull down IFT27 regardless of the nucleotide-bound state of IFT27. The proteins were pre-incubated for 30 min at 20°C with 5 mM GDP, 5 mM GTP or with 10 mM of EDTA before incubating for 1h with GSH-beads. After washing the beads 3 times, the protein was eluted with 30 mM glutathione (B) Pull-down of WT IFT27 using CBP-tagged WT (CBP-25DC^{WT}) or mutant (CBP-25DC^{mut}, V38R, T40R and T125E triple mutant) IFT25. Since the proteins are co-expressed and IFT25 is expressed to a much higher degree than IFT27, the band for IFT25 is stronger than that for IFT27. Whereas WT IFT25 can pull-down IFT27, the interface mutant of IFT25 no longer precipitates IFT27 consistent with the results shown in Figure 2B.

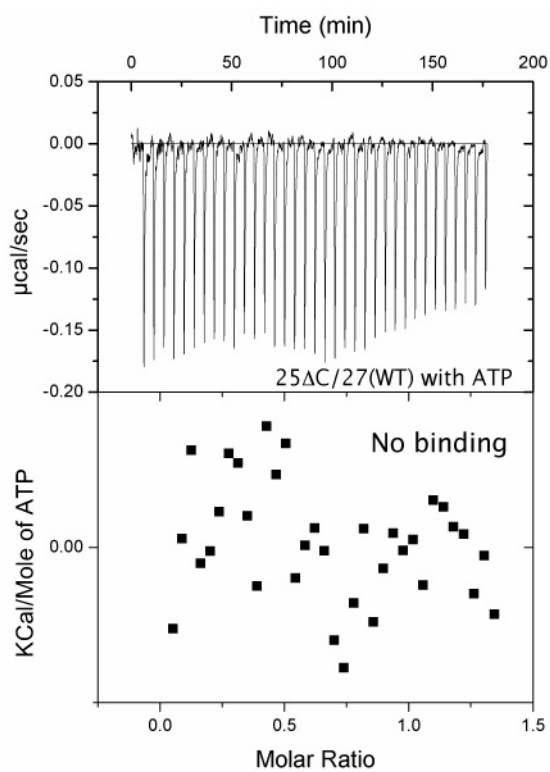


Figure S6 IFT25DC/27 does not bind ATP

To test if the IFT25DC/27 complex binds ATP, 50mM of the complex was titrated with 500 μM of ATP in an ITC experiment. The titration curve demonstrates that IFT25DC/27 does not bind ATP.

Table S1 Putative GAPs for CrIFT27

Gene accession code	Localization	E value	Conservation of catalytic motifs IxxDxxR and YxQ
XP_001698588.1	Unknown	5e-05	yes
XP_001701653.1	Unknown	8e-08	yes
XP_001697170.1	Unknown	2e-08	yes
XP_001690894.1	Unknown	5e-63	yes
XP_001692974.1	Unknown	6e-09	yes
XP_001693283.1	Unknown	6e-22	yes
XP_001700441.1	Unknown	2e-09	yes
XP_001699577.1	Cilia (Pazour et al., 2005)	5e-06	No

Since IFT27 has very low intrinsic GTPase activity and belongs to the Rab family of small GTPases it may be regulated by a TBC-domain GAP as seen for other Rabs. To find putative candidates, the TBC-domain Rab-GAP Gyp1p from yeast was blasted against the Chlamydomonas genome and significant hits (E value $> 10^{-3}$) listed in the table above. One of the candidates (code: XP_001699577.1) was found in the cilium in a previous study (Pazour et al., 2005) but does not contain the classical catalytic sequence motifs of Rab-GAPs.

Extended discussion

Finding a RabGAP specific for IFT25/27

Structural and biochemical analyses carried out in this article point towards a possible TBC domain containing protein acting as a GTPase activating protein (GAP) for IFT27. Such a GAP could regulate the GTPase activity of IFT27 and in turn cilia formation/function. Identifying and characterizing such a GAP would greatly help us to understand the cellular role of the IFT25/27 heterodimer. The human genome contains 44 genes coding for TBC domain containing proteins. Testing each RabGAP for their specificity towards IFT27 would be cumbersome and may also involve many false positives (as a single RabGAP can stimulate the activity of a broad range of Rabs *in vitro*) complicating the search. Here I present a strategy to narrow down the list of potential IFT27 specific RabGAPs.

It is reasonable to assume that the IFT27 GAP would have cilia-related functions. Therefore, one approach is to test the effect of deletion or overexpression of these 44 GAPs on cilia formation. Interestingly, such a study exists where the investigators have overexpressed all the human RabGAPs and screened for their effect on ciliogenesis in serum starved RPE1 cells (Yoshimura et al., 2007). Only 3 out of 44 exhibited a strong effect on ciliogenesis. These were TBC1D7, TBC1D30 and EVI5-like protein. Both TBC1D7 and TBC1D30 were shown to localize to the base of the cilium. Intriguingly, this is the place where the IFT particles accumulate before being injected into the cilium for transport (Deane et al., 2001; Ludington et al., 2013), so it is possible that one of these proteins acts as a GAP for IFT27. Sequence analysis of these GAPs indicates that TBC1D7 is an unconventional GAP that does not contain both of the catalytic residues responsible for the dual finger GTPase activation mechanism (Figure 6.1) (Frasa et al., 2012; Pan et al., 2006). Hence it is expected to

be an inactive GAP. Interestingly a significant number of human RabGAPs do not contain at least one of the catalytic residues. TBC1D3 (also called PRC17) is one such RabGAP lacking a catalytic residue. Unlike the typical transient interaction between GTPases and GAPs, TBC1D3 binds constitutively to the GTPase Rab5 (Pei et al., 2002). Hence it was proposed that the unconventional RabGAPs lacking one or both catalytic residues bind GTPases with higher affinity and act as effectors rather than activators (Frasa et al., 2012). Notably, mutating the catalytic arginine in TBC1D30 displaces it from the base of the cilium to inside the cilium, strongly suggesting that its partner GTPase is a ciliary RabGTPase (Yoshimura et al., 2007). TBC1D7 was shown to be a key player in mTORC1 signaling (Dibble et al., 2012), which is known to occur in cilia (Boehlke et al., 2010). Curiously, the mTORC pathway was linked to aging in *C.elegans*, as was the IFT22 orthologue IFTA-2 (Schafer et al., 2006; Smith et al., 2008). It would be interesting to see if this functional interaction translates into a biochemical one. In summary, characterization of these three GAPs should remain the main focus of future research to test if they are specific to IFT27 or IFT22.

IFT25 as a Ca²⁺ sensor in the Shh pathway

The article above also describes the Ca²⁺-binding of IFT25 via coordination with two conserved side chains, D30 and T35 (Figure 2A). The close proximity of the C-terminal extended helix in IFT27 and the Ca²⁺-binding loop of IFT25 initially led us to speculate that Ca²⁺-binding may be regulating IFT25/27 complex formation (Figure 2A). However, treatment of the purified complex with excess EGTA did not



Figure 6.1 Sequence alignment of TBC1D7, TBC1D30, EV5I-like and gyp1p. TBC1D7 is an atypical RabGAP lacking the catalytic motifs.

affect complex formation (Figure S4B). Moreover, the Ca²⁺-binding loop of IFT25 in the crystal structure of IFT25/27 does not show any significant difference from that of IFT25 alone (Figure S3A). This indicates that the interaction between IFT25 and IFT27 is independent of Ca²⁺ binding to IFT25.

Mutations in mouse IFT88 and IFT172 resulted in cilia malformation and also showed severe defects in Shh signaling, indicating that Shh signaling depends on cilia formation (Huangfu et al., 2003). Furthermore, the knockout of IFT25 in the mouse resulted in early death with severe Shh signaling defects (Keady et al., 2012).

Interestingly, the onset of Shh signaling in embryonic spinal cells is associated with Ca^{2+} spike activity in neuronal cilia (Belgacem and Borodinsky, 2011). It is possible that IFT25 is sensing intracellular Ca^{2+} levels during the onset of Shh signaling and in turn is helping in transducing the Shh signal to a known or as yet unidentified downstream player of the pathway. Future experiments involving the mutation of the Ca^{2+} binding site in IFT25 and testing its effect on Shh signaling *in vivo* will shed light on this. Additionally, quantification of the Ca^{2+} affinity to IFT25 is also important, as it would tell us if the affinity is compatible with the predicted function of IFT25 in sensing intracellular Ca^{2+} levels.

Chapter II

Intraflagellar transport proteins IFT74 and IFT81 form a tubulin-binding module required for ciliogenesis.

Intraflagellar transport proteins IFT74 and IFT81 form a tubulin-binding module required for ciliogenesis

Sagar Bhogaraju¹, Lukas Cajanek², Kristina Weber¹, Michael Taschner¹, Naoko Mizuno¹, Stefan Lamla³, Erich A. Nigg² and Esben Lorentzen^{1*}

¹ Department of Structural Cell Biology, Max-Planck-Institute of Biochemistry, Am Klopferspitz 18, D-82152 Martinsried, Germany

² Biozentrum, University of Basel, Klingelbergstrasse 50/70, CH-4056 Basel, Switzerland

³ Department of Cell Biology, Max-Planck-Institute of Biochemistry, Am Klopferspitz 18, D-82152 Martinsried, Germany. Current address: Anni-Albers-Straße 11, D-80807 München, Germany

E-mail: lorentze@biochem.mpg.de

* Corresponding author

Phone: + 49 (89) 8578 – 3479

Fax: + 49(89) 8578 – 3605

Highlights: N-termini of IFT74 and IFT81 are dispensable for normal IFT. IFT81 N-terminus contains a MT/tubulin-binding CH domain. N-termini of IFT74/81 form a tubulin-binding module. Mutant IFT81 with reduced tubulin binding affects ciliogenesis.

Summary

The cilium is an important organelle for motility and sensory reception of eukaryotic cells. Cilia are built and maintained by intraflagellar transport (IFT) of ciliary precursors such as tubulin from the cytoplasm to the ciliary tip. The molecular mechanisms of how IFT proteins recognize and transport ciliary cargo are currently poorly understood. Here, we show that the N-termini of the two core IFT proteins IFT74 and IFT81 contain an $\alpha\beta$ -tubulin binding module composed of a calponin-homology domain in IFT81 and a highly basic region in IFT74. Biochemical experiments demonstrate that IFT81 specifically recognizes the globular part of $\alpha\beta$ -tubulin whereas IFT74 binds the tubulin E-hooks providing increased affinity. Moreover, our knock-down and rescue experiments demonstrate the importance of this tubulin-binding module for ciliogenesis in human cells. We propose a model where tubulin is recognized as an IFT cargo by the IFT complex via a dedicated module in IFT74/81 that directly binds and transports $\alpha\beta$ -tubulin to the ciliary tip.

Introduction

Cilia are hair-like projections found on the surface of most cells in the mammalian body where they function in cell motility, signaling and sensory reception. The cilium has recently attracted a lot of attention as many human genetic disorders such as polycystic kidney disease (Pazour et al., 2000) are found to result from ciliary defects (Fliegauf et al., 2007; Hildebrandt et al., 2011). Although cilia serve different functions on different cell types, they share a common architecture of a microtubule(MT)-based axoneme surrounded by a ciliary membrane that is continuous with the plasma membrane (Ishikawa and Marshall, 2011). The cilium is anchored in the cytoplasm via a basal-body, which is derived from the centriole (Nigg and Raff, 2009; Bornens, 2012; Gönczy, 2012). Centrioles function in the mitotic spindle during cell division and so cilia are disassembled and reassembled during the cell cycle in most organisms (Tucker et al., 1979; Cole, 2003; Jékely and Arendt, 2006). As the cilium is separated from the cytoplasm by the transition zone that act as a ciliary pore and lacks protein synthesis machinery (Rosenbaum and Witman, 2002), cilia formation and maintenance require active transport of ciliary proteins and precursors to the tip of the cilium. This bi-directional translocation process between the base and the tip of the cilium is known as intraflagellar transport (IFT) (Kozminski et al., 1993) and relies on the movement of molecular motors kinesin 2 (Walther et al., 1994; Kozminski et al., 1995; Cole et al., 1998) and dynein 2/1b (Pazour et al., 1999; Porter et al., 1999; Perrone et al., 2003; Hou et al., 2004; Engel et al., 2012) moving along axonemal MTs. In addition to molecular motors, IFT relies on the IFT complex that contains 20 subunits (~1.5 MDa), sub-divided into a 6 subunit IFT-A complex and a 14 subunit IFT-B complex with a biochemically stable core of 9 proteins (Cole et al., 1998; Piperno et al., 1998; Lucker, 2005). IFT complex

proteins are found at the base of the cilium as well as inside the cilium where they undergo bi-directional movement between the base and the tip (Deane et al., 2001; Pedersen et al., 2006; Wang et al., 2009; Buisson et al., 2012; Ludington et al., 2013). Furthermore, IFT proteins are rich in predicted protein-protein interaction motifs such as coiled-coils, WD40 and TPR domains and are believed to mediate the interaction between IFT motors and ciliary cargo (Cole, 2003; Jékely and Arendt, 2006). However, with the exception of the interaction between IFT46 and outer dynein arm (ODA) precursor complexes via ODA16 (Hou et al., 2007; Ahmed et al., 2008), little is known about the molecular mechanisms underlying cargo recognition by the IFT complex.

Microtubules in the cytoplasm are highly dynamic structures that turn over rapidly. However, MTs in the ciliary axoneme are remarkably stable as a result of acetylation of α -tubulin, a hallmark posttranslational modification of axonemal MTs (L'Hernault and Rosenbaum, 1985; Webster and Borisy, 1989). As cilia do not shorten in the presence of MT-depolymerizing drugs such as colchicine, these organelles were long thought to be rather static (Tilney and Gibbins, 1968). However, pulse-chase experiments have shown that tubulin and other ciliary precursors are not only incorporated into the axoneme during cilium growth but also at steady state when these organelles maintain a fixed length (Stephens, 1997; 2000; Song, 2001). The addition and turnover of tubulin subunits in axonemal MTs were shown to occur at the tip of the cilium both during growth (Johnson and Rosenbaum, 1992) and at steady state (Marshall and Rosenbaum, 2001). Delivery of new tubulin subunits to the ciliary tip relies on IFT, as the addition of axonemal tubulins ceases in a temperature sensitive *Chlamydomonas reinhardtii* (*C.reinhardtii* or Cr) mutant (known as fla10)

of the IFT motor kinesin 2 at the nonpermissive temperature (Huang et al., 1977; Marshall and Rosenbaum, 2001). The inhibition of IFT results in the reabsorption of full-length cilia, demonstrating the requirement for a continuous supply of axonemal precursors to maintain cilium length (Huang et al., 1977; Kozminski et al., 1995). Consistent with these observations, studies of *Caenorhabditis elegans* sensory cilia have suggested that tubulin and axonemal dynein subunits are also delivered by IFT suggesting a conserved mechanism (Hao et al., 2011; Scholey, 2012). Although the transport of tubulin to the tip of the cilium is known to rely on IFT, it is currently not known whether the IFT complex directly recognizes tubulin as a ciliary cargo or if this occurs via an indirect mechanism, perhaps involving as yet unidentified adaptor proteins.

In an effort to characterize the molecular basis for ciliary cargo recognition by the IFT machinery, we focused on the two IFT-B core proteins IFT74 and IFT81. We show that the N-termini of IFT74 and IFT81 form a module that binds $\alpha\beta$ -tubulin with 1 μ M affinity. This tubulin-binding module is not required for IFT-B complex formation or localization of IFT proteins to cilia, but mutation of tubulin-binding residues results in ciliogenesis defects. Our data support a model where a conserved and dedicated module in IFT74/81 directly binds $\alpha\beta$ -tubulin heterodimers in the cytoplasm and transports these components via IFT to the ciliary tip where they are incorporated into the axoneme.

Results

The N-termini of IFT81 and IFT74 are not required for IFT-B core complex formation

The IFT-B complex is composed of 14 proteins and contains a salt-stable core of 8-9 members (Lucker, 2005). IFT81 and IFT74 are two conserved members of the IFT-B core complex and are believed to form a binding platform for the additional IFT-B proteins (Lucker, 2005; Follit et al., 2009; Lucker et al., 2010; Taschner et al., 2011). Sequence analysis reveals that both IFT74 and IFT81 contain relatively short uncharacterized regions at their N-termini (~120 residues for IFT81N and 80-180 residues for IFT74N) followed by longer (~500 residues) C-terminal domains of predicted coiled-coil structure (Fig. 1A) (Cole, 2003; Jékely and Arendt, 2006). Whereas the N-terminal domain of IFT81 (IFT81N) is highly conserved across species and likely constitutes a small domain, the N-terminus of IFT74 (IFT74N) is not well conserved in sequence and, according to structure prediction programs (Gasteiger et al., 2005), is likely to be disordered (Figs. 1A and S1). Yeast-two-hybrid studies have shown that IFT74 and IFT81 form a heteromeric complex via their coiled-coil domains (Lucker, 2005). Additionally, the IFT74/81 complex is known to interact with the additional IFT-B proteins IFT25/27 and IFT52 (Lucker et al., 2010; Taschner et al., 2011). To test if the N-terminal regions of IFT74/81 are required for IFT-B core complex formation, an N-terminally truncated IFT74 Δ N/81 Δ N complex (IFT74¹²⁸⁻⁶⁴¹ and 81¹³³⁻⁶⁵⁵) from *C.reinhardtii* was co-expressed with IFT25/27 in insect cells and subsequently co-purified. Size exclusion chromatography demonstrated that the interaction between IFT74/81 and IFT25/27 does not require the N-terminal regions of IFT74 and IFT81 (Fig. 1B). To investigate if the truncated IFT25/27/74 Δ N/81 Δ N can form larger IFT-B core complexes, we incubated the

purified complex shown in Fig. 1B with trimeric IFT46/52/70 and isolated a stoichiometric heptameric IFT-B core complex by size exclusion chromatography (Fig. 1C). These results show that only the C-terminal coiled-coil domains of IFT74/81 are required for IFT-B core complex formation and suggest that IFT74N and IFT81N may serve different functions.

The crystal structure of IFT81N reveals a calponin-homology domain

To gain insights into the function of the conserved N-terminal region of IFT81, residues 1-121 of *Homo sapiens* (Hs) IFT81 and 1-126 of CrIFT81 were purified and screened for crystallization (Fig. S2). Purified CrIFT81N yielded crystals diffracting to 2.3Å resolution, which allowed for structure determination (Fig. 2A and Table 1). The structure demonstrates that the CrIFT81N domain adopts a globular fold consisting of four central α -helices surrounded by three connecting α -helices (Fig. 2A). Given the reasonably high degree of sequence conservation between CrIFT81N and HsIFT81N (39% identity and 62% similarity), a homology model for HsIFT81N can be constructed with confidence (Fig. 2B) (Sali, 1995); (<http://salilab.org/modeller/>). Three-dimensional structure searches using the DALI server (Holm and Rosenström, 2010) revealed that IFT81N adopts a calponin-homology (CH) fold, a ~15kDa domain with MT and/or actin binding properties (Gimonaa et al., 2002). When compared to all structures available in the protein data bank, IFT81N displays the highest structural similarity to the CH-domain of MT-binding proteins with NDC80, a kinetochore complex component, as the closest structural homolog (root-mean-square-deviation (rmsd) of 2.6Å for 97 C α atoms, see Fig. 2C) (Wei et al., 2006). The well-characterized plus-end tracking MT-binding protein EB1 can also be superimposed with IFT81N although the overall structural

similarity is not as strong as for NDC80 (rmsd of 3.8Å for 90 C α atoms, Fig. 2D). Lower overall structural similarity is detected with CH-domains of actin-binding proteins (rmsd's of 3.3Å-5.5Å for 90-100 C α atoms). The closest structural homolog of IFT81N with actin-binding properties is the CH-domain of Fimbrin (rmsd of 3.3Å for 95 C α atoms). Most CH-domain-containing actin-binding proteins such as Fimbrin contain two CH-domains that bind actin in tandem (Goldsmith et al., 1997). As only a short linker (residues 122-135) connects the CH-domain to the predicted coiled-coil region, IFT81 is unlikely to contain more than one CH-domain. When compared to NDC80 and EB1, IFT81N has two noticeable structural differences (Fig. 2A-D and F). First, helix $\alpha 3'$ connecting $\alpha 3$ and $\alpha 4$ is considerably longer in IFT81N. Second, the C-terminal helix $\alpha 4$ of IFT81N is sharply bent towards $\alpha 2$ and $\alpha 3$, dividing the longer C-terminal $\alpha 4$ helix found in NDC80 and EB1 into two smaller helices $\alpha 4I$ and $\alpha 4II$. The most C-terminal helix $\alpha 4II$ connects the CH-domain to the coiled coil region of IFT81 through a small flexible linker, of which the first 8 residues are visible in the structure. Although most of $\alpha 4II$ is solvent exposed, the position of this helix is stabilized by several conserved hydrophobic contacts with the $\alpha 2$, $\alpha 3$ and the $\alpha 2$ - $\alpha 3$ connecting loop (highlighted in grey in Fig 2E). The atypical conformation of $\alpha 4II$ is significant as this helix harbors several functionally important residues (see the following sections).

To explore whether the IFT81N CH-domain structure is compatible with MT- and/or actin-binding, the IFT81N structure was superposed onto the molecular structures of CH-domains bound to either MT or F-actin (Fig. S3) (Alushin et al., 2010; Galkin et al., 2010). The results show that the IFT81N structure complements the MT surface well, but clashes significantly with F-actin due to a significantly longer helix $\alpha 3'$

found in the IFT81N structure (Fig. S3). The structural analyses of IFT81N thus point to a potential MT- and/or tubulin-binding function.

IFT81N interacts with MT and $\alpha\beta$ -tubulin but not with actin

As a direct test of the putative filament-binding properties of IFT81N, MT-sedimentation experiments and F-actin pull-down experiments were carried out. GST-tagged HsIFT81N was used to pull-down rabbit skeletal muscle F-actin, followed by Western blot analysis with anti-F-actin antibody (Fig. S4). Consistent with the structural analysis, we did not observe any binding of HsIFT81N to F-actin. Next, we evaluated the ability of IFT81N to bind Mts and $\alpha\beta$ -tubulin heterodimers. MT co-sedimentation assays were carried out with HsIFT81N (residues 1-121) and taxol-stabilized bovine brain MTs. Untagged HsIFT81N at 3 μ M concentration failed to co-sediment with MTs (4 μ M concentration) above background levels, indicating no binding or low binding affinity (Fig. 3A). At higher concentrations (50 μ M GST-tagged HsIFT81N, 6 μ M MT), binding was observed in co-sedimentation experiments by a small fraction of the available IFT81N (Fig. 3B). Consistent with a dissociation constant (K_d) in the double-digit μ M range, GST-IFT81N decorated MTs at 10 μ M but not at 1 μ M concentration, as judged by negative stain electron microscopy (EM) (Fig. 3C).

As IFT81 is known to be a core protein for IFT, a process required for the delivery of tubulin to the tip of the cilium (Marshall and Rosenbaum, 2006; Hao et al., 2011), we were interested to see if IFT81N binds $\alpha\beta$ -tubulin heterodimers. Binding was first evaluated in GSH pull-down assays by combining bovine brain $\alpha\beta$ -tubulin heterodimers with GST-HsIFT81N (Fig 3H). Western blots using anti- α -tubulin

antibody suggested that HsIFT81N binds to $\alpha\beta$ -tubulin, albeit weakly (Fig. 3H, lane 9). To quantify the affinity of the interaction, fluorescently labeled $\alpha\beta$ -tubulin was titrated with untagged HsIFT81N in microscale thermophoresis (MST) assays. The results of these experiments show that HsIFT81N binds $\alpha\beta$ -tubulin with a K_d of $16\pm 2\mu\text{M}$, consistent with the pull-down results (Fig. 3I). The measured affinity is weak when compared to the affinity of NDC80 complex^{Bonsai} towards MTs ($K_d\sim 40$ nM,) (Ciferri et al., 2008) but is comparable to that of the plus end tracking protein EB1 ($K_d\sim 20.3\mu\text{M}$) (Zhu et al., 2009).

IFT81N binds $\alpha\beta$ -tubulin via a patch of conserved positively-charged residues

To investigate the molecular basis for $\alpha\beta$ -tubulin-binding by IFT81N, we sought to identify the residues important for the interaction. Analysis of the molecular surface of the IFT81N structure reveals a prominent basic patch of residues (Fig. 3F). Interestingly, this patch partly overlaps with residues known to be involved in MT-binding by the NDC80 and EB1 CH-domains (Fig. 3E) (Hayashi and Ikura, 2003; Slep and Vale, 2007; Ciferri et al., 2008). The basic patch on IFT81N is formed by conserved K73 and K75 (numbers refer to the HsIFT81 sequence) in the loop connecting helices $\alpha 3$ and $\alpha 3'$ as well as K113, K114 and R115 within the C-terminal $\alpha 4\text{II}$ helix that adopts an unusually bent conformation in IFT81N compared to other CH-domain structures. Additionally, R87 from helix $\alpha 3'$ is found in an equivalent position to K166 of NDC80 (Fig. 3D, 3E), a residue shown to play an important role in MT-binding (Ciferri et al., 2008). All of these 5 basic residues are highly conserved among IFT81 proteins from different species (Fig. 2E and Fig. 3G). Based on these observations, charge-reversal point mutations of HsIFT81N were designed and tested for their ability to bind $\alpha\beta$ -tubulin in pull-down and MST experiments. Whereas the

R87E single point mutation did not affect binding, the K73E/K75E double mutation (mut¹) significantly reduced the affinity towards $\alpha\beta$ -tubulin in pull-down assays (Fig. 3H, lanes 10 and 11). Mutating all of the five residues K73/K75/K113/K114/R115 to glutamates (mut²) resulted in an even stronger reduction in tubulin-binding (Fig. S5). All mutants used in this study were soluble and folded as judged from size exclusion chromatography (Fig. S2). Quantification of binding affinities using MST showed that the HsIFT81Nmut¹ mutant binds $\alpha\beta$ -tubulin with ~12 fold reduced affinity ($K_d=187\pm 37\mu\text{M}$) compared to wild type HsIFT81N (Fig 3J). Together, these experiments demonstrate that the IFT81N-tubulin interaction is specific and occurs via a highly conserved basic patch on IFT81.

IFT74N/81N binds $\alpha\beta$ -tubulin with 1 μM affinity

The experiments described above point to a specific but rather weak binding of IFT81N towards MTs and $\alpha\beta$ -tubulin. The measured affinity of 16 μM for IFT81N towards $\alpha\beta$ -tubulin is likely too low to be physiologically relevant in the context of tubulin IFT. Interestingly, very weak MT-binding is also observed for the isolated NDC80 CH-domain (Ciferri et al., 2008). Robust MT-binding by NDC80 requires a ~100 residue sequence of unstructured and highly basic amino acids located N-terminally to the CH-domain that probably interacts with the acidic C-terminal tails of tubulin (E-hooks). This amino acid stretch is essential for high affinity MT interaction, as its deletion results in ~100 fold weaker binding (Ciferri et al., 2008). Inspection of the IFT81 sequence does not reveal a similar basic region flanking the CH-domain. However, the N-terminus of IFT74, a direct binding partner of IFT81, contains a highly basic stretch of amino acids (Fig. S1). Although the exact position of the basic residues is not well conserved between different organisms, the overall

basic nature of IFT74N is highly conserved with predicted pIs ranging from 12.1-12.6. This basic sequence of IFT74 is variable in length and ranges from ~80 residues in zebrafish to ~180 residues in *C.elegans*. In human IFT74, the N-terminal stretch is ~90 residues long and is predicted to have a pI of 12.6.

Based on these observations we reasoned that IFT74N could be involved in $\alpha\beta$ -tubulin binding, resulting in a significant increase in affinity when compared to IFT81N alone. To test this hypothesis, we carried out binding experiments between $\alpha\beta$ -tubulin and the HsIFT74/81 complex. Since full-length HsIFT74 and HsIFT81 proved to be insoluble when recombinantly co-expressed in *E.coli* or insect cells (data not shown), various truncated versions of the complex encompassing the entire IFT74N and IFT81N regions followed by different coiled-coil lengths were generated and co-expressed in *E.coli*. Co-expression tests demonstrated that HsIFT74¹⁻²⁷² and HsIFT81¹⁻²¹⁵ were soluble and formed a complex (referred to as HsIFT74/81_CC) that remained stable throughout purification (Fig. 4A). Given that IFT74 and IFT81 interact via their naturally occurring dimerization interface in this HsIFT74/81_CC complex, it is reasonable to assume that the IFT74N and IFT81N domains have the same relative orientations as in the native IFT complex. The IFT74/81_CC complex was first tested for its ability to co-sediment with MTs. We observed that 3 μ M of IFT74/81_CC were sufficient to bind MTs at a concentration of 4 μ M (Fig. 4B). Noticeably, this co-sedimentation was observed at concentrations where IFT81N alone did not co-sediment with MT above background levels (compare lane 4 in Fig. 4B to lane 4 in Fig. 3A). In agreement with the co-sedimentation results, we found that the IFT74/81_CC complex substantially decorated MTs at a concentration of 1.5 μ M in negative-stain EM experiments (Fig. 4C). Measurement of the affinity of

IFT74/81_CC towards $\alpha\beta$ -tubulin by MST revealed a dissociation constant of $0.9\pm 0.2\mu\text{M}$ (Fig. 4D), which represents an ~ 18 fold increase in affinity when compared to IFT81N alone. Given the cellular concentration of $\alpha\beta$ -tubulin is in the low μM range (Hiller and Weber, 1978), the measured affinity of $\sim 1\mu\text{M}$ between IFT74/81 and $\alpha\beta$ -tubulin could support IFT of tubulin.

IFT81N binds the globular domain of tubulin whereas IFT74N binds the E-hooks

Since IFT81N is a CH-domain and IFT74N forms a highly basic unstructured sequence, it is reasonable to hypothesize that IFT81N binds the $\alpha\beta$ -tubulin globular domains providing specificity, whereas IFT74N binds the E-hooks to enhance affinity. To test this hypothesis, we prepared protease-treated $\alpha\beta$ -tubulin samples where the acidic tail of β -tubulin or the tails of both α - and β -tubulin were removed (Sackett et al., 1985), and tested the interaction with HsIFT81N in MST experiments (Fig. S6A). Interestingly, core $\alpha\beta$ -tubulin without the C-terminal acidic tails displayed the same affinity for IFT81N as untreated $\alpha\beta$ -tubulin (Figs. 4E and S6B). This suggests that IFT81N recognizes the globular fold of $\alpha\beta$ -tubulin without significantly interacting with the tubulin tails. To evaluate the binding site for IFT74N, MTs were treated with protease to remove the acidic tail of β -tubulin and then used in co-sedimentation assays with IFT74/81_CC. The MT-binding of IFT74/81_CC was reduced to background levels in the absence of the β -tubulin E-hook (Fig. 4F). These data are in agreement with a model where IFT81N binds the core of $\alpha\beta$ -tubulin to provide specificity and IFT74N recognizes the β -tubulin tail to increase affinity (Fig. 4G).

Tubulin-binding of IFT81 is required for ciliogenesis but not for IFT81 localization in human RPE-1 cells

To examine the role of tubulin-binding by IFT81 in a cellular system, we first used transient transfection in U2OS cells. We observed co-localizing of both Flag-HsIFT81 and Flag-HsIFT81 Δ N with or in close proximity to the centriolar marker protein Cep152 (Fig 5A). These results suggest that the N-terminal portion of IFT81 is not required for its localization to the centrosome. To test the impact of the IFT81 tubulin-binding domain on ciliogenesis, we transiently expressed Flag-HsIFT81 or Flag-HsIFT81 Δ N in RPE-1 cells and induced formation of primary cilia either by treatment with 0.5 μ M cytochalasin D or serum starvation. In these experiments, centrioles and cilia were visualized by staining for CAP350 and the small GTPase Arl13b, respectively (Fig. 5B). We detected both Flag-HsIFT81 and Flag-HsIFT81 Δ N at the tip of the primary cilium, and to a minor extent also along the axoneme (Fig S7A), suggesting that the N-terminal part of IFT81 is not required for the transport of IFT81 within the primary cilium. This observation is in agreement with our *in vitro* results demonstrating that stable IFT-B complexes can be assembled using N-terminally truncated IFT81 protein (Fig. 1B-C). Remarkably, however, the expression of Flag-HsIFT81 Δ N had a strong negative impact on the extent of ciliogenesis induced by cytochalasin D treatment (Fig. 5B and C) or serum starvation (Fig. 5D, and data not shown), suggesting that excess IFT81 Δ N caused a dominant-negative effect, presumably through formation of non-functional IFT complexes.

To corroborate the above conclusion and further test the function of the tubulin-binding domain of IFT81 in ciliogenesis, we carried out siRNA-rescue experiments. As expected for a key component of an IFT complex, siRNA-mediated depletion of

IFT81 strongly reduced the percentage of ciliated cells (Fig. 5E-F and Fig. S7B), and this defect could be rescued by co-expression of an siRNA-resistant full-length IFT81 (Fig. 5E-F). In striking contrast, none of the IFT81 mutants shown to be deficient in tubulin-binding *in vitro* (IFT81 Δ N, HsIFT81mut¹, and HsIFT81mut², see Figs. 3H and S5) could fully compensate for the depletion of endogenous IFT81. Whereas expression of the deletion mutant (HsIFT81 Δ N) or the mutant with reduced tubulin binding ability (HsIFT81mut¹) resulted in partial rescue (with about 45-50% of the RPE-1 cells being ciliated; Fig. 5F), expression of HsIFT81mut² in which the entire tubulin-binding patch is mutated, completely failed to rescue the siRNA-mediated knockdown of IFT81 (Fig. 5F). Together, these results demonstrate that the tubulin-binding CH-domain of IFT81 is not needed for IFT81 localization to cilia or its transport within cilia but is required for normal ciliogenesis. These observations are in agreement with our *in vitro* experiments and suggest that the IFT81 CH-domain functions in intraflagellar transport of tubulin.

The affinity between IFT74/81 and tubulin is optimal for the regulation of ciliary length through IFT of tubulin

Intraflagellar transport is known to play a direct role in ciliary length control as partial inhibition of IFT in a *C.reinhardtii* mutant resulted in shorter flagella (Marshall and Rosenbaum, 2001). To assess whether the modulation of tubulin transport is another plausible mechanism for controlling cilium length, we used the measured affinity ($K_d=0.9\mu\text{M}$) to calculate the fraction of IFT complexes bound to $\alpha\beta$ -tubulin as a function of tubulin concentration (Fig. 6A). This calculation predicts that 90% of IFT complexes have tubulin bound when the cellular concentration of free tubulin is $8\mu\text{M}$, whereas only 10% of IFT complexes have tubulin bound at a

tubulin concentration of 0.1 μ M. As the cellular tubulin concentration is estimated to be in the low μ M range (Hiller and Weber, 1978), the affinity to IFT74/81 is thus optimal for such a regulatory mechanism. Tubulin is concentrated at the transition zone fibres emanating from the basal body (Stephan et al., 2007), a location where IFT protein also concentrate (Deane et al., 2001). Furthermore, tubulin expression is induced at the onset of ciliogenesis followed by a gradual decrease in tubulin concentration during cilium growth (Weeks and Collis, 1976; Stephens, 1977; Guttman and Gorovsky, 1979; Silflow, 1981; Stolc et al., 2005). This implies that the tubulin-loading of IFT74/81 is maximal during the early stages of ciliogenesis and may decrease as the cilium elongates and the concentration of free tubulin in the cytoplasm is reduced (Fig. 6B). As a result, less tubulin would be delivered to the tip of the cilium as it continues to grow. Combined with modulating IFT, this mechanism could provide an additional important control of cilium length.

Discussion

An NDC80-like MT/tubulin-binding CH-domain in IFT81

In this paper, we describe the structural and functional characterization of a conserved MT/tubulin-binding module in the intraflagellar transport proteins IFT74 and IFT81. We show that IFT81N contains a CH-domain that recognizes the globular fold of tubulin, whereas IFT74N contains a basic stretch of residues that bind the acidic E-hooks of tubulin. This binding-mode is similar to MT-recognition by the NDC80 complex in spindle assembly during cell division (Ciferri et al., 2008; Alushin et al., 2010), suggesting a common ancestry between NDC80 and IFT81. Indeed, the NDC80 CH-domain is the closest structural homolog of the IFT81 CH-domain present in the protein data bank, and both proteins contain long stretches of coiled-

coil structure C-terminal to the CH-domain. Another striking similarity between the NDC80 and IFT81 CH-domains is that robust MT-binding requires a basic disordered stretch of amino acids (Fig. 3A and 4C) (Ciferri et al., 2008). In NDC80, the basic residues precede the CH-domain, whereas for the IFT81 CH-domain the basic residues are provided by IFT74, a direct binding partner of IFT81. Another important difference between NDC80 and IFT81 is that the NDC80 complex does not interact with soluble tubulin *in vitro* (Ciferri et al., 2008), whereas the IFT74N/81N complex binds tubulin with $\sim 1\mu\text{M}$ affinity (Fig. 4D). The implication of the structural and functional analyses is that the CH-domains of IFT81 and NDC80 evolved from a common ancestor to serve different molecular functions. The molecular basis for the different functionalities likely reside in helices $\alpha 3'$ and $\alpha 4\text{II}$ that harbor MT/tubulin-binding residues and adopt different conformations in IFT81N and NDC80 CH-domains. Interestingly, to our knowledge IFT81N constitutes the first reported CH-domain to bind soluble tubulin, and may thus found a new functional class of CH-domains.

A well-conserved and dedicated tubulin-binding module in the IFT complex

IFT is well-established as the mechanism of assembly for almost all cilia and flagella raising the question of how ciliary proteins are recognized by the IFT-machinery (Ishikawa and Marshall, 2011). Ciliary targeting sequences have been described for some proteins destined for the cilium (Tam et al., 2000; Corbit et al., 2005; Geng et al., 2006; Berbari et al., 2008; Follit et al., 2010) but general ZIP-codes for transport to the cilium have not yet been established. A prime candidate for cargo recognition is the IFT complex, with 20 subunits of which many are predicted to contain protein-protein interaction domains (Cole, 2003). It is therefore surprising that there are no

examples in the literature of well-characterized interactions between IFT proteins and ciliary cargos, likely a reflection of our limited knowledge of IFT proteins at the molecular level. Moreover, it is clear that some cargoes are not directly bound to the IFT complex but associate via adaptor proteins such as Tulp3 (some G-protein coupled receptors) (Mukhopadhyay et al., 2010) or ODA16 (outer dynein arms) (Hou et al., 2007; Ahmed et al., 2008). Whereas some of the less abundant ciliary proteins might compete for the same binding sites on the IFT machinery via similar ciliary targeting sequences, very abundant cargos may have dedicated binding sites. Tubulin is probably the most abundant protein in the cilium, and a robust mechanism is expected for tubulin transport into cilia as it is required for both assembly and maintenance of this organelle. Additionally, since all cilia, whether primary or motile, consist of a MT-based axoneme, the transport of tubulin seems likely to rely on the conserved core machinery of IFT and not on the more variable and species-specific adaptor proteins. Consistent with this hypothesis, we find a specific $\alpha\beta$ -tubulin binding module within the IFT-B core proteins IFT74 and IFT81. This module is conserved from single celled eukaryotes such as *C.reinhardtii* to mammals and is also found in organisms that only require IFT for making primary sensory cilia such as *Drosophila melanogaster* (Vincensini et al., 2012). Additionally, the functional residues forming a basic patch on the IFT81N structure that directly binds tubulin are also highly conserved among different ciliated species (Fig. 2E and 3F-G). These observations support the notion of an ancient IFT74/81 tubulin-binding module, likely present in the first ciliated eukaryotic cell. The fact that CH-domains such as the one present in IFT81 specifically recognize the globular domain of tubulin means that this cargo-binding site is probably dedicated to the transport of tubulin as its sole cargo.

IFT of tubulin as a regulatory mechanism for cilium length control

Axonemal precursors such as tubulin are added to the tip of the cilium in a length-dependent manner (Johnson and Rosenbaum, 1992; Marshall and Rosenbaum, 2001). The removal of tubulin from the axonemal tip on the other hand appears to be constant with no dependence on cilium length (Marshall and Rosenbaum, 2001; Song, 2001). These observations inspired the balance-point model where the length of a mature cilium is the result of equal delivery and removal rates for axonemal precursors (Marshall and Rosenbaum, 2001; Marshall et al., 2005). Several studies have shown that tubulin is up-regulated upon deflagellation followed by a gradual decrease as tubulin subunits are used for axonemal assembly (Weeks and Collis, 1976; Stephens, 1977; Guttman and Gorovsky, 1979; Silflow, 1981; Stolc et al., 2005). Experiments with human cells have revealed a correlation between the available tubulin pool and cilium length. When free tubulin was depleted through stabilization of MTs with the drug taxol, cilium formation was less frequent and cilia grew significantly shorter (Sharma et al., 2011). Conversely, increasing the tubulin pool through MT depolymerization with the drug nocodazole induced the assembly of cilia under serum conditions where ciliogenesis normally does not occur that were twice the length of cilia on untreated cells (Sharma et al., 2011). Interestingly, while the concentration of free tubulin gradually decreases during ciliary assembly, it has been shown that the levels of IFT proteins within cilia remain constant (Marshall et al., 2005; Engel et al., 2009). This fact makes the ciliary assembly rate intrinsically length-dependent because the concentration of IFT complexes travelling base to tip (anterograde), and thus the capacity to deliver cargo to the ciliary tip, decreases as cilium length increases. We propose that the rate of tubulin delivery to the tip is set by two variables: the concentration of anterograde IFT complexes and the tubulin

occupancy of these complexes, which is influenced by the level of free tubulin in the cytoplasm. Indeed, the measured K_d of $\sim 1\mu\text{M}$ between IFT74/81 and tubulin is in the perfect range for such a control mechanism. These two variables may be independent of each other, or they could be coupled. During cilia growth, both anterograde IFT complex concentration and tubulin binding are negatively correlated with cilia length, resulting in a decreasing assembly rate as the cilium approaches steady state length (Fig. 6B-C). Modulation of one or both variables can produce a range of ciliary length phenotypes (Fig. 6D), and compensatory changes may help preserve normal length when either IFT or tubulin binding is compromised.

Further regulation of the IFT of axonemal precursors is likely to occur via post-translational modifications that modulate affinity to the IFT machinery. Tubulin itself is known to undergo a large number of modifications (Janke and Bulinski, 2011), primarily in the acidic C-terminal tail recognized by IFT74, and modifications in this region could thus change binding properties. Recently, the induction of arginine methylation, which is known to affect protein-protein interactions (Bedford and Clarke, 2009), was shown to occur during cilia resorption. The methylation pattern was punctate along the length of the cilium, reminiscent of IFT protein staining, indicating that one or more IFT proteins could be methylated (Schneider et al., 2008; Sloboda and Howard, 2009). Indeed, a protein post-translational modification database (PhosphoSitePlus[®]) search reveals that human IFT74 is methylated at R51 (Hornbeck et al., 2012). This residue is part of the basic IFT74 N-terminus required for the high affinity tubulin binding by IFT74/81 (Fig. 4D). Methylation of R51 may thus interfere with the function of IFT74 by neutralizing the critical positive charge required for binding to tubulin E-hooks (Fig. 4E) and hence may compromise tubulin

transport by the IFT complex. Methylation of IFT81/74 arginines to reduce the affinity for tubulin might thus be a regulatory pathway that is especially active during ciliary resorption, although further studies are required to elucidate its importance.

Materials and methods

Purification and reconstitution of IFT-B complexes

For purification of the *C.reinhardtii* IFT81 Δ N/74 Δ N/His₆-27/25 Δ C complex, insect cells (HighFive, Invitrogen) were infected with baculovirus expressing the complex and grown for 72 hours. Extract preparation was carried out as described previously (Taschner et al., 2011), and the complex purified using a combination of Ni-NTA, ion-exchange (monoQ column) and size exclusion chromatography. Purification of the IFT70/IFT52/IFT46 complex from *E.coli* was performed as described previously (Taschner et al., 2011). Reconstitution of the heptameric IFT81 Δ N/74 Δ N/70/52/46/His₆-27/25 Δ C complex was achieved by mixing equimolar amounts of the IFT81 Δ N/74 Δ N/His₆-27/25 Δ C complex and the IFT70/52/46 complex, followed by Superose6 size exclusion chromatography after an incubation at 4°C for 3 hours.

Protein purification and crystallization

His tagged CrIFT81 (residues 1-126) was expressed in *E.coli* BL21 (DE3) GOLD pLysS strain and lysed in a buffer containing 50mM Tris pH 7.5, 150mM NaCl and 10% glycerol. The protein was purified by Ni-NTA affinity chromatography followed by TEV cleavage to remove the His tag and size exclusion chromatography in a buffer of 10mM HEPES pH 7.5, 150mM NaCl using a superdex 75 or 200 column.

CrIFT81N was concentrated to 20mg/ml and crystallized by vapor diffusion. Crystals of CrIFT81N appeared in 0.8M (NH₄)₂SO₄, 0.1 M Tris pH 8.0 precipitant condition (Fig. S2B). HsIFT81N was purified using the same procedure. Point mutants of HsIFT81N were made using the Quikchange site directed mutagenesis protocol from Agilent Technologies[®] and all the mutants were expressed and purified like the WT protein.

Seleno-methionine (SeMET) labeled His₆-CrIFT81N protein was purified like the native protein but with the addition of 1mM DTT in the purification buffers. The IFT81/74_CC complex was produced by co-expression of His₆-HsIFT81 (residues 1-215) and His₆-HsIFT74 (residues 1-272) in the *E.coli* strain BL21 (DE3) GOLD pLysS. Cells were lysed and the proteins were purified using the same procedure as described above.

X-ray diffraction data collection and structure determination

Crystals of CrIFT81N were flash cooled in liquid nitrogen in mother liquor supplemented with 25% glycerol as a cryoprotectant. Diffraction data were collected at the Swiss light source (SLS, Villigen, Switzerland). The data were processed with the XDS package (Kabsch, 2010). Phases were obtained by single anomalous diffraction (SAD) X-ray diffraction experiments on tantalum bromide (Ta₆Br₁₂) soaked crystals. These crystals diffracted to higher resolution than the native crystals and the experimental phases were calculated using the PHENIX package (Adams et al., 2010). The program BUCCANEER (Cowtan, 2006) was used to automatically build ~80% of the CrIFT81N structure. The model was completed by iterative cycles of manual building in the program COOT (Emsley et al., 2010) and refinement in

PHENIX. The obtained structure was then used as a search model for molecular replacement with native data. Interestingly, the native structure has higher average B factors compared to the structure derivatized with Ta₆Br₁₂ indicating that the intermolecular contacts made by Ta₆Br₁₂ stabilize the CrIFT81N structure.

MT co-sedimentation assays

99% pure Bovine brain tubulin was obtained from Cytoskeleton[®] and MT were polymerized according to the manufacturers instructions. For co-sedimentation experiments, either 3 or 6μM of MTs were pre-incubated with protein (HsIFT81N, HsIFT81N-GST or HsIFT74/81_CC) at room temperature for 30 min in the BRB80 buffer (80mM Pipes-KOH pH 6.8, 1mM EGTA, 2mM MgCl₂) supplemented with 20μM taxol to a final reaction volume of 50 μL. This reaction mixture was then carefully pipetted on to 100 μL of cushion buffer (50% glycerol, 80 mM Pipes-KOH pH 6.8, 2mM MgCl₂, 1mM EGTA) supplemented with 20μM taxol. The resulting solution was centrifuged at 40,000 rpm for 30 min in a Beckmann TLA100 rotor. Supernatants and pellets were analyzed using SDS-PAGE followed by coomassie staining.

Electron microscopy

Taxol-stabilized MTs at a concentration of 2μM were mixed with different concentrations of GST-HsIFT81N or with 1.5μM of HsIFT74/81_CC in 50 μL of BRB80 buffer. The mixture was incubated for 30 min at room temperature and 5μL of this reaction mix were placed onto a glow discharged EM grid followed by 2-3 rounds of washing with BRB80 buffer. The sample was stained using 1% Uranyl

acetate solution. Images were collected using aFEI-CM200 microscope operating at 160 kV at 38,000X magnification corresponding to a pixel size of 2.78Å.

Tubulin co-precipitation assays (pull-assays)

Three μM of tubulin and 10 μM of GST tagged proteins were mixed together in 100 μL of BRB80 buffer and incubated on ice for 30 min. The reaction mixture was then added to 15 μL of pre-blocked GSH beads and incubated on a shaker for 1 hour at 4°C. The beads were washed extensively with the BRB80 buffer and the proteins bound to GSH beads were eluted with 30mM glutathione and analyzed using SDS-PAGE. Actin pulldowns were done using a similar protocol except for the use of lysis buffer rather than BRB80 buffer.

Microscale thermophoresis (MST)

Bovine tubulin was labeled on lysine side-chains using the Cy3 protein labeling kit from Jena Bioscience according to the manufacturers instructions. The average number of lysines labeled per $\alpha\beta$ -tubulin dimer was estimated to be 3.6. Labeled tubulin (a total of 200nM or nmol) were titrated with 0.03-2000 μM of HsIFT81N or HsIFT81Nmut1 and 10-16 thermophoresis measurements were carried out per sample. Each sample was incubated at room temperature for 10 min before measurement. For the HsIFT81/74_CC complex, a lower concentration of 0.003-200 μM was used. Thermophoresis measurements were carried out using the NanoTemper Monolith NT.115 instrument (NanoTemper Technologies GmbH) using 50% LED and 65% laser power with the laser on for 40 sec followed by an off period of 10 sec. The resulting raw data were analysed using the NanoTemper software to obtain binding curves.

Subtilisin treatment of tubulin/microtubules

Eight μM of preformed and taxol stabilized MTs were mixed with $1.25\mu\text{M}$ of subtilisin in BRB80 buffer containing $20\mu\text{M}$ taxol in a total volume of $50\mu\text{L}$. This reaction mixture was incubated at 30°C for 30 min and the proteolysis stopped by adding 1mM PMSF. Proteolysed MTs were spun at 40.000 rpm for 30 min in a Beckmann TLA100 rotor and the pellet re-dissolved in BRB80 buffer supplemented with $20\mu\text{M}$ taxol. For the subtilisin treatment of soluble tubulin, $25\mu\text{M}$ of tubulin were mixed with $1.25\mu\text{M}$ of subtilisin in a total of $120\mu\text{L}$ of BRB80 buffer. The solution was divided into two equal halves and incubated at 30°C for 30 and 120 min, respectively, followed by the addition of 1mM PMSF.

Cell culture and transfections

The RPE-1 and U2OS cells were cultured as previously described (Schmidt et al., 2009). For transient gene expression, cells were transfected with TransIT-LT1 (Mirus) according manufacturers instructions with pcDNA3.1-IFT81 F.L. and pcDNA3.1-IFT81 ΔN (human IFT81 sequences). For the rescue experiments, RNAi resistant plasmid was generated by making silent mutations in the siRNA spanning regions of IFT81 gene and subsequent cloning of this construct into pcDNA5.1 vector. This RNAi resistant pcDNA5.1-IFT81 F.L. plasmid was further used to generate the rescue plasmids with point and deletion mutations (mut¹, mut² and ΔN). In case of the rescue experiment, the RPE-1 cells were first transfected with control (GL2) or IFT81 siRNA (GGATATCAGTGCAATGGAA and CAGCTCATTAAGAGAGTT GAA, each at $50\mu\text{M}$) using Oligofectamine (Invitrogen) according manufacturers recommendations. Cells were subsequently

nucleofected with pcDNA5.1-IFT81 (F.L or mut1 or mut2 or Δ N) rescue plasmids using Amaxa 4D-Nucleofector (Lonza) and the DS137 program, 48h after the siRNA transfection. Following the plasmid transfection, the formation of primary cilia in RPE-1 cells was induced either by 0.5 μ M Cytochalasin D (Sigma) or by changing into serum-free media for 24h.

Immunofluorescence and microscopy

Cells grown on coverslips were washed with PBS and fixed in methanol (-20°C/5min). In case of the detection of acetylated tubulin, cells were cold treated (+4°C/30min) prior the methanol fixation. Blocking, incubation with primary and secondary antibodies, and washing were done as described before (Schmidt et al., 2009). The following primary and secondary antibodies were used: mouse anti-acetylated tubulin (6-11B-1, Sigma), rabbit anti-Arl13b (17711, Proteintech), mouse anti-Flag (M2, Sigma), rabbit anti-Flag (F7425, Sigma), rat anti-IFT81, goat anti-CAP350 (Yan et al., 2006), rabbit anti-Cep135 (Kleylein-Sohn et al., 2007) (both Alexa 647-labeled), rabbit anti-Cep152 (Sonnen et al., 2012)(Alexa 555-labeled), Alexa 488 anti-mouse, Alexa 488 anti-rabbit, Alexa 555 anti-mouse , Alexa 555 anti-rabbit (all from Invitrogen), and Cy2 anti-rat (Jackson Immuno Research). Direct labeling of primary antibodies was done with the Alexa-antibody labeling kit (Invitrogen). Coverslips were mounted on slides using Glycergel (Dako). Wide-field imaging was performed on a DeltaVision system (Applied Precision) with a 60x/1.2 or 100x/1.4 Apo plan oil immersion objective. Image stacks were taken with a z-distance of 0.2 μ m, deconvolved (conservative ratio, 3-5 cycles) and projected as maximal intensity image using SoftWoRX (Applied Precision). For cell counts, at

least 50 transfected cells per condition and experiment were analyzed for the presence/absence of primary cilia.

Statistical analyses

Statistical analyses (Students t-test, one-way ANOVA with Bonferroni's multiple comparison test) were performed using Prism 4 (GraphPad Software). $p < 0.05$ was considered as statistically significant difference (*), $p < 0.01$ (**), $p < 0.001$ (***). Results are presented as mean plus standard error of the mean (SEM).

Acknowledgements

We thank the staff at SLS for help with X-ray diffraction data collection, the crystallization facility of the Max Planck Institute of Biochemistry (Munich) for access to crystallization screening, the staff at Biozentrum Imaging Core Facility for assistance, Dr. Christophe Jung for help with MST. We also thank Atlanta Cook, Sutapa Chakrabarti and Ben Engel for carefully reading and correcting the manuscript. We acknowledge Michaela Morawetz and Marc Stiegler for technical assistance with molecular biology. This work was funded by an Emmy Noether grant (DFG; LO1627/1-1), the European Research Council (ERC grant 310343) and by the EMBO Young Investigator program. E.A.N. acknowledges support from the University of Basel and the Swiss National Science Foundation [31003A_132428/1]. M.T is the recipient of an Erwin-Schroedinger-stipend granted by the Austrian Science Fund J3148-B12, S.B was supported by the International Max Planck Research School for Molecular and Cellular Life Sciences (IMPRS) and L.C. was supported by the FEBS long-term fellowship.

References

- Adams, P.D., Afonine, P.V., Bunkóczi, G., Chen, V.B., Davis, I.W., Echols, N., Headd, J.J., Hung, L.-W., Kapral, G.J., Grosse-Kunstleve, R.W., et al. (2010). PHENIX: a comprehensive Python-based system for macromolecular structure solution. *Acta Crystallogr D Biol Crystallogr* 66, 213–221.
- Ahmed, N.T., Gao, C., Lucker, B.F., Cole, D.G., and Mitchell, D.R. (2008). ODA16 aids axonemal outer row dynein assembly through an interaction with the intraflagellar transport machinery. *The Journal of Cell Biology* 183, 313–322.
- Alushin, G.M., Ramey, V.H., Pasqualato, S., Ball, D.A., Grigorieff, N., Musacchio, A., and Nogales, E. (2010). The Ndc80 kinetochore complex forms oligomeric arrays along microtubules. *Nature* 467, 805–810.
- Bedford, M.T., and Clarke, S.G. (2009). Protein arginine methylation in mammals: who, what, and why. *Mol Cell* 33, 1–13.
- Berbari, N.F., Johnson, A.D., Lewis, J.S., Askwith, C.C., and Mykytyn, K. (2008). Identification of ciliary localization sequences within the third intracellular loop of G protein-coupled receptors. *Mol Biol Cell* 19, 1540–1547.
- Bornens, M. (2012). The Centrosome in Cells and Organisms. *Science* 335, 422–426.
- Buisson, J., Chenouard, N., Lagache, T., Blisnick, T., Olivo-Marin, J.-C., and Bastin, P. (2012). Intraflagellar transport proteins cycle between the flagellum and its base. *Journal of Cell Science* 1–50.
- Ciferri, C., Pasqualato, S., Screpanti, E., Varetta, G., Santaguida, S., Reis, Dos, G., Maiolica, A., Polka, J., De Luca, J.G., De Wulf, P., et al. (2008). Implications for kinetochore-microtubule attachment from the structure of an engineered Ndc80 complex. *Cell* 133, 427–439.
- Cole, D.G. (2003). The intraflagellar transport machinery of *Chlamydomonas reinhardtii*. *Traffic* 4, 435–442.
- Cole, D.G., Diener, D.R., Himelblau, A.L., Beech, P.L., Fuster, J.C., and Rosenbaum, J.L. (1998). *Chlamydomonas* kinesin-II-dependent intraflagellar transport (IFT): IFT particles contain proteins required for ciliary assembly in *Caenorhabditis elegans* sensory neurons. *Journal of Cell Biology* 141, 993–1008.
- Corbit, K.C., Aanstad, P., Singla, V., Norman, A.R., Stainier, D.Y.R., and Reiter, J.F. (2005). Vertebrate Smoothed functions at the primary cilium. *Nature* 437, 1018–1021.
- Cowtan, K. (2006). The Buccaneer software for automated model building. 1. Tracing protein chains. *Acta Crystallogr D Biol Crystallogr* 62, 1002–1011.
- Deane, J.A., Cole, D.G., Seeley, E.S., Diener, D.R., and Rosenbaum, J.L. (2001). Localization of intraflagellar transport protein IFT52 identifies basal body

transitional fibers as the docking site for IFT particles. *Current Biology* 11, 1586–1590.

Emsley, P., Lohkamp, B., Scott, W.G., and Cowtan, K. (2010). Features and development of Coot. *Acta Crystallogr D Biol Crystallogr* 66, 486–501.

Engel, B.D., Ishikawa, H., Wemmer, K.A., Geimer, S., Wakabayashi, K.I., Hirono, M., Craige, B., Pazour, G.J., Witman, G.B., Kamiya, R., et al. (2012). The role of retrograde intraflagellar transport in flagellar assembly, maintenance, and function. *The Journal of Cell Biology* 199, 151–167.

Engel, B.D., Ludington, W.B., and Marshall, W.F. (2009). Intraflagellar transport particle size scales inversely with flagellar length: revisiting the balance-point length control model. *The Journal of Cell Biology* 187, 81–89.

Fliegauf, M., Benzing, T., and Omran, H. (2007). When cilia go bad: cilia defects and ciliopathies. *Nat Rev Mol Cell Biol* 8, 880–893.

Follit, J. A., Li, L., Vucica, Y., & Pazour, G. J. (2010). The cytoplasmic tail of fibrocystin contains a ciliary targeting sequence. *The Journal of Cell Biology*, 188(1), 21–28.

Follit, J.A., Xu, F., Keady, B.T., and Pazour, G.J. (2009). Characterization of mouse IFT complex B. *Cell Motil. Cytoskeleton* 66, 457–468.

Galkin, V.E., Orlova, A., Salmazo, A., Djinovic-Carugo, K., and Egelman, E.H. (2010). Opening of tandem calponin homology domains regulates their affinity for F-actin. *Nat Struct Mol Biol* 17, 614–616.

Gasteiger, E., Hoogland, C., Gattiker, A., Duvaud, S., Wilkins, M.R., Appel, R.D., and Bairoch, A. (2005). Protein Identification and Analysis Tools on the ExPASy Server. (Totowa, NJ: Humana Press), pp. 571–607.

Geng, L., Okuhara, D., Yu, Z., Tian, X., Cai, Y., Shibasaki, S., and Somlo, S. (2006). Polycystin-2 traffics to cilia independently of polycystin-1 by using an N-terminal RVxP motif. *Journal of Cell Science* 119, 1383–1395.

Gimona, M., Djinovic-Carugob, K., & Kranewittera, W. J. (2002). Functional plasticity of CH domains. *FEBS Letters*, 513, 98–106.

Goldsmith, S.C., Pokala, N., Shen, W., Fedorov, A.A., Matsudaira, P., and Almo, S.C. (1997). The structure of an actin-crosslinking domain from human fimbrin. *Nat. Struct. Biol.* 4, 708–712.

Gönczy, P. (2012). Towards a molecular architecture of centriole assembly. *Nat Rev Mol Cell Biol* 13, 425–435.

Guttman, S.D., and Gorovsky, M.A. (1979). Cilia regeneration in starved tetrahymena: an inducible system for studying gene expression and organelle biogenesis. *Cell* 17, 307–317.

Hao, L., Thein, M., Brust-Mascher, I., Civelekoglu-Scholey, G., Lu, Y., Acar, S., Prevo, B., Shaham, S., and Scholey, J.M. (2011). Intraflagellar transport delivers tubulin isoforms to sensory cilium middle and distal segments. *Nature* *13*, 790–798.

Hayashi, I., and Ikura, M. (2003). Crystal structure of the amino-terminal microtubule-binding domain of end-binding protein 1 (EB1). *J Biol Chem* *278*, 36430–36434.

Hildebrandt, F., Benzing, T., and Katsanis, N. (2011). Ciliopathies. *N. Engl. J. Med.* *364*, 1533–1543.

Hiller, G., and Weber, K. (1978). Radioimmunoassay for tubulin: a quantitative comparison of the tubulin content of different established tissue culture cells and tissues. *Cell* *14*, 795–804.

Holm, L., and Rosenström, P. (2010). Dali server: conservation mapping in 3D. *Nucleic Acids Research* *38*, W545–W549.

Hornbeck, P.V., Kornhauser, J.M., Tkachev, S., Zhang, B., Skrzypek, E., Murray, B., Latham, V., and Sullivan, M. (2012). PhosphoSitePlus: a comprehensive resource for investigating the structure and function of experimentally determined post-translational modifications in man and mouse. *Nucleic Acids Research* *40*, D261–D270.

Hou, Y., Pazour, G.J., and Witman, G.B. (2004). A dynein light intermediate chain, D1bLIC, is required for retrograde intraflagellar transport. *Mol Biol Cell* *15*, 4382–4394.

Hou, Y., Qin, H., Follit, J.A., Pazour, G.J., Rosenbaum, J.L., and Witman, G.B. (2007). Functional analysis of an individual IFT protein: IFT46 is required for transport of outer dynein arms into flagella. *The Journal of Cell Biology* *176*, 653–665.

Huang, B., Rifkin, M.R., and Luck, D.J. (1977). Temperature-sensitive mutations affecting flagellar assembly and function in *Chlamydomonas reinhardtii*. *Journal of Cell Biology* *72*, 67–85.

Ishikawa, H., and Marshall, W.F. (2011). Ciliogenesis: building the cell's antenna. *Nat Rev Mol Cell Biol* *12*, 222–234.

Janke, C., and Bulinski, J.C. (2011). Post-translational regulation of the microtubule cytoskeleton: mechanisms and functions. *Nat Rev Mol Cell Biol* *12*, 773–786.

Jékely, G., and Arendt, D. (2006). Evolution of intraflagellar transport from coated vesicles and autogenous origin of the eukaryotic cilium. *Bioessays* *28*, 191–198.

Johnson, K. A., & Rosenbaum, J. L. (1992). Polarity of flagellar assembly in *Chlamydomonas*. *The Journal of Cell Biology*, *119*(6), 1605–1611.

Kabsch, W. (2010). XDS. *Acta Crystallographica Section D: Biological*

Crystallography, 66(2), 125–132.

Kleylein-Sohn, J., Westendorf, J., Le Clech, M., Habedanck, R., Stierhof, Y.-D., and Nigg, E.A. (2007). Plk4-induced centriole biogenesis in human cells. *Dev Cell* 13, 190–202.

Kozminski, K.G., Beech, P.L., and Rosenbaum, J.L. (1995). The *Chlamydomonas* kinesin-like protein FLA10 is involved in motility associated with the flagellar membrane. *Journal of Cell Biology* 131, 1517–1527.

Kozminski, K.G., Johnson, K.A., Forscher, P., and Rosenbaum, J.L. (1993). A motility in the eukaryotic flagellum unrelated to flagellar beating. *Proc Natl Acad Sci USA* 90, 5519–5523.

L'Hernault, S.W., and Rosenbaum, J.L. (1985). Reversal of the posttranslational modification on *Chlamydomonas* flagellar alpha-tubulin occurs during flagellar resorption. *Journal of Cell Biology* 100, 457–462.

Lucker, B.F. (2005). Characterization of the Intraflagellar Transport Complex B Core: DIRECT INTERACTION OF THE IFT81 AND IFT74/72 SUBUNITS. *Journal of Biological Chemistry* 280, 27688–27696.

Lucker, B. F., Miller, M. S., Dziedzic, S.A., Blackmarr, P.T., & Cole, D. G. (2010). Direct interactions of intraflagellar transport complex B proteins IFT88, IFT52, and IFT46. *JBC*, 285(28), 21508–21518.

Ludington, W. B., Wemmer, K. A., Lehtreck, K. F., Witman, G. B., & Marshall, W. F. (2013). Avalanche-like behavior in ciliary import. *Proceedings of the National Academy of Sciences of the United States of America*, 110(10), 3925–3930.

Marshall, W.F., and Rosenbaum, J.L. (2001). Intraflagellar transport balances continuous turnover of outer doublet microtubules: implications for flagellar length control. *Journal of Cell Biology* 155, 405–414.

Marshall, W.F., Qin, H., Rodrigo Brenni, M., and Rosenbaum, J.L. (2005). Flagellar length control system: testing a simple model based on intraflagellar transport and turnover. *Mol Biol Cell* 16, 270–278.

Mukhopadhyay, S., Wen, X., Chih, B., Nelson, C.D., Lane, W.S., Scales, S.J., and Jackson, P.K. (2010). TULP3 bridges the IFT-A complex and membrane phosphoinositides to promote trafficking of G protein-coupled receptors into primary cilia. *Genes & Development* 24, 2180–2193.

Nigg, E.A., and Raff, J.W. (2009). Centrioles, centrosomes, and cilia in health and disease. *Cell* 139, 663–678.

Pazour, G.J., Dickert, B.L., and Witman, G.B. (1999). The DHC1b (DHC2) isoform of cytoplasmic dynein is required for flagellar assembly. *Journal of Cell Biology* 144, 473–481.

Pazour, G.J., Dickert, B.L., Vucica, Y., Seeley, E.S., Rosenbaum, J.L., Witman, G.B.,

- and Cole, D.G. (2000). Chlamydomonas IFT88 and its mouse homologue, polycystic kidney disease gene tg737, are required for assembly of cilia and flagella. *Journal of Cell Biology* 151, 709–718.
- Pedersen, L.B., Geimer, S., and Rosenbaum, J.L. (2006). Dissecting the molecular mechanisms of intraflagellar transport in chlamydomonas. *Current Biology* 16, 450–459.
- Perrone, C.A., Tritschler, D., Taulman, P., Bower, R., Yoder, B.K., and Porter, M.E. (2003). A novel dynein light intermediate chain colocalizes with the retrograde motor for intraflagellar transport at sites of axoneme assembly in chlamydomonas and Mammalian cells. *Mol Biol Cell* 14, 2041–2056.
- Piperno, G., Siuda, E., Henderson, S., Segil, M., Vaananen, H., and Sassaroli, M. (1998). Distinct mutants of retrograde intraflagellar transport (IFT) share similar morphological and molecular defects. *The Journal of Cell Biology* 143, 1591–1601.
- Porter, M.E., Bower, R., Knott, J.A., Byrd, P., and Dentler, W. (1999). Cytoplasmic dynein heavy chain 1b is required for flagellar assembly in Chlamydomonas. *Mol Biol Cell* 10, 693–712.
- Rosenbaum, J.L., and Witman, G.B. (2002). Intraflagellar transport. *Nat Rev Mol Cell Biol* 3, 813–825.
- Sackett, D.L., Bhattacharyya, B., and Wolff, J. (1985). Tubulin subunit carboxyl termini determine polymerization efficiency. *J Biol Chem* 260, 43–45.
- Sali, A. (1995). Comparative protein modeling by satisfaction of spatial restraints. *Molecular Medicine Today*, 1(6), 270–277.
- Schmidt, T.I., Kleylein-Sohn, J., Westendorf, J., Le Clech, M., Lavoie, S.B., Stierhof, Y.-D., and Nigg, E.A. (2009). Control of centriole length by CPAP and CP110. *Curr Biol* 19, 1005–1011.
- Schneider, M. J., Ulland, M., & Sloboda, R. D. (2008). A Protein Methylation Pathway in Chlamydomonas Flagella Is Active during Flagellar Resorption. *Molecular biology of the cell*, 19, 4319–4327.
- Scholey, J.M. (2012). Kinesin-2 motors transport IFT-particles, dyneins and tubulin subunits to the tips of Caenorhabditis elegans sensory cilia: Relevance to vision research? *Vision Res* 75, 44–52.
- Sharma, N., Kosan, Z.A., Stallworth, J.E., Berbari, N.F., and Yoder, B.K. (2011). Soluble levels of cytosolic tubulin regulate ciliary length control. *Mol Biol Cell* 22, 806–816.
- Silflow, C. (1981). Multiple α - and β -tubulin genes in chlamydomonas and regulation of tubulin mRNA levels after deflagellation. *Cell* 24, 81–88.
- Slep, K.C., and Vale, R.D. (2007). Structural basis of microtubule plus end tracking

by XMAP215, CLIP-170, and EB1. *Mol Cell* 27, 976–991.

Sloboda, R. D., & Howard, L. (2009). Protein methylation in full length *Chlamydomonas* flagella. *Cell Motility and the Cytoskeleton*, 66(8), 650–660.

Song, L. (2001). Flagellar Protein Dynamics in *Chlamydomonas*. *Journal of Biological Chemistry* 276, 29754–29763.

Sonnen, K.F., Schermelleh, L., Leonhardt, H., and Nigg, E.A. (2012). 3D-structured illumination microscopy provides novel insight into architecture of human centrosomes. *Biol Open* 1, 965–976.

Stephan, A., Vaughan, S., Shaw, M.K., Gull, K., and McKean, P.G. (2007). An Essential Quality Control Mechanism at the Eukaryotic Basal Body Prior to Intraflagellar Transport. *Traffic* 8, 1323–1330.

Stephens, R. E. (1977). Differential protein synthesis and utilization during cilia formation in sea urchin embryos. *Developmental Biology*, 61(2), 311–329.

Stephens, R.E. (1997). Synthesis and turnover of embryonic sea urchin ciliary proteins during selective inhibition of tubulin synthesis and assembly. *Mol Biol Cell* 8, 2187–2198.

Stephens, R.E. (2000). Preferential incorporation of tubulin into the junctional region of ciliary outer doublet microtubules: a model for treadmilling by lattice dislocation. *Cell Motil. Cytoskeleton* 47, 130–140.

Stolc, V., Samanta, M.P., Tongprasit, W., and Marshall, W.F. (2005). Genome-wide transcriptional analysis of flagellar regeneration in *Chlamydomonas reinhardtii* identifies orthologs of ciliary disease genes. *Proc Natl Acad Sci USA* 102, 3703–3707.

Tam, B.M., Moritz, O.L., Hurd, L.B., and Papermaster, D.S. (2000). Identification of an outer segment targeting signal in the COOH terminus of rhodopsin using transgenic *Xenopus laevis*. *The Journal of Cell Biology* 151, 1369–1380.

Taschner, M., Bhogaraju, S., Vetter, M., Morawetz, M., and Lorentzen, E. (2011). Biochemical Mapping of Interactions within the Intraflagellar Transport (IFT) B Core Complex: IFT52 BINDS DIRECTLY TO FOUR OTHER IFT-B SUBUNITS. *Journal of Biological Chemistry* 286, 26344–26352.

Tilney, L.G., and Gibbins, J.R. (1968). Differential effects of antimitotic agents on the stability and behavior of cytoplasmic and ciliary microtubules. *Protoplasma* 65, 167–179.

Tucker, R.W., Scher, C.D., and Stiles, C.D. (1979). Centriole deciliation associated with the early response of 3T3 cells to growth factors but not to SV40. *Cell* 18, 1065–1072.

Vincensini, L., Blisnick, T., and Bastin, P. (2012). 1001 model organisms to study cilia and flagella. *Biol. Cell* 103, 109–130.

- Walther, Z., Vashishtha, M., and Hall, J.L. (1994). The *Chlamydomonas* FLA10 gene encodes a novel kinesin-homologous protein. *Journal of Cell Biology* 126, 175–188.
- Wang, Z., Fan, Z.-C., Williamson, S.M., and Qin, H. (2009). Intraflagellar Transport (IFT) Protein IFT25 Is a Phosphoprotein Component of IFT Complex B and Physically Interacts with IFT27 in *Chlamydomonas*. *PLoS ONE* 4, e5384.
- Webster, D.R., and Borisy, G.G. (1989). Microtubules are acetylated in domains that turn over slowly. *Journal of Cell Science* 92 (Pt 1), 57–65.
- Weeks, D.P., and Collis, P.S. (1976). Induction of microtubule protein synthesis in *Chlamydomonas reinhardi* during flagellar regeneration. *Cell* 9, 15–27.
- Wei, R. R., Al-Bassam, J., & Harrison, S. C. (2006). The Ndc80/HEC1 complex is a contact point for kinetochore-microtubule attachment. *Nature Structural & Molecular Biology*, 14(1), 54–59.
- Yan, X., Habedanck, R., and Nigg, E.A. (2006). A complex of two centrosomal proteins, CAP350 and FOP, cooperates with EB1 in microtubule anchoring. *Mol Biol Cell* 17, 634–644.
- Zhu, Z.C., Gupta, K.K., Slabbekoorn, A.R., Paulson, B.A., Folker, E.S., and Goodson, H.V. (2009). Interactions between EB1 and Microtubules.

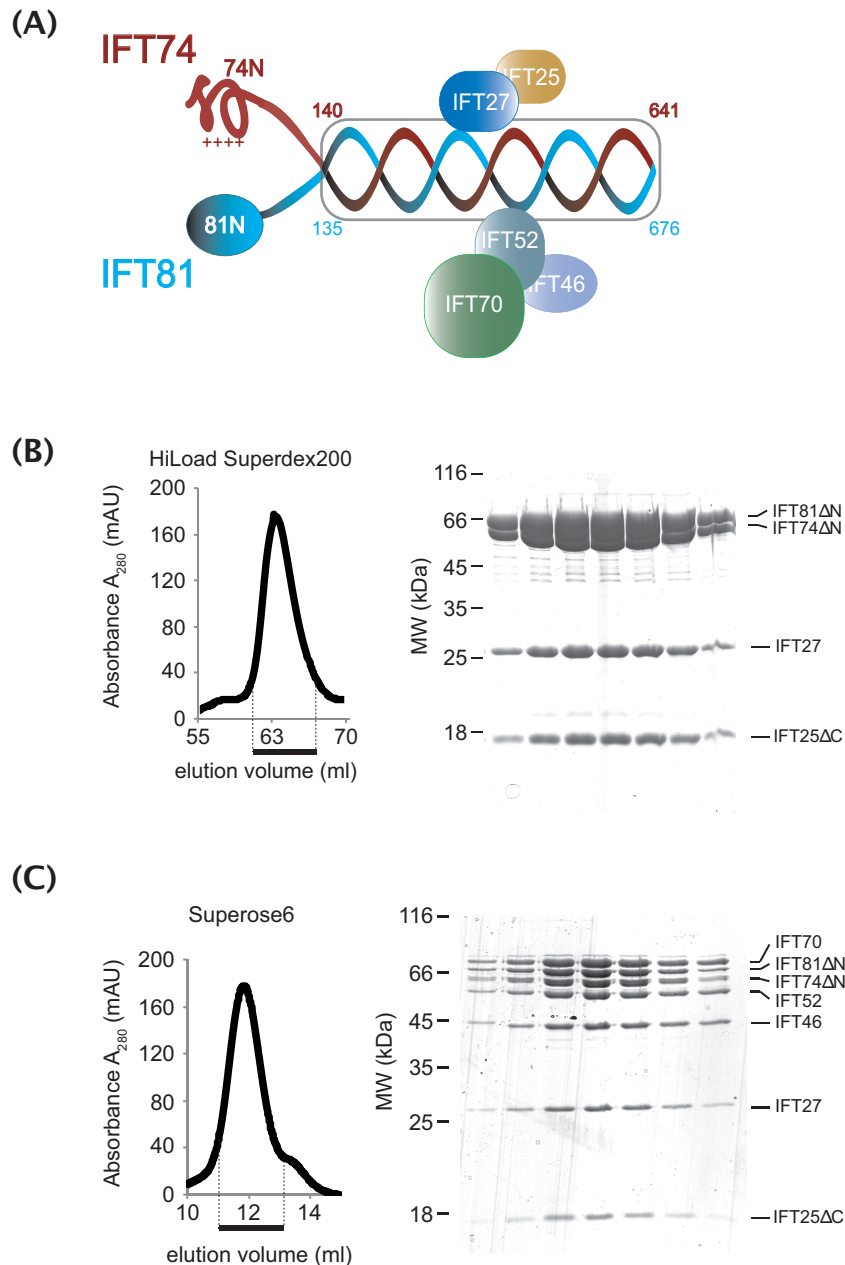


Figure 1: The N-terminal domains of IFT74 and IFT81 are not required for IFT-B core complex formation. **(A)** Schematics of the IFT-B core complex with 7 of the 9 core subunits depicted. The schematics illustrate that both the IFT25/27 and the IFT46/52/70 sub-complexes associate with the coiled coil regions of IFT74/81. **(B)** Chromatogram from size exclusion purification (left) and associated coomassie-stained SDS-PAGE gel of the indicated peak fraction (right) for purified *C.reinhardtii* IFT25DC/27/74DN/81DN complex lacking the N-terminal regions of IFT74 and IFT81. **(C)** Purification of a heptameric IFT-B core complex obtained by mixing the tetramer shown in (B) with a trimeric IFT46/52/70 complex followed by purification using size exclusion chromatography. The results show that IFT74N and IFT81N are dispensable for complex formation with IFT25/27 and IFT46/52/70.

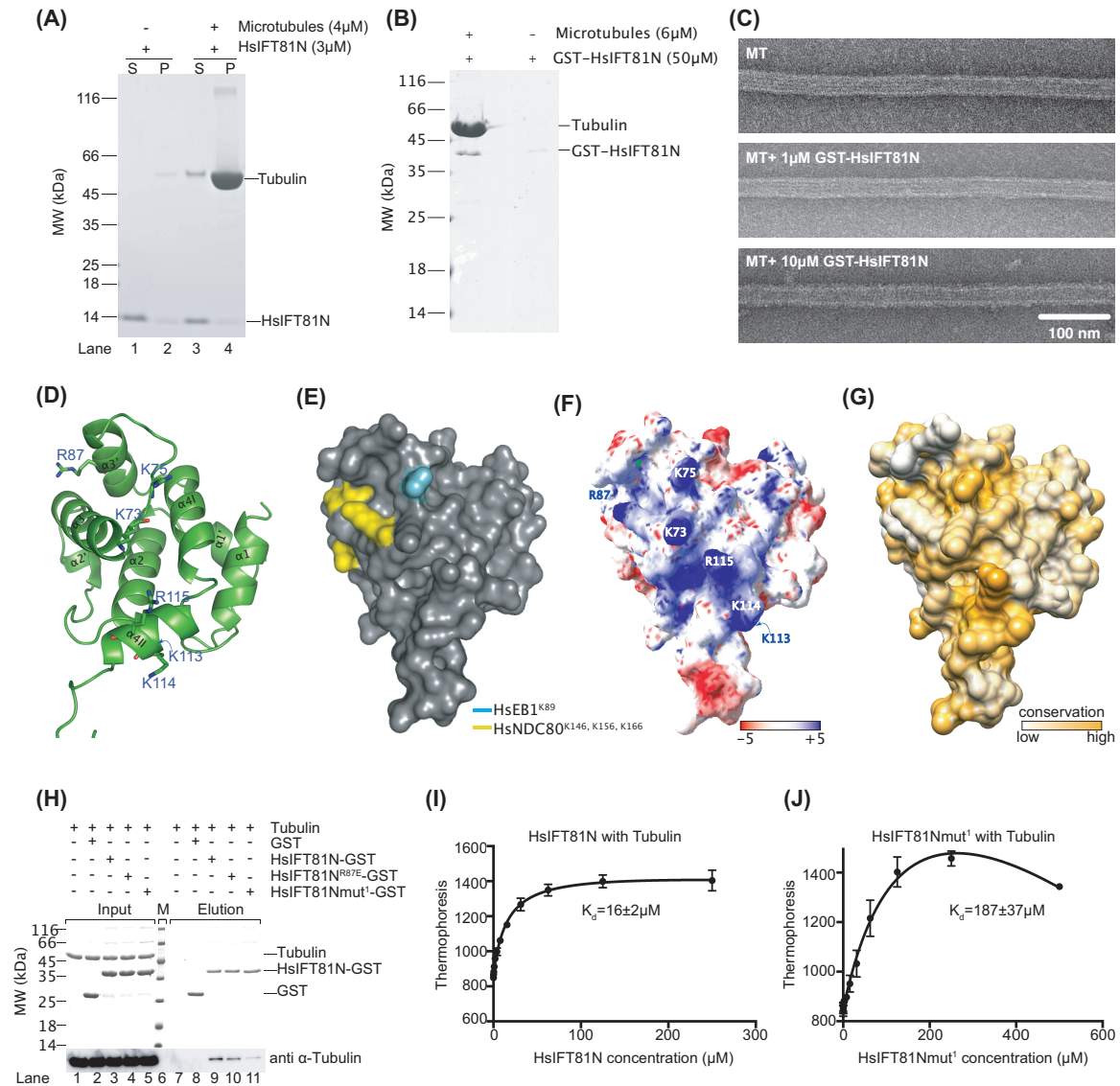


Figure 3: IFT81N binds tubulin via a conserved positively-charged patch. **(A)** MT-sedimentation assay with HsIFT81N and subsequent SDS-PAGE analysis of the supernatant (S) and the pellet (P) reveal only background levels of HsIFT81N co-sedimenting with MT. **(B)** At higher concentrations, a significant amount of GST-HsIFT81N co-sediments with MTs although the band intensity indicates only weak binding. **(C)** Negative-stain EM of taxol stabilized MT alone (top panel) and incubated with either 1 mM (middle) or 10 mM (bottom) GST-HsIFT81N demonstrating decoration only at the higher protein concentration. **(D)** Cartoon representation of the CrIFT81N domain in the same orientation as Figure 2A with conserved lysines and arginines implicated in tubulin/MT-binding shown as sticks. **(E)** Surface representation of the IFT81N structure with the characterized MT-binding residues of NDC80 and EBI colored in yellow and cyan, respectively. **(F)** Electrostatic surface potential of IFT81N displaying the positively-charged patch with the residues labelled according to the HsIFT81 sequence. **(G)** Surface conservation of IFT81N demonstrates that the basic patch is well conserved among different species. **(H)** Tubulin-binding evaluated by GSH affinity pull-down of *ab*-tubulin using GST-HsIFT81N. Whereas tubulin does not bind the GSH-beads and is not pulled down by GST alone, a significant portion is pulled down by GST-HsIFT81N demonstrating binding. Whereas the single point mutation R87E does not significantly impair binding, the K73K75/EE double mutant (*mut*¹) results in reduced amounts of pulled-down tubulin indicating reduced binding. **(I)** Quantification of tubulin

binding to untagged HsIFT81N by microscale thermophoresis reveals a K_d of 16mM. (J) The HsIFT81N mut^I has significantly reduced binding with a K_d of 187mM showing that the basic patch is required for tubulin binding. The curves in (I) and (J) are calculated for 3 independent experiments and the error bars represent the standard deviation.

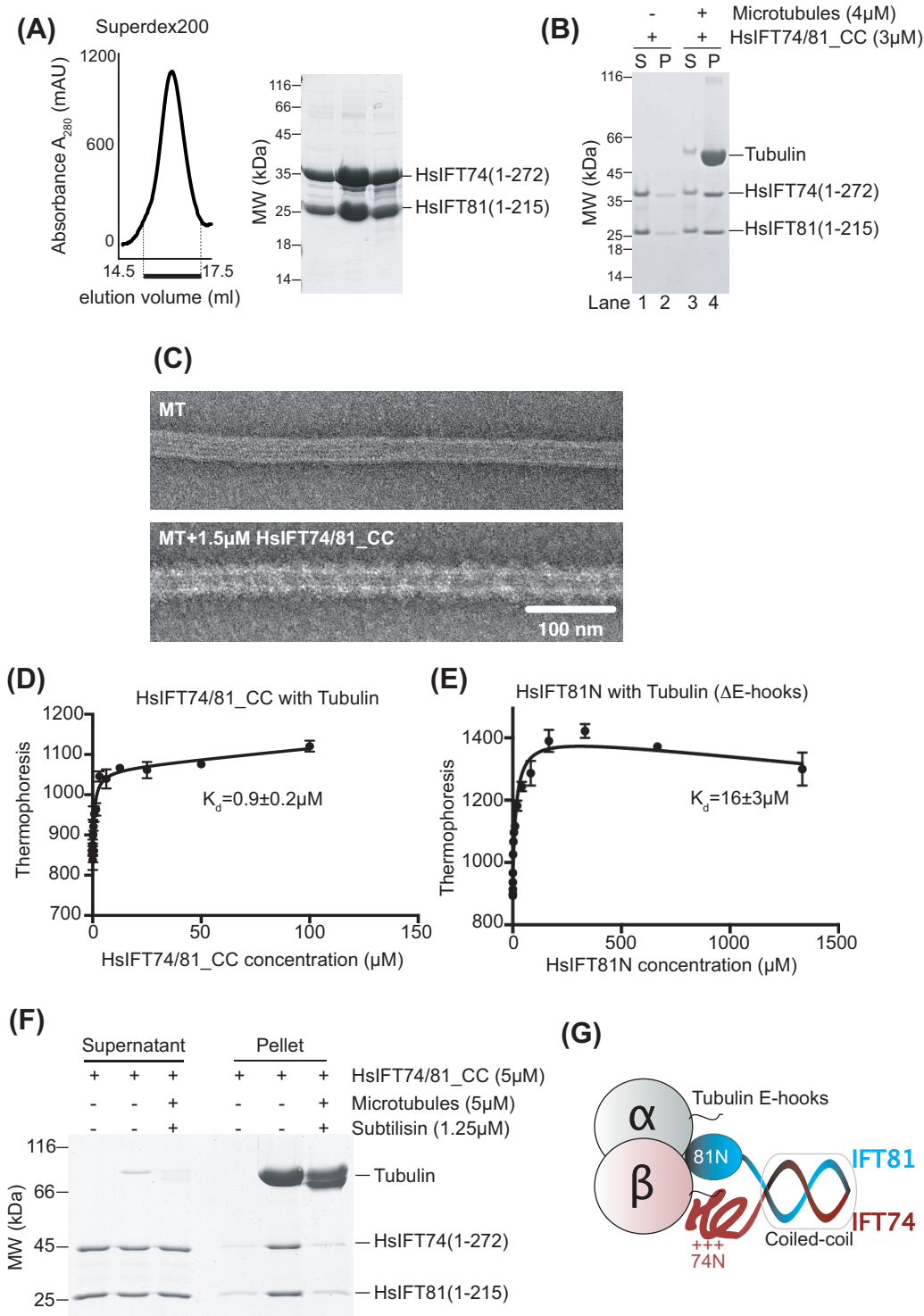


Figure 4: IFT74 increases the affinity of IFT81 towards tubulin by 18-fold (A) Purification of truncated HsIFT74/81 complex (HsIFT7481_CC) by size exclusion chromatography. The complex contains all of the N-terminal domains and a sufficient portion of the coiled-coil domains to form a stable interaction. (B) MT-sedimentation of the HsIFT74/81_CC complex shown in (A) demonstrates interaction with MT at low mM concentration (S=supernatant and P=pellet). (C) Negative stain EM of taxol stabilized MT incubated with 1.5 μ M of HsIFT74/81_CC complex, showing a thick decoration of microtubules (D) Microscale thermophoresis titration of tubulin with HsIFT7481_CC reveals a K_d of 0.9 mM. (E) Microscale thermophoresis titration of ab-tubulin lacking both the acidic C-terminal tails with HsIFT81N gives a K_d of 16mM. This is equivalent affinity to what is observed for full-

length tubulin and suggests that IFT81N does not interact with the C-terminal tubulin tails (curves in D and E are from 3 independent experiments). **(F)** MT-sedimentation experiments where full-length α -tubulin or tubulin lacking the C-terminal tail of β -tubulin is titrated with the HsIFT74/81_CC complex demonstrates that the high-affinity interaction mediated by IFT74N requires the C-terminal tail of β -tubulin. **(G)** The experiments shown in panel D-F suggest a model in which IFT81N recognizes the core-fold of tubulin providing specificity whereas IFT74N binds the acidic tail of β -tubulin providing increased affinity.

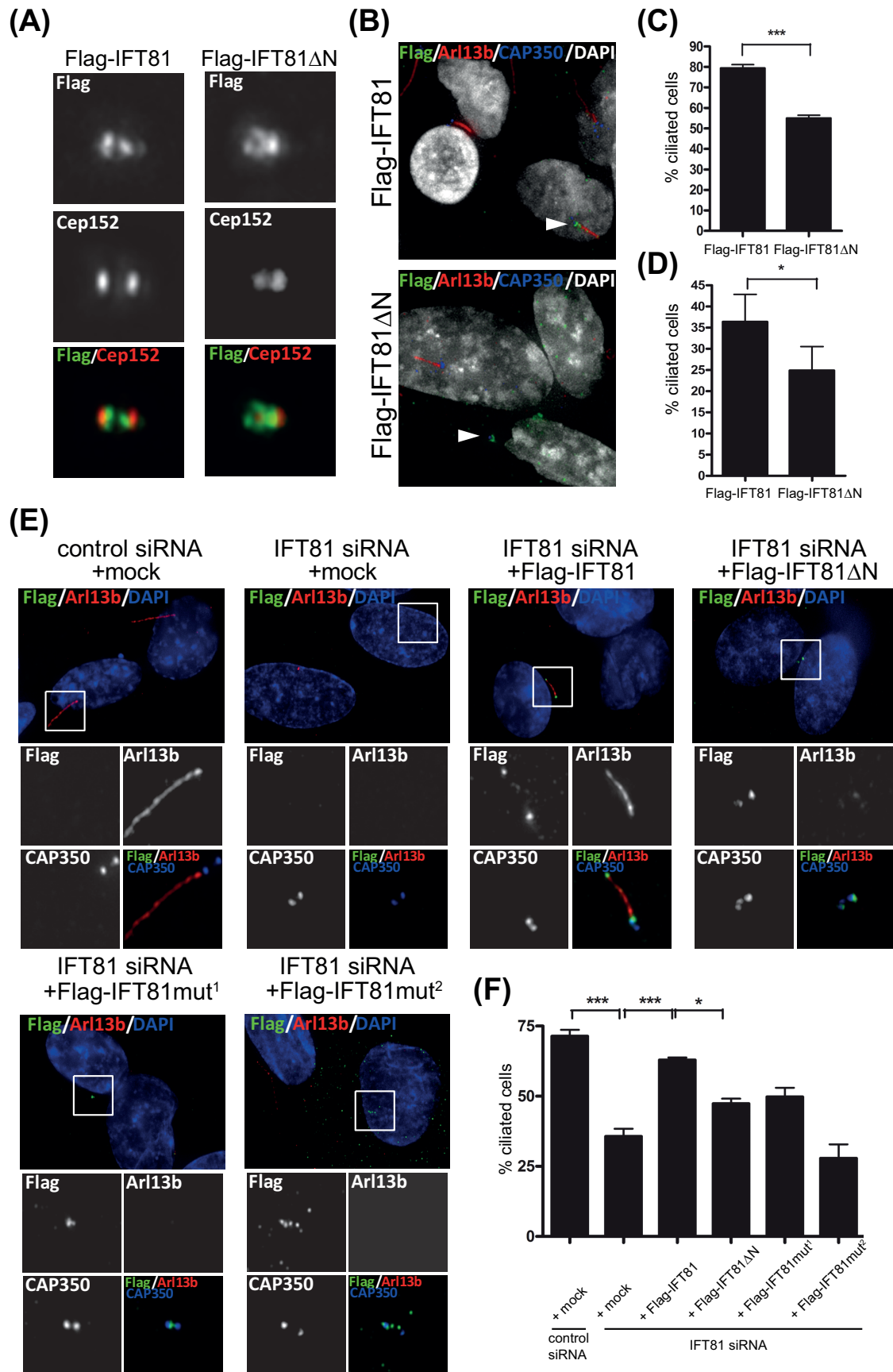


Figure 5: Tubulin-binding of IFT81 is required for ciliogenesis in human cells. (A) Both Flag-IFT81 and Flag-IFT81 Δ N (in green) localize to the centrosome (detected by anti-Cep152

staining, in red) in U2OS cells. **(B)** Transient expression of Flag-IFT81 Δ N, but not Flag-IFT81 (in green) impairs formation of primary cilia induced by 24h treatment with 0.5 μ M cytochalasin D in RPE1 cells. Primary cilia were detected by Arl13b immuno-staining (in red), CAP350 (in blue) was used to visualize centrosomes. Arrowheads show Flag positive cells. **(C)** Quantification of the effects of Flag-IFT81 and Flag-IFT81 Δ N expression on the presence of primary cilia induced by 0.5 μ M cytochalasin D. $n=3$, $p<0.001$ (***) by Student's *t*-test. **(D)** Quantification of the effects of Flag-IFT81 and Flag-IFT81 Δ N expression on the presence of primary cilia induced 24h serum starvation. $n=4$, $p<0.05$ (*) by Student's *t*-test. **(E)** Transient expression of Flag-IFT81, but not the tubulin binding-deficient IFT81 mutants (in green) rescues the ciliogenesis defect after the IFT81 siRNA knockdown. Primary cilia were induced by 0.5 μ M cytochalasin D and detected by Arl13b antibody (in red). CAP350 (in blue, inset images only) was used to visualize centrosomes. **(F)** Quantification of the rescue experiment shown in (E), $n=3$, statistical analyses by one-way ANOVA.

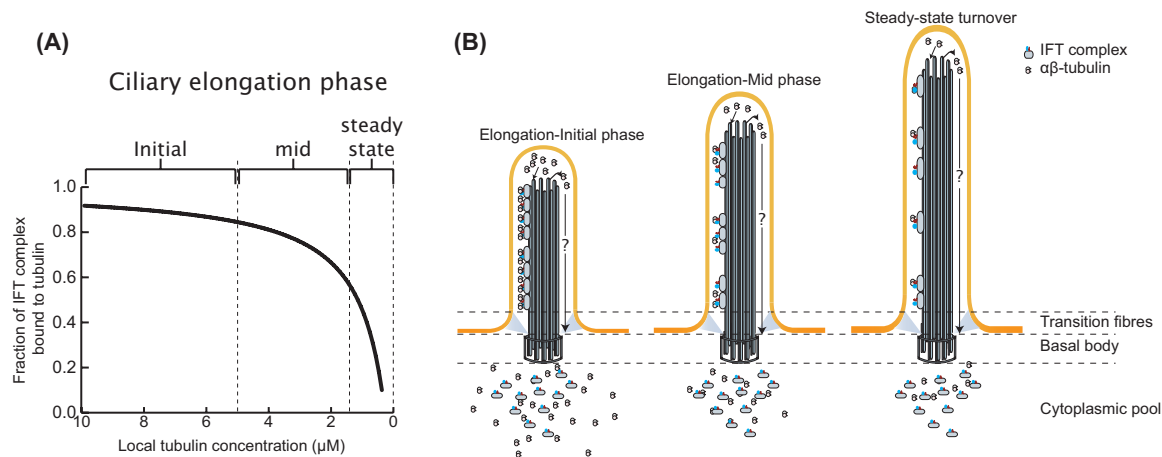


Figure 6: (A) Fraction of IFT complex bound to tubulin at varying tubulin concentration is plotted using the equation $O_{IFT} = [Tub]/\{K_d + [Tub]\}$ (see supplementary material for the derivation). O_{IFT} is the fraction of IFT bound to tubulin, K_d is the binding constant that is experimentally determined in this study as $0.9\mu\text{M}$ and $[Tub]$ is the local concentration of free tubulin at the base of the cilium. (B) Model for ciliary length control: 3 representative phases of cilia growth are shown. Each phase is characterized by a varying fraction of IFT complexes bound to tubulin. O_{IFT} is highest in the initial elongation phase and gradually decreases as the cilia approaches its steady state length.

HsIFT74N	-----	MASN	4
CfIFT81N	-----	MASN	4
DrIFT74N	-----		
CrIFT74N	-----	MDRPSSRGALALGAGGLGKA	20
CeIFT74N	MEIYLELLTNQNGLSKLIISFNYSALSHIFHSWSVLVSMTTKHASTTNTRMERPPSTASSR		60
HsIFT74N	HKSSAARPV---SRGGVGLTGRPPSGIRP--LSGNIRVATAMPPGTAR-----	PGSR	51
CfIFT81N	HKPSAARPV---SRGGIGLPGRPPSGIRP--PSGNTRVATGLPPGTAR-----	PGSR	51
DrIFT74N	--MSAQRPA---SRGSFG-----PGAGRP--QTAS-RVGTAMAPGTAR-----	PGTR	39
CrIFT74N	PTGGAVQQP---DRPMTGQRGAAPAGPMR--APAGASIIIGAGPPGTAMRG-----	GPGPA	70
CeIFT74N	PRTSTGRAPSARARPPSAMRAPPQPTYENRPTTGMSMRNGGPPVPPSRSGMIPVPPSR		120
	.: : * . *	. . : . * .	*
HsIFT74N	GCPIGTG----GVLS-----SQIKVAHRPVTQQGLTGMKTGTK-G		86
CfIFT81N	GGPIGTG----GVLS-----SQIKVADRPVTQQGLSGMKTGMK-G		86
DrIFT74N	GAHLATP----GVLS-----AQIKVADRPVTQQGLSGMKTGIK-G		74
CrIFT74N	GGPPGTAYK-RMGTASQRPQTGQQAAAAAAAAARAGQQLQVENRPIITNHGVSGMKTAAA-G		128
CeIFT74N	GGPPAPMPVSRAGGPPRAPTSMGGRPMTG---MARPPTAGLRPVTQQGLRAPPSSRMGTG		176
	* .. *	. **:*:*:* . : *	
	Predicted pI		
HsIFT74N	PQRQ	90	12.55
CfIFT81N	PQRQ	90	12.55
DrIFT74N	PQRQ	78	12.48
CrIFT74N	VGRQ	132	12.08
CeIFT74N	NSRQ	180	12.18
	**		

Figure S1: Sequence alignment of the N-terminal region preceding the predicted coiled-coil domain of IFT74 from different organisms. Conservation is indicated below the sequence. Positively- and negatively-charged residues are shown in blue and red, respectively. The

theoretical pI 's calculated for the shown sequence using the program ProtParam (<http://web.expasy.org/protparam/>) are indicated.

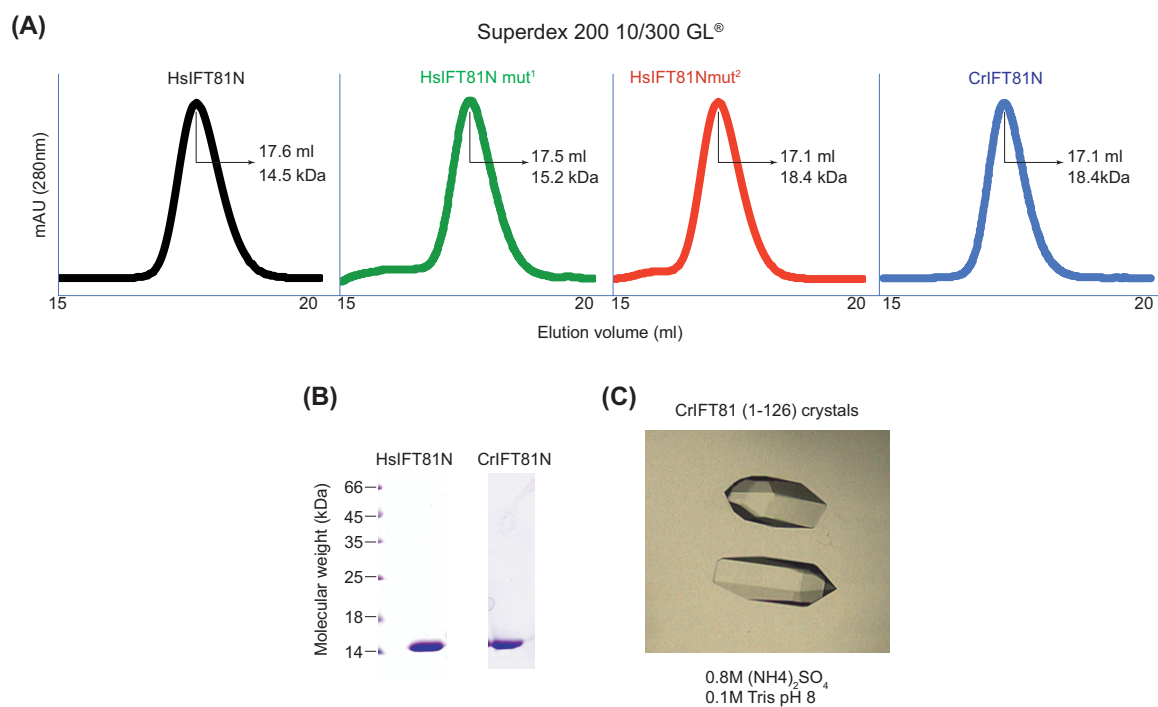


Figure S2: (A) Size exclusion profiles of IFT81N wild-type and mutant proteins showing that all the mutants are folded. (B) Coomassie stained SDS-PAGE gels of purified HsIFT81N and CrIFT81N. (C) Hexagonal crystals of CrIFT81N grown by vapor diffusion.

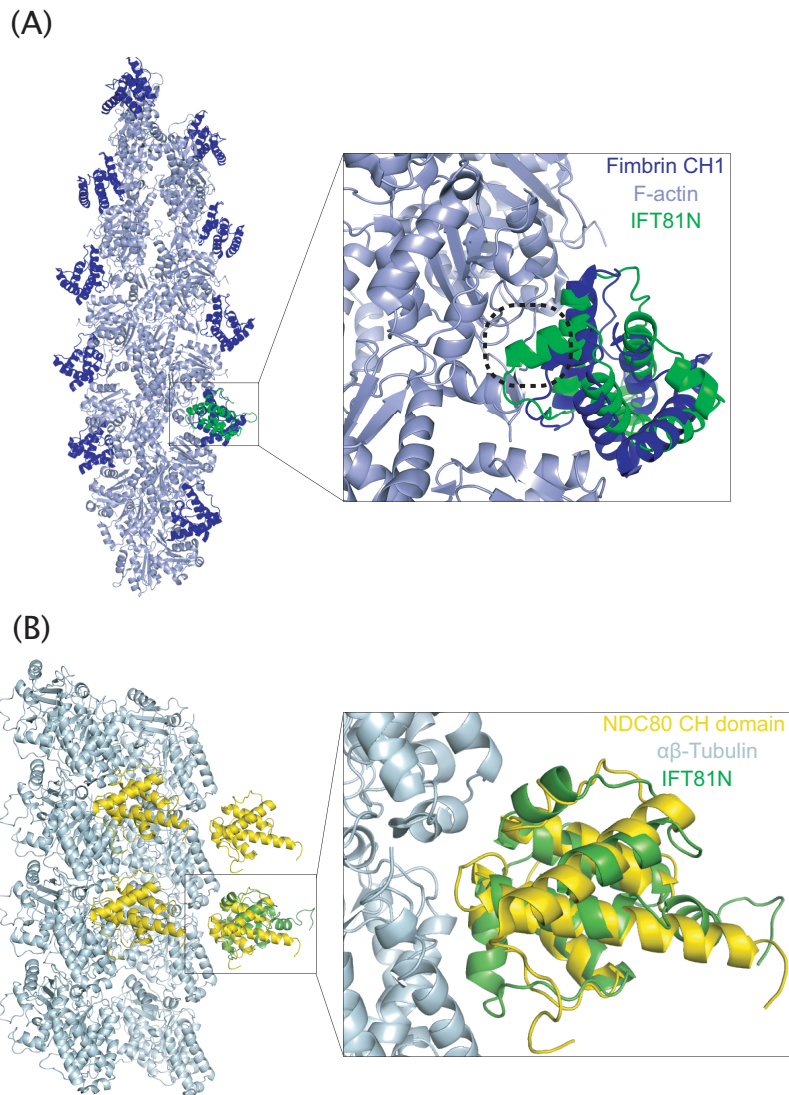


Figure S3: The IFT81N structure is compatible with MT-binding but not actin-binding. **(A)** Superpositioning of the CrIFT81N structure (green) onto the CH-domain of α -actinin (dark blue, only one of the two CH-domains is shown) bound to F-actin (light blue) (Galkin et al., 2010). The figure shows that α -helix $\alpha 3'$ clashes with F-actin (dotted circle) and would have to undergo a significant conformational change to allow binding. **(B)** Superpositioning of CrIFT81N (green) onto the CH-domain of NDC80 (yellow, only the CH-domain closest to the tubulin globular domains is shown) bound to MT (cyan) (Alushin et al., 2010). The conformation of the CrIFT81N structure is compatible with MT-binding.

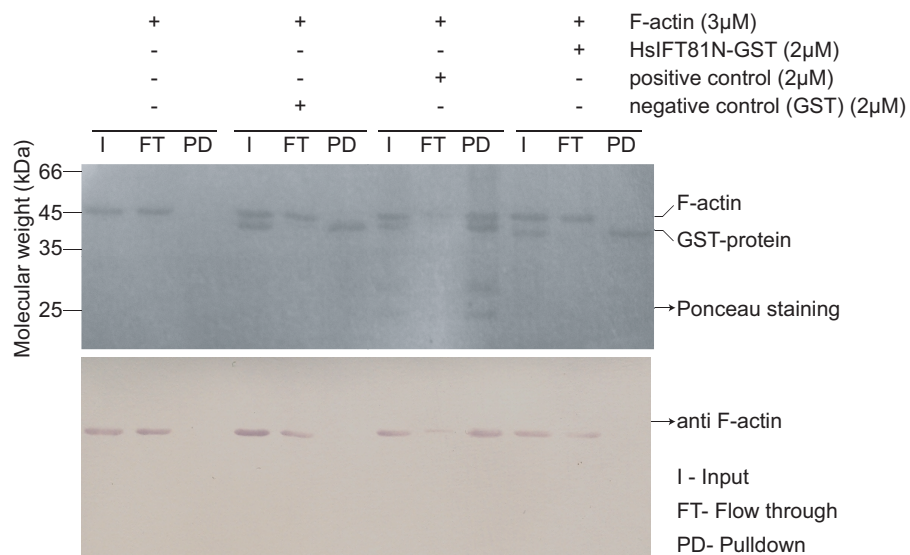


Figure S4: *HsIFT81N* does not bind actin in pull-down experiments. Pull-down of rabbit muscle F-actin by GST-tagged protein using GSH-beads and subsequent western-blotting with anti-F-actin antibodies. The experiment shows that *HsIFT81N* does not interact with F-actin.

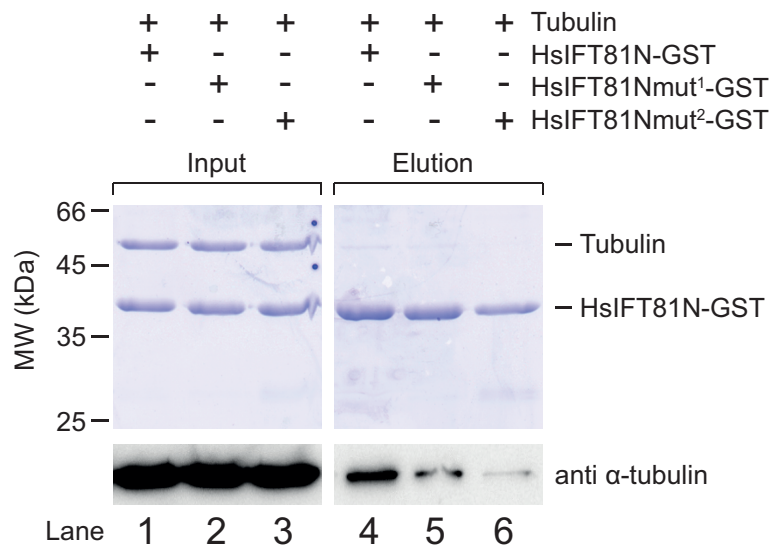


Figure S5: *ab*-tubulin pull-down with wildtype and mutant GST-HsIFT81N proteins. (Top) Coomassie-stained SDS gel of input and eluted proteins. (Bottom) Western-blot using anti α -tubulin antibody to visualize the amount of tubulin pulled-down by GST-HsIFT81N. Mutation of conserved basic residues of IFT81N reduces the affinity for tubulin.

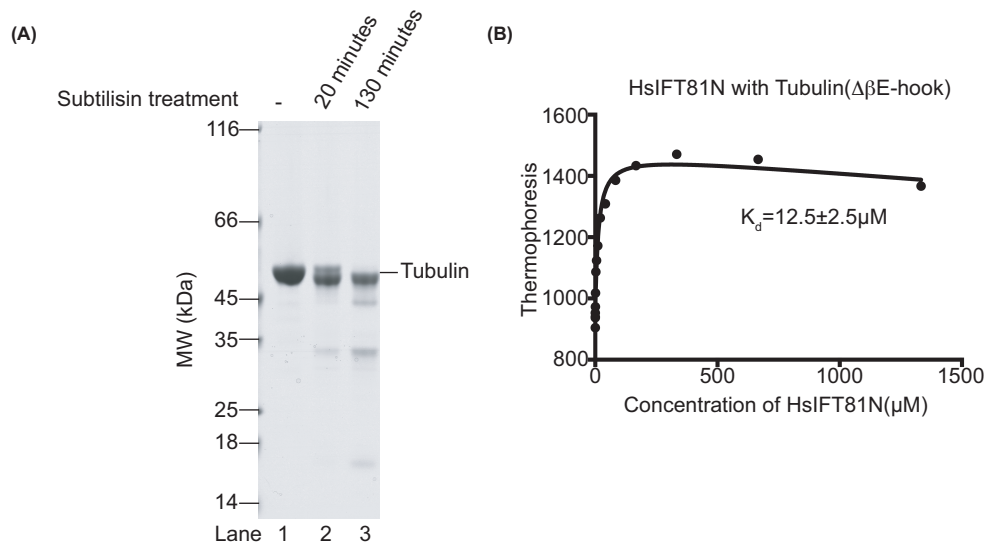


Figure S6: (A) Coomassie-stained SDS-PAGE gel showing subtilisin treatment of ab-tubulin to remove the E-hook of b-tubulin (after 20 min) or both a- and b-tubulin (after 130 min). (B) Microscale thermophoresis titration of ab-tubulin lacking the C-terminal tail of b-tubulin (tubulin $\Delta\beta$ E-hook) with HsIFT81N (panel (A), 20 min treatment) showing a similar affinity as observed for ab-tubulin with E-hooks intact.

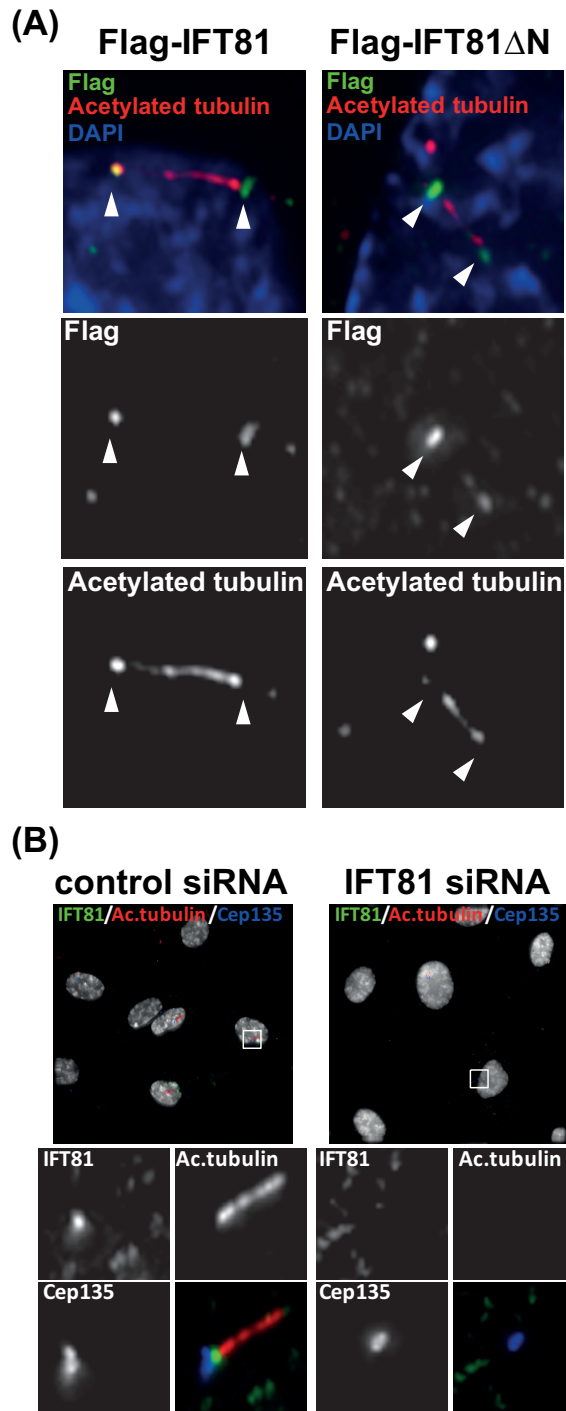


Figure S7: **(A)** Both *Flag-IFT81* and *Flag-IFT81 Δ N* (in green) are detected at the basal body and the tip of the primary cilium in RPE1 cells (see the arrowheads). Acetylated tubulin immuno-staining (in red) was used to visualize primary cilium. **(B)** *IFT81* siRNA efficiently depletes *IFT81* protein levels of the centrosome (in green) 48h after transfection and prevents the formation of acetylated tubulin positive primary cilium (in green). *Cep135* antibody staining (in blue) was used to detect centrosomes.

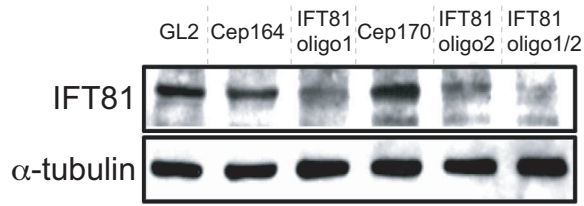


Figure S8: *IFT81* siRNA knockdown efficiency was probed by testing the levels of *IFT81* protein with anti-*IFT81*. Transfection of either *IFT81* oligo1 or *IFT81* oligo2 reduced the protein levels. Combination of oligo1 and oligo2 had the maximum effect on the *IFT81* protein levels and hence it was used in the SiRNA rescue experiments shown in Fig. 5. Various control RNAi (GL2, Cep164 & Cep170) did not affect *IFT81* levels. Levels of α -tubulin in each lane are indicated as a loading control.

Table 1. Data collection and refinement statistics.

	Cr81N_Native	Cr81N_Ta6Br12
Wavelength (Å)	0.9793	1.2545
Resolution range (Å)	37.92 - 2.51 (2.60 - 2.51)	38.28 - 2.32 (2.41 - 2.32)
Space group	P 64 2 2	P 64 2 2
Unit cell	75.05 75.05 93.38 90 90 120	76.07 76.07 94.06 90 90 120
Multiplicity	12.0 (12.0)	20.1 (20.0)
Completeness (%)	99.51 (96.91)	99.81 (98.14)
Mean I/sigma(I)	21.90 (3.06)	49.21 (12.37)
R-sym	0.051 (0.644)	0.034 (0.200)
R-factor	0.2374 (0.3769)	0.2141 (0.2736)
R-free	0.2897 (0.3936)	0.2391 (0.3218)
Number of atoms	948	1006
macromolecules	948	981
ligands	NA	4
water	0	21
Protein residues	124	124
RMS(bonds)	0.009	0.009
RMS(angles)	1.50	1.30
Average B-factor	98.70	57.10
macromolecules	98.70	57.00
solvent	NA	57.20

Statistics for the highest-resolution shell are shown in parentheses.

Extended discussion

The IFT74/81 tubulin binding module in mitosis

In addition to the well established role of IFT in ciliogenesis, the IFT complex was also shown to be involved in non-ciliary processes such as mitosis and the formation of the immune synapse (Delaval et al., 2011; Finetti et al., 2009). Depletion of IFT88 in cultured human cells resulted in the loss of astral MTs and spindle disorientation during mitosis. Immuno precipitation analysis revealed that other IFT proteins such as IFT52 and IFT20 were also part of a cytoplasmic dynein-driven complex involved in the transport of these astral MTs. This indicates that an IFT-like transport is involved in the assembly of astral MTs during mitosis, allowing proper orientation of the spindle (Delaval et al., 2011). Interestingly, IFT81 was also shown to localize to centrosomes and their periphery during mitosis in human RPE1 cells (Lamla, 2008). MT co-pelleting assays and electron microscopic analysis done in the current study show that the IFT74/81 tubulin-binding module is also able to bind MTs (Figure 3B & C and Figure 4B & C). Taken together, these data suggest that a single tubulin/MT-binding module in IFT74/81 may play an essential role in the assembly of both the ciliary axoneme and the astral MTs. However, the effect of depleting IFT81 levels on mitosis is not assessed in my study. Further research aimed at testing the effect of tubulin/MT binding mutants of IFT81 in the transport of astral MTs will shed light on this interesting possibility.

The life cycle of ciliary tubulin

From the point of tubulin synthesis in the cytoplasm to its incorporation into the ciliary axoneme, tubulin undergoes an extraordinary journey of several steps involving proper folding, selection for the properly folded pool at the base of the

cilium, and the actual transport into the cilium. In this section, I review the published literature on this pathway and try to connect the individual reports to the results and the predictions of this study. One of the earliest steps in cilium formation involves the localization of tubulin mRNA to the base of the cilium (Han et al., 1997). Sorting of mRNAs is a common mechanism for the spatially restricted translation of different proteins leading to their correct localization to the respective cellular compartments; and ciliary tubulin probably follows the same mechanistic principles (St Johnston, 2005). Newly synthesized tubulin must undergo cytosolic chaperonin (CCT complex) assisted folding to form $\alpha\beta$ -tubulin dimers capable of forming axonemal MTs (Yaffe et al., 1992). The properly folded tubulin then docks on to the transition fibers extending from the mature basal body with the help of another chaperone TBCC. TBCC, an orthologue of human RP2 (a gene mutated in the human ciliopathy: Retinitis pigmentosa), is proposed to play a role in yet another quality control step of the tubulin dimers involving testing of their GTPase activity (Stephan et al., 2007). The IFT complex, which is also known to dock to the transition fibers, binds and transports the assembly-qualified tubulin to the tip of the cilium where it is incorporated into the axoneme (Deane et al., 2001; Hao et al., 2011; Marshall and Rosenbaum, 2001b). In this study, we identify the probable molecular players of this particular step of the pathway by showing that the IFT74/81 complex directly binds $\alpha\beta$ -tubulin (Figure 3H, 3I and 4D). We also show that IFT81N binds to the globular domain of tubulin and that IFT74N recognizes the C-terminal acidic tails of this protein. This suggests a coupled quality control and transport mechanism wherein IFT81N recognizes only the properly folded tubulin subunits, adding another level of tubulin quality control. The tubulin incorporated into the axoneme turns over and must be transported back to the base of the cilium for recycling (Coyne and

Rosenbaum, 1970; Marshall and Rosenbaum, 2001a). Akin to the ciliary axonemal MTs, tubulin subunits in cytoplasmic MTs also turn over constantly at the + end of the MTs. However, the molecular mechanism of this tubulin turnover and reutilization in ciliary assembly is unclear. Several CCT complex components which are known to participate in proper tubulin folding after synthesis in the cytosol also localize to the tip of the cilium (Seixas et al., 2003). These CCT components are essential for the proper assembly of the axoneme and cilia formation in *Trypanosoma brucei* (Seixas et al., 2010). It is possible that this CCT complex localized at the tip of the cilium is involved in the recycling of tubulin. Although the study presented in this thesis uncovers the molecular mechanism of tubulin transport to the ciliary tip via IFT, the molecular details of the other steps of the tubulin life cycle essentially remain elusive. Further research is thus needed to characterize the molecular players in the tubulin folding and recycling pathways.

7. Abbreviations

Å	Angstrom, $1\text{Å} = 10^{-10}\text{ m}$
BBS	Bardet-Biedl syndrome
Ca ²⁺	Calcium
cGMP	Cyclic guanosine monophosphate
cAMP	Cyclic adenosine monophosphate
Cr	Chlamydomonas reinhardtii
EGTA	Ethylene glycol tetraacetic acid
GAP	GTPase activating protein
GTP	Guanosine triphosphate
GPCR	G-protein coupled receptor
IFT	Intraflagellar transport
IFT81N	N-terminus of IFT81
IFT74N	N-terminus of IFT74
ITC	Isothermal titration calorimetry
MST	Microscale thermophoresis
MT	Microtubule
ODA	Outer dynein arm
ORC	Olfactory receptor cell
PC	Polycystin
PKD	Polycystic kidney disease
Ptc1	Patched-1
RP	Retinitis pigmentosa
RPE	Retinal pigment epithelium
Shh	Sonic hedgehog
Smo	Smoothed
TPR	Tetratricopeptide repeat
TULP3	Tubby-like protein 3

8. References

- Adhiambo, C., Blisnick, T., Toutirais, G., Delannoy, E., and Bastin, P. (2009). A novel function for the atypical small G protein Rab-like 5 in the assembly of the trypanosome flagellum. *Journal of Cell Science* *122*, 834–841.
- Afzelius, B. (1959). Electron Microscopy of the Sperm Tail Results Obtained with a New Fixative. *The Journal of biophysical and biochemical cytology*, *5*(2).
- Ahmed, N.T., Gao, C., Lucker, B.F., Cole, D.G., and Mitchell, D.R. (2008). ODA16 aids axonemal outer row dynein assembly through an interaction with the intraflagellar transport machinery. *The Journal of Cell Biology* *183*, 313–322.
- Arts, H.H., Bongers, E.M.H.F., Mans, D.A., van Beersum, S.E.C., Oud, M.M., Bolat, E., Spruijt, L., Cornelissen, E.A.M., Schuurs-Hoeijmakers, J.H.M., de Leeuw, N., et al. (2011). C14ORF179 encoding IFT43 is mutated in Sensenbrenner syndrome. *Journal of Medical Genetics* *48*, 390–395.
- Bacaj, T., Lu, Y., and Shaham, S. (2008). The Conserved Proteins CHE-12 and DYF-11 Are Required for Sensory Cilium Function in *Caenorhabditis elegans*. *Genetics* *178*, 989–1002.
- Badano, J. L., Mitsuma, N., & Beales, P. L. (2006). The Ciliopathies: An Emerging Class of Human Genetic Disorders. *Annu Rev Genomics and Human Genetics*, *7*, 125–148.
- Banizs, B. (2005). Dysfunctional cilia lead to altered ependyma and choroid plexus function, and result in the formation of hydrocephalus. *Development* *132*, 5329–5339.
- Barber, C. F., Heuser, T., Carbajal-González, B. I., Botchkarev, V. V., & Nicastro, D. (2012). Three-dimensional structure of the radial spokes reveals heterogeneity and interactions with dyneins in *Chlamydomonas* flagella. *Molecular biology of the cell*, *23*, 111–120.
- Beales, P.L., Bland, E., Tobin, J.L., Bacchelli, C., Tuysuz, B., Hill, J., Rix, S., Pearson, C.G., Kai, M., Hartley, J., et al. (2007). IFT80, which encodes a conserved intraflagellar transport protein, is mutated in Jeune asphyxiating thoracic dystrophy. *Nat Genet* *39*, 727–729.
- Beatson, S., & Ponting, C. P. (2004). GIFT domains: linking eukaryotic intraflagellar transport and glycosylation to bacterial gliding. *Trends in biochemical sciences*, *29*(8), 396–399.
- Behal, R.H., Miller, M.S., Qin, H., Lucker, B.F., Jones, A., and Cole, D.G. (2012). Subunit Interactions and Organization of the *Chlamydomonas reinhardtii* Intraflagellar Transport Complex A Proteins. *Journal of Biological Chemistry* *287*, 11689–11703.
- Belgacem, Y. H., & Borodinsky, L. N. (2011). Sonic hedgehog signaling is decoded by calcium spike activity in the developing spinal cord. *Proceedings of the National Academy of Sciences of the United States of America*, *108*, 4482–4487.

- Benton, R., Sachse, S., Michnick, S.W., and Vosshall, L.B. (2006). Atypical Membrane Topology and Heteromeric Function of *Drosophila* Odorant Receptors In Vivo. *Plos Biol* 4, e20.
- Berbari, N.F., O'Connor, A.K., Haycraft, C.J., and Yoder, B.K. (2009). The Primary Cilium as a Complex Signaling Center. *Current Biology* 19, R526–R535.
- Blacque, O.E., Michael, R.J., Chunmei, L., Jonathan, M., and Leroux, M.R. (2004). Loss of *C. elegans* BBS-7 and BBS-8 protein function results in cilia defects and compromised intraflagellar transport. *Genes & Development* 18, 1630–1642.
- Boehlke, C., Kotsis, F., Patel, V., Braeg, S., & Voelker, H. (2010). Primary cilia regulate mTORC1 activity and cell size through Lkb1 : Nature Cell Biology : Nature Publishing Group. *Nature Cell Biology*, 12, 1115–1125.
- Bornens, M. (2012). The Centrosome in Cells and Organisms. *Science*, 335(6067), 422–426.
- Cano, D.A., Sekine, S., and Hebrok, M. (2006). Primary Cilia Deletion in Pancreatic Epithelial Cells Results in Cyst Formation and Pancreatitis. *Gastroenterology* 131, 1856–1869.
- Cavalcanti, D.P., Huber, C., Le Quan Sang, K.H., Baujat, G., Collins, F., Delezoide, A.L., Dagoneau, N., Le Merrer, M., Martinovic, J., Mello, M.F.S., et al. (2011). Mutation in IFT80 in a fetus with the phenotype of Verma-Naumoff provides molecular evidence for Jeune-Verma-Naumoff dysplasia spectrum. *Journal of Medical Genetics* 48, 88–92.
- Cole, D.G., Diener, D.R., Himelblau, A.L., Beech, P.L., Fuster, J.C., and Rosenbaum, J.L. (1998). Chlamydomonas kinesin-II-dependent intraflagellar transport (IFT): IFT particles contain proteins required for ciliary assembly in *Caenorhabditis elegans* sensory neurons. *The Journal of Cell Biology* 141, 993–1008.
- Coyne, B., and Rosenbaum, J.L. (1970). Flagellar elongation and shortening in *Chlamydomonas* II. Re-utilization of flagellar proteins. *The Journal of Cell Biology*, 47(3), 777–781.
- Davis, E.E., Zhang, Q., Liu, Q., Diplas, B.H., Davey, L.M., Hartley, J., Stoetzel, C., Szymanska, K., Ramaswami, G., Logan, C.V., et al. (2011). TTC21B contributes both causal and modifying alleles across the ciliopathy spectrum. *Nat Genet* 43, 189–196.
- Deane, J.A., Cole, D.G., Seeley, E.S., Diener, D.R., and Rosenbaum, J.L. (2001). Localization of intraflagellar transport protein IFT52 identifies basal body transitional fibers as the docking site for IFT particles. *Current Biology* 11, 1586–1590.
- Delaval, B., Bright, A., Lawson, N.D., and Doxsey, S. (2011). The cilia protein IFT88 is required for spindle orientation in mitosis. *Nature Cell Biology* 13, 461–468.
- Dibble, C.C., Elis, W., Menon, S., Qin, W., Klekota, J., Asara, J.M., Finan, P.M., Kwiatkowski, D.J., Murphy, L.O., and Manning, B.D. (2012). TBC1D7 Is a Third Subunit of the TSC1-TSC2 Complex Upstream of mTORC1. *Mol Cell* 47, 535–546.

Duchateau, G. S., Merkus, F., Zuidema, J., & MD, G. K. (1985). Correlation Between Nasal Ciliary Beat Frequency and Mucus Transport Rate in Volunteers. *The Laryngoscope*, *95*(7), 854–859.

Elias, R. V., Sezate, S. S., Cao, W., & McGinnis, J. F. (2004). Temporal kinetics of the light/dark translocation and compartmentation of arrestin and alpha-transducin in mouse photoreceptor cells. *Mol Vis*, *10*, 672–681.

Engel, B.D., Ludington, W.B., and Marshall, W.F. (2009). Intraflagellar transport particle size scales inversely with flagellar length: revisiting the balance-point length control model. *The Journal of Cell Biology* *187*, 81–89.

Fan, Z.C., Behal, R.H., Geimer, S., Wang, Z., Williamson, S.M., Zhang, H., Cole, D.G., and Qin, H. (2010). Chlamydomonas IFT70/CrDYF-1 Is a Core Component of IFT Particle Complex B and Is Required for Flagellar Assembly. *Mol Biol Cell* *21*, 2696–2706.

Finetti, F., Paccani, S.R., Riparbelli, M.G., Giacomello, E., Perinetti, G., Pazour, G.J., Rosenbaum, J.L., and Baldari, C.T. (2009). Intraflagellar transport is required for polarized recycling of the TCR/CD3 complex to the immune synapse. *Nature Cell Biology* *11*, 1332–1339.

Fisch, C., and Dupuis-Williams, P. (2012). Ultrastructure of cilia and flagella - back to the future! *Biology of the Cell* *103*, 249–270.

Fliegauf, M., Benzing, T., and Omran, H. (2007a). When cilia go bad: cilia defects and ciliopathies. *Nat Rev Mol Cell Biol* *8*, 880–893.

Follit, J.A., Tuft, R.A., Fogarty, K.E., and Pazour, G.J. (2006). The Intraflagellar Transport Protein IFT20 Is Associated with the Golgi Complex and Is Required for Cilia Assembly. *Mol Biol Cell* *17*, 3781–3792.

Follit, J.A., San Agustin, J.T., Xu, F., Jonassen, J.A., Samtani, R., Lo, C.W., and Pazour, G.J. (2008). The Golgin GMAP210/TRIP11 Anchors IFT20 to the Golgi Complex. *PLoS Genet* *4*, e1000315.

Follit, J.A., Xu, F., Keady, B.T., and Pazour, G.J. (2009). Characterization of mouse IFT complex B. *Cell Motil. Cytoskeleton* *66*, 457–468.

Frasa, M.A.M., Koessmeier, K.T., Ahmadian, M.R., and Braga, V.M.M. (2012). Illuminating the functional and structural repertoire of human TBC/RABGAPs. *13*, 67–73.

Garcia-Gonzalo, F.R., Corbit, K.C., Sirerol-Piquer, M.S., Ramaswami, G., Otto, E.A., Noriega, T.R., Seol, A.D., Robinson, J.F., Bennett, C.L., Josifova, D.J., et al. (2011). A transition zone complex regulates mammalian ciliogenesis and ciliary membrane composition. *43*, 776–784.

Gilula, N.B. (1972). THE CILIARY NECKLACE: A Ciliary Membrane Specialization. *The Journal of Cell Biology* *53*, 494–509.

Gorivodsky, M., Mukhopadhyay, M., Wilsch-Braeuninger, M., Phillips, M., Teufel,

- A., Kim, C., Malik, N., Huttner, W., and Westphal, H. (2009). Intraflagellar transport protein 172 is essential for primary cilia formation and plays a vital role in patterning the mammalian brain. *Developmental Biology* 325, 24–32.
- Gouttenoire, J., Valcourt, U., Bougault, C., Aubert-Foucher, E., Arnaud, E., Giraud, L., and Mallein-Gerin, F. (2007). Knockdown of the Intraflagellar Transport Protein IFT46 Stimulates Selective Gene Expression in Mouse Chondrocytes and Affects Early Development in Zebrafish. *Journal of Biological Chemistry* 282, 30960–30973.
- Gönczy, P. (2012). Towards a molecular architecture of centriole assembly. *Nature Reviews Molecular Cell Biology*, 13(7), 425–435.
- Guo, C.-W., Xiong, S., Liu, G., Wang, Y.-F., He, Q.-Y., Zhang, X.-E., Zhang, Z.-P., Ge, F., and Kitazato, K. (2010). Proteomic analysis reveals novel binding partners of MIP-T3 in human cells. *Proteomics* 10, 2337–2347.
- Han, J. W., Park, J. H., Kim, M., & Lee, J. (1997). mRNAs for Microtubule Proteins Are Specifically Colocalized during the Sequential Formation of Basal Body, Flagella, and Cytoskeletal Microtubules in the Differentiation of *Naegleria gruberi*. *The Journal of Cell Biology*, 137, 871–879.
- Han, Y.-G., Spassky, N., Romaguera-Ros, M., Garcia-Verdugo, J.-M., Aguilar, A., Schneider-Maunoury, S., and Alvarez-Buylla, A. (2008). Hedgehog signaling and primary cilia are required for the formation of adult neural stem cells. *Nat Neurosci* 11, 277–284.
- Hao, L., Thein, M., Brust-Mascher, I., Civelekoglu-Scholey, G., Lu, Y., Acar, S., Prevo, B., Shaham, S., and Scholey, J.M. (2011). Intraflagellar transport delivers tubulin isotypes to sensory cilium middle and distal segments. *Nature* 13, 790–798.
- Haycraft, C. J., Banizs, B., Aydin-Son, Y., & Zhang, Q. (2005). Gli2 and Gli3 localize to cilia and require the intraflagellar transport protein polaris for processing and function. *PLoS Genetics*, 1(4), e53.
- Hou, Y., Qin, H., Follit, J.A., Pazour, G.J., Rosenbaum, J.L., and Witman, G.B. (2007). Functional analysis of an individual IFT protein: IFT46 is required for transport of outer dynein arms into flagella. *The Journal of Cell Biology* 176, 653–665.
- Huangfu, D., Cho, E., Petruk, S., Cherbas, L., Smith, S.T., Jones, R.S., Cherbas, P., Canaani, E., Jaynes, J.B., and Mazo, A. (2003). Hedgehog Signalling in the mouse requires intraflagellar transport proteins. 426, 83–87.
- Ibanez-Tallon, I. (2004). Dysfunction of axonemal dynein heavy chain Mdnah5 inhibits ependymal flow and reveals a novel mechanism for hydrocephalus formation. *Human Molecular Genetics* 13, 2133–2141.
- Iomini, C., Babaev-Khaimov, V., Sassaroli, M., & Piperno, G. (2001). Protein particles in *Chlamydomonas* flagella undergo a transport cycle consisting of four phases. *Journal of Cell Biology*, 153(1), 13–24.
- Ishikawa, H., and Marshall, W.F. (2011). Ciliogenesis: building the cell's antenna.

Nat Rev Mol Cell Biol 12, 222–234.

Jékely, G., and Arendt, D. (2006). Evolution of intraflagellar transport from coated vesicles and autogenous origin of the eukaryotic cilium. *Bioessays* 28, 191–198.

Johnson, K. A. (1992). Polarity of flagellar assembly in *Chlamydomonas*. *The Journal of Cell Biology*, 119(6), 1605–1611.

Keady, B.T., Le, Y.Z., and Pazour, G.J. (2011). IFT20 is required for opsin trafficking and photoreceptor outer segment development. *Mol Biol Cell* 22, 921–930.

Keady, B.T., Samtani, R., Tobita, K., Tsuchiya, M., San Agustin, J.T., Jonassen, J.A., Subramanian, R., Lo, C.W., and Pazour, G.J. (2012). IFT25 Links the Signal-Dependent Movement of Hedgehog Components to Intraflagellar Transport. *Dev Cell* 22, 940–951.

Khanna, H. (2005). RPGR-ORF15, Which Is Mutated in Retinitis Pigmentosa, Associates with SMC1, SMC3, and Microtubule Transport Proteins. *Journal of Biological Chemistry* 280, 33580–33587.

Kikuchi, T., Takasaka, T., & Tonosaki, A. (1989). Fine structure of guinea pig vestibular kinocilium. *Acta Otolaryngol (Stockh)*, 108, 26–30.

Kim, J., Kato, M., and Beachy, P.A. (2009). Gli2 trafficking links Hedgehog-dependent activation of *Smoothed* in the primary cilium to transcriptional activation in the nucleus. *Proc Natl Acad Sci USA* 106, 21666–21671.

Kobayashi, T., Gengyo-Ando, K., Ishihara, T., Katsura, I., and Mitani, S. (2007). IFT-81 and IFT-74 are required for intraflagellar transport in *C. elegans*. *Genes Cells* 12, 593–602.

Kozminski, K.G., Beech, P.L., and Rosenbaum, J.L. (1995). The *Chlamydomonas* kinesin-like protein FLA10 is involved in motility associated with the flagellar membrane. *The Journal of Cell Biology* 131, 1517–1527.

Kozminski, K.G., Johnson, K.A., Forscher, P., and Rosenbaum, J.L. (1993). A motility in the eukaryotic flagellum unrelated to flagellar beating. *90*, 5519–5523.

Krock, B.L., and Perkins, B.D. (2008). The intraflagellar transport protein IFT57 is required for cilia maintenance and regulates IFT-particle-kinesin-II dissociation in vertebrate photoreceptors. *Journal of Cell Science* 121, 1907–1915.

Kulaga, H.M., Leitch, C.C., Eichers, E.R., Badano, J.L., Lesemann, A., Hoskins, B.E., Lupski, J.R., Beales, P.L., Reed, R.R., and Katsanis, N. (2004). Loss of BBS proteins causes anosmia in humans and defects in olfactory cilia structure and function in the mouse. *Nat Genet* 36, 994–998.

Kunitomo, H., and Iino, Y. (2008). *Caenorhabditis elegans* DYF-11, an orthologue of mammalian Traf3ip1/MIP-T3, is required for sensory cilia formation. *Genes to Cells* 13, 13–25.

Lamla, S. (2008). Functional Characterisation of the Centrosomal Protein Cep170.

- Lehman, J.M., Michaud, E.J., Schoeb, T.R., Aydin-Son, Y., Miller, M., and Yoder, B.K. (2008). The Oak Ridge Polycystic Kidney mouse: Modeling ciliopathies of mice and men. *Dev. Dyn.* 237, 1960–1971.
- Liem, K.F., Ashe, A., He, M., Satir, P., Moran, J., Beier, D., Wicking, C., and Anderson, K.V. (2012). The IFT-A complex regulates Shh signaling through cilia structure and membrane protein trafficking. *The Journal of Cell Biology* 197, 789–800.
- Lindemann, C. B., & Lesich, K. A. (2010). Flagellar and ciliary beating: the proven and the possible. *Journal of Cell Science*, 123, 519–528.
- Ling, L., and Goeddel, D.V. (2000). MIP-T3, a Novel Protein Linking Tumor Necrosis Factor Receptor-associated Factor 3 to the Microtubule Network. *Journal of Biological Chemistry* 275, 23852–23860.
- Lucker, B.F., Behal, R.H., Qin, H., Siron, L.C., Taggart, D.W., Rosenbaum, J.L., and Cole, D.G. (2005). Characterization of the Intraflagellar Transport Complex B Core: DIRECT INTERACTION OF THE IFT81 AND IFT74/72 SUBUNITS. *Journal of Biological Chemistry* 280, 27688–27696.
- Lucker, B. F., Miller, M. S., Dziedzic, S. A., Blackmarr, P. T., & Cole, D. G. (2010). Direct interactions of intraflagellar transport complex B proteins IFT88, IFT52, and IFT46. *JBC*, 285(28), 21508–21518.
- Ludington, W. B., Wemmer, K. A., Lehtreck, K. F., Witman, G. B., & Marshall, W. F. (2013). Avalanche-like behavior in ciliary import. *Proceedings of the National Academy of Sciences of the United States of America*, 110(10), 3925–3930.
- Lyons, R.A. (2006). The reproductive significance of human Fallopian tube cilia. *Human Reproduction Update* 12, 363–372.
- Marshall, W.F., and Rosenbaum, J.L. (2001). Intraflagellar transport balances continuous turnover of outer doublet microtubules: implications for flagellar length control. *155*, 405–414.
- Marshall, W.F., Qin, H., Rodrigo Brenni, M., and Rosenbaum, J.L. (2005). Flagellar length control system: testing a simple model based on intraflagellar transport and turnover. *Mol Biol Cell* 16, 270–278.
- McEwen, D. P., Jenkins, P. M., & Martens, J. R. (2008). Olfactory Cilia: Our Direct Neuronal Connection to the External World. *Current topics in developmental biology*, 85, 333–370.
- Mitchell, D. R. (2000). Chlamydomonas flagella. *Journal of Phycology*, 36, 261–273.
- Mizuno, N., Taschner, M., Engel, B. D., & Lorentzen, E. (2012). Structural Studies of Ciliary Components. *Journal of Molecular Biology*, 422, 163–180.
- Mukhopadhyay, S., Wen, X., Ratti, N., Loktev, A., & Rangell, L. (2013). The Ciliary G-Protein-Coupled Receptor Gpr161 Negatively Regulates the Sonic Hedgehog Pathway via cAMP Signaling. *Cell*, 152, 210–223.

- Mukhopadhyay, S., Wen, X., Ben Chih, Nelson, C.D., Lane, W.S., Scales, S.J., and Jackson, P.K. (2010). TULP3 bridges the IFT-A complex and membrane phosphoinositides to promote trafficking of G protein-coupled receptors into primary cilia. *24*, 2180–2193.
- Nagao, S., Nishii, K., Yoshihara, D., & Kurahashi, H. (2008). Kidney International - Calcium channel inhibition accelerates polycystic kidney disease progression in the *Cy//+* rat. *Kidney International*, *73*, 269–277.
- Nauli, S. M., Alenghat, F. J., Luo, Y., & Williams, E. (2003). Polycystins 1 and 2 mediate mechanosensation in the primary cilium of kidney cells. *Nature Genetics*, *33*, 129–137.
- Nicastro, D. (2006). The Molecular Architecture of Axonemes Revealed by Cryoelectron Tomography. *Science* *313*, 944–948.
- Nicastro, D., McIntosh, J.R., and Baumeister, W. (2005). 3D structure of eukaryotic flagella in a quiescent state revealed by cryo-electron tomography. *Proc Natl Acad Sci USA* *102*, 15889–15894.
- Nigg, E. A., & Raff, J. W. (2009). Centrioles, Centrosomes, and Cilia in Health and Disease. *Cell*, *139*(4), 663–678.
- Nonaka, S., Tanaka, Y., Okada, Y., Takeda, S., Harada, A., Kanai, Y., et al. (1998). Randomization of left–right asymmetry due to loss of nodal cilia generating leftward flow of extraembryonic fluid in mice lacking KIF3B motor protein. *Cell*, *95*(6), 829–837.
- Nonaka, S., Shiratori, H., Saijoh, Y., and Hamada, H. (2002). Determination of left–right patterning of the mouse embryo by artificial nodal flow. *Nature* *418*, 96–99.
- Omori, Y., Zhao, C., Saras, A., Mukhopadhyay, S., Kim, W., Furukawa, T., Sengupta, P., Veraksa, A., and Malicki, J. (2008). *elipsa* is an early determinant of ciliogenesis that links the IFT particle to membrane-associated small GTPase Rab8. *Nature Cell Biology* *10*, 437–444.
- Osawa, S., Jo, R., Xiong, Y., Reidel, B., Tserentsoodol, N., Arshavsky, V.Y., Iuvone, P.M., and Weiss, E.R. (2011). Phosphorylation of G Protein-coupled Receptor Kinase 1 (GRK1) Is Regulated by Light but Independent of Phototransduction in Rod Photoreceptors. *Journal of Biological Chemistry* *286*, 20923–20929.
- Ou, G., E Blacque, O., Snow, J.J., Leroux, M.R., and Scholey, J.M. (2005). Functional coordination of intraflagellar transport motors. *Nature* *436*, 583–587.
- Ounjai, P., Kim, K. D., Liu, H., Dong, M., Tauscher, A. N., Witkowska, H. E., & Downing, K. H. (2013). Architectural Insights into a Ciliary Partition. *Current Biology*, *23*, 1–6.
- Pan, X., Eathiraj, S., Munson, M., & Lambright, D. G. (2006). TBC-domain GAPs for Rab GTPases accelerate GTP hydrolysis by a dual-finger mechanism. *Nature*, *442*(7100), 303–306.

- Pathak, N., Obara, T., Mangos, S., Liu, Y., and Drummond, I.A. (2007). The Zebrafish fleer Gene Encodes an Essential Regulator of Cilia Tubulin Polyglutamylation. *Mol Biol Cell* 18, 4353–4364.
- Pazour, G. J. (2004). Intraflagellar Transport and Cilia-Dependent Renal Disease: The Ciliary Hypothesis of Polycystic Kidney Disease. *Journal of the American Society of Nephrology*, 15(10), 2528–2536.
- Pazour, G.J., Dickert, B.L., and Witman, G.B. (1999). The DHC1b (DHC2) isoform of cytoplasmic dynein is required for flagellar assembly. *The Journal of Cell Biology* 144, 473–481.
- Pazour, G., Dickert, B.L., Vucica, Y., Seeley, E.S., Rosenbaum, J.L., Witman, G.B., and Cole, D.G. (2000). Chlamydomonas IFT88 and Its Mouse Homologue, Polycystic Kidney Disease Gene Tg737, Are Required for Assembly of Cilia and Flagella. *The Journal of Cell Biology* 151, 709–718.
- Pedersen, L. B., Miller, M. S., Geimer, S., Jeffery, L. M., Rosenbaum, J. L., & Cole, D. G. (2005). Chlamydomonas IFT172 Is Encoded by FLA11, Interacts with CrEB1, and Regulates IFT at the Flagellar Tip. *Current Biology*, 15, 262–266.
- Pei, L., Peng, Y., Yang, Y., Ling, X. B., van Eindhoven, W. G., Nguyen, K. C. Q., et al. (2002). PRC17, a Novel Oncogene Encoding a Rab GTPase-activating Protein, Is Amplified in Prostate Cancer. *Cancer research*, 62, 5420–5424.
- Piperno, G., and Mead, K. (1997). Transport of a novel complex in the cytoplasmic matrix of Chlamydomonas flagella. *Proc Natl Acad Sci USA* 94, 4457–4462.
- Piperno, G., Siuda, E., Henderson, S., Segil, M., Vaananen, H., and Sassaroli, M. (1998). Distinct mutants of retrograde intraflagellar transport (IFT) share similar morphological and molecular defects. *The Journal of Cell Biology* 143, 1591–1601.
- Qian, F., Germino, F.J., Cai, Y., Zhang, X., Somlo, S., and Germino, G.G. (1997). PKD1 interacts with PKD2 through a probable coiled-coil domain. *Nat Genet* 16, 179–183.
- Qin, H. (2004). Intraflagellar transport (IFT) cargo: IFT transports flagellar precursors to the tip and turnover products to the cell body. *The Journal of Cell Biology* 164, 255–266.
- Qin, H., Barr, M.M., Diener, D.R., and Rosenbaum, J.L. (2001). Intraflagellar Transport particles complex A and B play different roles in C. elegans cilia formation. *International C. Elegans Meeting* (2001).
- Qin, H., Wang, Z., Diener, D., and Rosenbaum, J. (2007). Intraflagellar transport protein 27 is a small G protein involved in cell-cycle control. *Current Biology* 17, 193–202.
- Ramelot, T.A., Raman, S., Kuzin, A.P., Xiao, R., Ma, L.-C., Acton, T.B., Hunt, J.F., Montelione, G.T., Baker, D., and Kennedy, M.A. (2008). Improving NMR protein structure quality by Rosetta refinement: A molecular replacement study. *Proteins* 75, 147–167.

- Richey, E.A., and Qin, H. (2012). Dissecting the Sequential Assembly and Localization of Intraflagellar Transport Particle Complex B in *Chlamydomonas*. *PLoS ONE* 7, e43118.
- Ringo, D. L. (1967). Flagellar Motion and Fine Structure of the Flagellar Apparatus in *Chlamydomonas*. *The Journal of Cell Biology*, 33(3), 543–571.
- Rix, S., Calmont, A., Scambler, P. J., & Beales, P. L. (2011). An Ift80 mouse model of short rib polydactyly syndromes shows defects in hedgehog signalling without loss or malformation of cilia. *Human Molecular Genetics*, 20(7), 1306–1314.
- Rohatgi, R., Milenkovic, L., & Scott, M. P. (2007). Patched1 Regulates Hedgehog Signaling at the Primary Cilium. *Science*, 317, 372–376.
- Rosenbaum, J. L., & Witman, G. B. (2002). Intraflagellar transport. *Nature Reviews Molecular Cell Biology*, 3(11), 813–825.
- Sang, L., Miller, J. J., Corbit, K. C., Giles, R. H., & Brauer, M. J. (2011). Mapping the NPHP-JBTS-MKS Protein Network Reveals Ciliopathy Disease Genes and Pathways. *Cell*, 145, 513–528.
- Schafer, J. C., Winkelbauer, M. E., Williams, C. L., Haycraft, C. J., Desmond, R. A., & Yoder, B. K. (2006). IFTA-2 is a conserved cilia protein involved in pathways regulating longevity and dauer formation in *Caenorhabditis elegans*. *Journal of Cell Biology*, 119, 4088–4100.
- Sedmak, T., and Wolfrum, U. (2012). Intraflagellar transport proteins in ciliogenesis of photoreceptor cells. *Biology of the Cell* 103, 449–466.
- Seixas, C., Casalou, C., Melo, L. V., Nolasco, S., Brogueira, P., & Soares, H. (2003). Subunits of the chaperonin CCT are associated with *Tetrahymena* microtubule structures and are involved in cilia biogenesis. *Experimental cell research*, 290(2), 303–321.
- Seixas, C., Cruto, T., Tavares, A., Gaertig, J., & Soares, H. (2010). CCT α and CCT δ Chaperonin Subunits Are Essential and Required for Cilia Assembly and Maintenance in *Tetrahymena*. *PLoS ONE*, 5(5), e10704.
- Silva, D.A., Huang, X., Behal, R.H., Cole, D.G., and Qin, H. (2012). The RABL5 homolog IFT22 regulates the cellular pool size and the amount of IFT particles partitioned to the flagellar compartment in *Chlamydomonas reinhardtii*. *Cytoskeleton* 69, 33–48.
- Smith, E.D., Tsuchiya, M., Fox, L.A., Dang, N., Hu, D., Kerr, E.O., Johnston, E.D., Tchao, B.N., Pak, D.N., Welton, K.L., et al. (2008). Quantitative evidence for conserved longevity pathways between divergent eukaryotic species. *Genome Research* 18, 564–570.
- Sobkowicz, H.M., Slapnick, S.M., and August, B.K. (1995). The kinocilium of auditory hair cells and evidence for its morphogenetic role during the regeneration of stereocilia and cuticular plates. *24*, 633–653.

- St Johnston, D. (2005). Developmental Cell Biology: Moving messages: the intracellular localization of mRNAs. *Nat Rev Mol Cell Biol* 6, 363–375.
- Stayner, C., and Zhou, J. (2001). Polycystin channels and kidney disease. *Trends in Pharmacological Sciences* 22, 543–546.
- Stenmark, H. (2009). Rab GTPases as coordinators of vesicle traffic. *Nat Rev Mol Cell Biol* 10, 513–525.
- Stephan, A., Vaughan, S., Shaw, M.K., Gull, K., and McKean, P.G. (2007). An Essential Quality Control Mechanism at the Eukaryotic Basal Body Prior to Intraflagellar Transport. *Traffic* 8, 1323–1330.
- Strissel, K.J. (2005). Recoverin Undergoes Light-dependent Intracellular Translocation in Rod Photoreceptors. *Journal of Biological Chemistry* 280, 29250–29255.
- Sui, H., and Downing, K.H. (2006). Molecular architecture of axonemal microtubule doublets revealed by cryo-electron tomography. *Nature Cell Biology* 442, 475–478.
- Taschner, M., Bhogaraju, S., and Lorentzen, E. (2012). Architecture and function of IFT complex proteins in ciliogenesis. *Differentiation* 83, S12–S22.
- Taschner, M., Bhogaraju, S., Vetter, M., Morawetz, M., and Lorentzen, E. (2011). Biochemical Mapping of Interactions within the Intraflagellar Transport (IFT) B Core Complex. *Journal of Biological Chemistry* 286, 26344–26352.
- Tukachinsky, H., Lopez, L. V., & Salic, A. (2010). A mechanism for vertebrate Hedgehog signaling: recruitment to cilia and dissociation of SuFu–Gli protein complexes. *The Journal of Cell Biology*, 191(2), 415–428.
- Wang, Z., Fan, Z.-C., Williamson, S.M., and Qin, H. (2009). Intraflagellar Transport (IFT) Protein IFT25 Is a Phosphoprotein Component of IFT Complex B and Physically Interacts with IFT27 in *Chlamydomonas*. *PLoS ONE* 4, e5384.
- Warner, F. D., & Satir, P. (1974). The Structural Basis of Ciliary Bend Formation. *The Journal of Cell Biology*, 63, 35–63.
- Yaffe, M. B., Farr, G. W., Miklos, D., Horwich, A. L., & Sternlicht, M. L. (1992). TCP1 complex is a molecular chaperone in tubulin biogenesis. *Nature*, 358, 245–248.
- Yang, S., and Wang, C. (2012). The intraflagellar transport protein IFT80 is required for cilia formation and osteogenesis. *Bone* 51, 407–417.
- Yoshida, S., Shiratori, H., Kuo, I. Y., & Kawasumi, A. (2012). Cilia at the Node of Mouse Embryos Sense Fluid Flow for Left-Right Determination via Pkd2. *Science*, 338, 226–231.
- Yoshimura, S.I., Egerer, J., Fuchs, E., Haas, A.K., and Barr, F.A. (2007). Functional dissection of Rab GTPases involved in primary cilium formation. *The Journal of Cell Biology* 178, 363–369.

9. Acknowledgements

Firstly, I sincerely thank my supervisor Dr. Esben Lorentzen for his patience and belief in me during testing times and teaching me all that I know about crystallography. He has been a great mentor and a role model to me. He created a unique lab environment that can be best described as “easy to thrive”. I thank my thesis advisory committee members Prof. Dr. Elena Conti, Prof. Dr. Karl-Peter Hopfner and Dr. Gáspár Jékely for their valuable inputs into my projects.

I thank Andre, Kristina, Marc, Melanie, Michaela and Taschi for being the best lab-mates I could hope for and making my lab work huge fun. Special thanks go to Taschi for proof reading my thesis. I also thank all the people in the Conti department for being very cooperative. Special thanks go to Dr. Naoko Mizuno and Dr. Claire Basquin for their great technical support in EM and ITC respectively. I am grateful to Jerome, Karina, Sabine and Laura for providing an excellent crystallization facility. I want to thank the core facility of the MPI Biochemistry for their excellent technical support. I also want to thank the staff of IMRS-LS graduate program for being very kind and supportive, especially during the initial times of my stay in Germany.

I thank my parents (Father: B. Venugopala Rao; Mother: M. Vijaya Laxmi). Despite being wary of me doing PhD in Germany in the beginning, their support from the very early was unconditional. My brother Satyam is my best friend and a great support; I am fortunate to have him by my side all the time. Sissy is the best companion I could ever ask for, her support during my professional and personal troubled times was really helpful. Our shared passion for science and movies made the weekends we spent together fun and fruitful.

Finally, I thank all the people who helped me through the course of carrying out this research work. I apologize if I missed mentioning anybody by name.

10. Curriculum vitae

Personal data

Full Name	Sagar Bhogaraju
Date and Place of Birth	04/06/1985, Nizamabad, India.
Nationality	Indian

Education

07/2002-04/2006	Bachelor degree in Biotechnology, JNTU, Hyderabad, India
06/2006-07/2008	Masters degree in Biological sciences and Bioengineering, Indian Institute of Technology, Kanpur, India.

Industry Experience

07/2008-06/2009	Senior Research Analyst, EVALUESERVE, Gurgaon, India.
-----------------	---

Research Experience

02/2007-07/2008	Masters thesis in Structural biology lab, Indian Institute of Technology, Kanpur, India.
10/2009-04/2013	PhD studies in Dr. Esben Lorentzen's lab, MaxPlanck Institute for Biochemistry, Martinsried, Germany.

Publications

- 1) **Bhogaraju S**, Cajanek L, Fort C, Blisnick T, Weber K, Taschner M, Mizuno N, Lamla S, Bastin P, Nigg EA, Lorentzen E. (2013). Molecular basis of tubulin transport within the cilium by IFT74 and IFT81. *SCIENCE*, 341(6149), 1009-1012
- 2) **Bhogaraju S**, Engel B, Lorentzen E. (2013). Intraflagellar transport complex structure and cargo interactions. *Cilia*, 2:10
- 3) Taschner, M., **Bhogaraju, S.**, and Lorentzen, E. (2012). Architecture and function of IFT complex proteins in ciliogenesis. *Differentiation* 83, S12–S22.
- 4) **Bhogaraju, S.**, Taschner, M., Morawetz, M., Basquin, C., & Lorentzen, E. (2011). Crystal structure of the intraflagellar transport complex 25/27. *The EMBO Journal*, 30(10), 1907–1918.
- 5) Taschner, M., **Bhogaraju, S.**, Vetter, M., Morawetz, M., and Lorentzen, E. (2011). Biochemical Mapping of Interactions within the Intraflagellar Transport (IFT) B Core Complex. *Journal of Biological Chemistry* 286, 26344–26352.
- 6) Baskaran, A., Surana, P., **Bhogaraju, S.**, Pahari, S., & Prakash, B. (2009). Circularly permuted GTPase YqeH binds 30S ribosomal subunit: Implications for its role in ribosome assembly, *Biochemical and Biophysical Research Communications*, 386(4), 602-606.

Award

2011	MPI Biochemistry Junior research award
------	--